Supplementary Information

An unprecedented genre of lanthanide-based coordination polymers to widen the scopes of CO_2 fixation

Vaibhav Singh, Vajeeha Urunikulavan, Arun Kumar Bar*

Corresponding author: a.bar@iisertirupati.ac.in

The PDF file includes:

Experimental Section

Supplementary text

Mechanistic Proposition

Figures: S1 to S56

Tables: S1 to S12

Schemes: S1 to S16

References: 1-8

Other Supplementary Materials for this manuscript include the following:

Videos: S1 to S4

Crystallographic Information Files (CIFs): 1 to 13

CheckCIFs: 1 to 13

Table of Contents

EXPERIMENTAL SECTION

Materials and methods: All the reagents and solvents used for the syntheses were used as received from the commercial suppliers. The Schiff base ligand $\mathbf{H_2L}^{i}$ was synthesized following the reported procedure.[1,2] Synthetic manipulations and sample processing for all the characterizations in solutions are carried out under inert conditions for all the complexes unless otherwise mentioned. All the spectroscopic studies were carried out under ambient conditions. UV-Vis spectral studies were carried out on μ(M) methanol solutions of the complexes with Agilent 8454 diode array UV-Vis spectrometer. The ^{1}H spectral studies were carried out in the deuterated solvents (CD_3OD) with a Bruker model Ascend 400 FT-NMR spectrometer. Fourier transform infrared (FT-IR) spectroscopic studies were performed on the thin layers of neat samples with a Bruker-Alpha Eco-ATR FT-IR spectrometer. ESI – MS data were recorded on ThermoScientific Orbitrap Exploris™ 120 mass spectrometer.

X-ray crystallographic studies: Suitable single crystals for X-ray diffraction were coated with paratone oil and mounted onto the goniometer. The X-ray crystallographic data were obtained from Bruker D8 Venture diffractometer equipped with a Photon III detector using MoKα radiation source. Temperature control was achieved using an Oxford Cryosystem. The structures were solved by intrinsic phasing methods using ShelXT and refined by means of least-square procedures on F^2 using SHELXL as implemented in the Olex2 software package. The scattering factors for all the atoms were used as listed in the International Tables for X-ray Crystallography.[3] Absorption correction was performed using a multi-scan procedure. The H atoms were repositioned geometrically. The H atoms were initially refined with soft restraints on the bond lengths and angles to regularize their geometry and U~iso~(H) (in the range 1.2-1.5 times U~eq~ of the parent atom), after which the positions were refined with riding constraints. All non-hydrogen atoms were refined anisotropically. Crystallographic data and refinement parameters for the single-crystal X-ray data analyses for all the complexes are summarized in Tables S5-S6. The selected bond parameters are provided in Table S7. CIF has been deposited at CCDC (http://www.ccdc.cam.ac.uk) with references **2441095-2441103**, **2441106, 2475746**, **2475747, 2475749** for complexes **1·Ln - 11·Ln**. The solid-state phase purity of the isolated polycrystalline solid samples of the complexes was confirmed by powder X-ray diffraction (PXRD) using a Rigaku (SmartLab) diffractometer with Cu(Kα) radiation source radiation, λ=1.5406 Å. The PXRD studies were carried out with 2θ ranging from 5 to 50° with a step size of 0.01.

Computational studies: The computational studies for conformational analyses were carried out using DFT on GAUSSIAN-09 platform[4] utilizing hybrid B3LYP basis functions[5] with mixed basis sets: 6-311G*[6] for all elements except for Y and La, and the small-core Hay-Wadt pseudopotential (indicated in the Gaussian code as LANL2DZ)[7] for Y and La. For the single-point structure-based computations, the crystallographic coordinates of the respective single-crystal X-ray molecular structures were employed. The Gaussian in-build Onsager model was employed for self-consistent reaction field (SCRF) of MeOH solvent with steered molecular dynamics (SMD). The isosurface maps were plotted with isovalue 0.02 using GassView4.1 software and are presented in 4×10-4 μB $Å^3$ isosurface.

Synthetic procedures:

General Information: The reactions detailed here were carried out using a Schlenk line in an inert argon environment unless stated. Freeze-pump-thaw cycles were utilized to degas commercially available methanol and methanol was dried from magnesium methoxide.

1·La: A suspension of the ligand **H_2L^1** (40 mg, 0.1 mmol) and La $(OTf)_3 \cdot 6H_2O$ (70 mg, 0.1 mmol) in 10 mL of commercially available methanol was stirred at room temperature for 1 hour, resulting in a clear yellow solution. The mixture was filtered and allowed to evaporate slowly at ambient conditions. Upon near-complete evaporation, colorless plate-shaped crystals were formed. These crystals were manually isolated under a microscope and subsequently characterized by single-crystal X-ray diffraction and NMR spectroscopy.

Isolated yield 10% (14 mg). NMR (CD_3OD): δ ppm: ^{1}H: 2.80 (s,12H, $–CH_3$), 7.37–7.48 (m, 8H, Aromatic-CH), 7.56–7.67 (m, 12H, Aromatic-CH), 8.45–8.58 (m,6H, aromatic –CH).

2·La: A 25 mL Schlenk tube was charged with a magnetic stirring bar, followed by the addition of **3·La** polymer (0.05 mmol ,28mg) and 10 ml of degassed methanol. Carbon dioxide gas was purged into the reaction mixture till the solution turned clear yellow and the whole solution was stirred for 1 hour. The reaction mixture was filtered and then concentrated under reduced pressure which gave bright yellow plate-shaped crystals. These crystals were isolated and redissolved in $CHCl_3$ and kept for slow evaporation, which finally gave yellow plate shaped crystals suitable for X-ray diffraction.

Isolated yield 60% (40 mg). UV-Vis: λ_{max} = 306 nm; ε = 3.9x10^4 L mol^{-1} cm^{-1}; λ_{max} = 245 nm; ε = 3. 2x10^4 L mol^{-1} cm^{-1}. NMR (CD_3OD): δ ppm: ^{1}H: 2.48 (s, 12H, $-CH_3$) ,7.18-7.27 (m, 8H, Aromatic-CH), 7.32-7.42 (m, 4H, Aromatic-CH), 7.49-7.57 (m, 8H, Aromatic-CH), 8.01-8.08 (d, 4H, Aromatic-CH), 8.23-8.31 (t, 2H, aromatic -CH).

2′·Y and 2″·Y: A suspension of the ligand $\mathbf{H_2L^1}$ (40 mg, 0.1 mmol) and $Y(OTf)_3 \cdot 6H_2O$ (64 mg, 0.1 mmol) in 10 mL of commercially available methanol was stirred at room temperature for 1 hour, resulting in a clear yellow solution. The mixture was filtered and allowed to evaporate slowly at ambient conditions. Upon near-complete evaporation, colorless plate-shaped and yellow rod-shaped crystals were formed. Upon X-ray diffraction, colorless crystals gave the structure **2″·Y** and the yellow rod-shaped crystals gave the structure **2′·Y.** The colorless crystals (**2″·Y)** were manually isolated under a microscope and subsequently characterized by NMR spectroscopy.

NMR (CD_3OD): δ ppm: ^1H: 2.83 (s, 12H, $-CH_3$) ,7.66-7.72 (m, 8H, Aromatic-CH), 7.80-7.90 (m, 6H, Aromatic-CH), 8.21-8.25 (m, 6H, Aromatic-CH), 8.41-8.48 (m, 4H, Aromatic-CH), 8.54-8.60 (m, 2H, aromatic -CH).

3·La: A 25 mL Schlenk tube was charged with a magnetic stirring bar, followed by the addition of lanthanide salt (0.25 mmol, 173.5 mg of La $(OTf)_3.6H_2O$) and ligand (0.25 mmol, 100 mg of $\mathbf{H_2L^1}$). Subsequently, 10 mL of degassed methanol was introduced, and the resulting mixture was refluxed for 1 hour. The solution was then filtered into another Schlenk tube, to which Triethylamine (NEt_3, 1.25 mmol, 209 µL) was added, leading to the immediate formation of a yellow precipitate. The reaction mixture was stirred for 24 hours, after which the precipitate was collected by filtration and washed thrice with methanol. The obtained polymer was suspended in methanol and heated at 45–50°C under continuous stirring for 48 hours. Finally, the polymer was isolated by filtration and was dried under vacuum.

Isolated yield 51% (77 mg). IR (cm^{-1}): 1504 (m), 1557(m),1583(s). Elemental analysis (%) calcd. $C_{24.5}H_{26}N_5O_{4.5}La$ (FW = 601.41 g/mol): C 48.91; H 4.32; N 11.64; found: C 48.86; H 4.35; N 11.62.

NMR (CD_3OD): δ ppm: ^1H: 2.71 (s, 6H, $-CH_3$) ,7.38-7.55 (m, 6H, Aromatic-CH), 8.0-8.06 (m, 2H, Aromatic-CH), 8.19-8.34 (m, 5H, Aromatic-CH).

4·La: A 25 mL Schlenk tube was charged with a magnetic stirring bar, followed by the addition of lanthanide salt (0.25 mmol, 146.5 mg of La $(OTf)_3$) and ligand (0.25 mmol, 100 mg of $\mathbf{H_2L^1}$). Subsequently, 10 mL of dried and degassed methanol was introduced, and the resulting mixture was refluxed for 1 hour. The solution was then filtered into another Schlenk tube, to which Triethylamine (NEt_3, 1.25 mmol, 209 µL) was added, leading to the immediate formation of a yellow precipitate. The reaction mixture was stirred for 24 hours, after which the precipitate was collected by filtration and washed thrice with methanol. The obtained polymer was suspended in methanol and heated at 45–50°C under continuous stirring for 48 hours. Finally, the polymer was isolated by filtration and was dried under vacuum.

Isolated yield 49% (78 mg). IR (cm^{-1}): 1506 (s),1559(m),1586(m). Elemental analysis (%) calcd. $C_{26.4}H_{31.37}N_5O_{5.34}La$ (FW = 642.36 g/mol): C 49.35; H 4.93; N 10.90; found: C 49.40; H 4.90; N 10.93.

NMR (CD_3OD): δ ppm: ^1H: 2.71 (s, 6H, $-CH_3$) ,7.34-7.53 (m, 6H, Aromatic-CH), 7.9-8.03 (m, 2H, Aromatic-CH), 8.15-8.30 (m, 4H, Aromatic-CH), 8.54 (s, 1H, Aromatic-CH).

3·Y: A 25 mL Schlenk tube was charged with a magnetic stirring bar, followed by the addition of lanthanide salt (0.25 mmol, 161 mg of $Y(OTf)_3.6H_2O$) and ligand (0.25 mmol, 100 mg of $\mathbf{H_2L^1}$). Subsequently, 10 mL of degassed methanol was introduced, and the resulting mixture was refluxed for 1 hour. The solution was then filtered into another Schlenk tube, to which Triethylamine (NEt_3, 1.25 mmol, 209 µL) was added, leading to the immediate formation of a yellow precipitate. The reaction mixture was stirred for 24 hours, after which the precipitate was collected by filtration and washed thrice with methanol. The obtained polymer was suspended in methanol and heated at 45–50°C under continuous stirring for 48 hours. Finally, the polymer was isolated by filtration and was dried under vacuum.

Isolated yield 48% (68.5 mg). IR (cm^{-1}): 1508 (s),1563(m),1583(m). Elemental analysis (%) calcd. $C_{24}H_{28}N_5O_6Y$ (FW = 571.42 g/mol): C 50.45; H 4.94; N 12.26; found: C 50.36; H 4.99; N 12.22.

NMR (CD_3OD): δ ppm: ^1H: 2.70 (s, 6H, $-CH_3$) ,7.32-7.53 (m, 6H, Aromatic-CH), 8.0-8.10 (m, 2H, Aromatic-CH), 8.18-8.37 (m, 5H, Aromatic-CH).

4·Y: A 25 mL Schlenk tube was charged with a magnetic stirring bar, followed by the addition of lanthanide salt (0.25 mmol, 134 mg of $Y(OTf)_3$) and ligand (0.25 mmol, 100 mg of $\mathbf{H_2L^1}$). Subsequently, 10 mL of dried and degassed methanol was introduced, and the resulting mixture was refluxed for 1 hour. The solution was then filtered into another Schlenk tube, to which Triethylamine (NEt_3, 1.25 mmol, 209 µL) was added, leading to the immediate formation of a yellow precipitate. The reaction mixture was stirred for 24 hours, after which the precipitate was collected by filtration and washed thrice with methanol. The obtained polymer was suspended in methanol and heated at 45–50°C under continuous stirring for 48 hours. Finally, the polymer was isolated by filtration and was dried under vacuum.

Isolated yield 47% (70 mg). IR (cm^{-1}): 1508 (s),1561(m),1585(m). Elemental analysis (%) calcd. $C_{26.4}H_{31.37}N_5O_{5.34}Y$ (FW = 592.36 g/mol): C 53.52; H 5.34; N 11.82; found: C 53.47; H 5.30; N 11.86.

NMR (CD_3OD): δ ppm: ^1H: 2.70 (s, 6H, $-CH_3$) ,7.33-7.55 (m, 6H, Aromatic-CH), 8.0-8.10 (m, 2H, Aromatic-CH), 8.18-8.37 (m, 5H, Aromatic-CH).

5·La: A 25 mL Schlenk tube was charged with a magnetic stirring bar, followed by the addition of lanthanide salt (0.25 mmol, 146.5 mg of La $(OTf)_3$) and ligand (0.25 mmol, 107 mg of $\mathbf{H_2L^2}$). Subsequently, 10 mL of degassed methanol was introduced, and the resulting mixture was refluxed for 1 hour. The solution was then filtered into another Schlenk tube, to which Triethylamine (NEt_3, 1.25 mmol, 209 µL) was added, leading to the immediate formation of a yellow precipitate. The reaction mixture was stirred for 24 hours, after which the precipitate was collected by filtration and washed thrice with methanol. The obtained polymer was suspended in methanol and heated at 45–50°C under continuous stirring for 48 hours. Finally, the polymer was isolated by filtration and was dried under vacuum.

Isolated yield 56% (88 mg). IR (cm^{-1}): 1493(s),1553(m), 1580(m),1608(w). Elemental analysis (%) calcd. $C_{26}H_{30}N_5O_5La$ (FW = 631.46 g/mol): C 49.45; H 4.79; N 11.09; found: C 49.40; H 4.87; N 10.98.

6·La: A 25 mL Schlenk tube was charged with a magnetic stirring bar, followed by the addition of lanthanide salt (0.25 mmol, 146.5 mg of La $(OTf)_3$) and ligand (0.25 mmol, 107 mg of $\mathbf{H_2L^2}$). Subsequently, 10 mL of dried and degassed methanol was introduced, and the resulting mixture was refluxed for 1 hour. The solution was then filtered into another Schlenk tube, to which Triethylamine (NEt_3, 1.25 mmol, 209 µL) was added, leading to the immediate formation of a yellow precipitate. The reaction mixture was stirred for 24 hours, after which the precipitate was collected by filtration and washed thrice with methanol. The obtained polymer was suspended in methanol and heated at 45–50°C under continuous stirring for 48 hours. Finally, the polymer was isolated by filtration and was dried under vacuum.

Isolated yield 55% (95 mg). IR (cm^{-1}): 1500(s),1555(m),1580(m),1610(w). Elemental analysis (%) calcd. $C_{29}H_{38}N_5O_6La$ (FW = 691.55 g/mol): C 50.37; H 5.54; N 10.13; found: C 50.40; H 5.59; N 10.20.

5·Y: A 25 mL Schlenk tube was charged with a magnetic stirring bar, followed by the addition of lanthanide salt (0.25 mmol, 161 mg of $Y(OTf)_3.6H_2O$) and ligand (0.25 mmol, 107 mg of $\mathbf{H_2L^2}$). Subsequently, 10 mL of dried and degassed methanol was introduced, and the resulting mixture was refluxed for 1 hour. The solution was then filtered into another Schlenk tube, to which Triethylamine (NEt_3, 1.25 mmol, 209 µL) was added, leading to the immediate formation of a yellow precipitate. The reaction mixture was stirred for 24 hours, after which the precipitate was collected by filtration and washed thrice with methanol. The obtained polymer was suspended in methanol and heated at 45–50°C under continuous stirring for 48 hours. Finally, the polymer was isolated by filtration and was dried under vacuum.

Isolated yield 69% (100 mg). IR (cm^{-1}): 1504 (s),1561(m),1579(m),1608(w). Elemental analysis (%) calcd. $C_{26}H_{30}N_5O_5Y$ (FW = 581.46 g/mol): C 53.71; H 5.20; N 12.04; found: C 53.66; H 5.28; N 12.10.

6·Y: A 25 mL Schlenk tube was charged with a magnetic stirring bar, followed by the addition of lanthanide salt (0.25 mmol, 134 mg of $Y(OTf)_3$) and ligand (0.25 mmol, 107 mg of $\mathbf{H_2L^2}$). Subsequently, 10 mL of dried and degassed methanol was introduced, and the resulting mixture was refluxed for 1 hour. The solution was then filtered into another Schlenk tube, to which Triethylamine (NEt_3, 1.25 mmol, 209 µL) was added, leading to the immediate formation of a yellow precipitate. The reaction mixture was stirred for 24 hours, after which the precipitate was collected by filtration and washed thrice with methanol. The obtained polymer was suspended in methanol and heated at 45–50°C under continuous stirring for 48 hours. Finally, the polymer was isolated by filtration and was dried under vacuum.

Isolated yield 70% (95 mg). IR (cm^{-1}): 1504 (s),1561(m),1579(m),1608(w). Elemental analysis (%) calcd. $C_{29}H_{38}N_5O_6Y$ (FW = 641.55 g/mol): C 54.29; H 5.97; N 10.92; found: C 54.25; H 5.90; N 10.85.

7·Y: A 25 mL Schlenk tube was charged with a magnetic stirring bar, followed by the addition of **3·Y** polymer (0.05 mmol ,25mg) and 15 ml of degassed methanol. Carbon dioxide gas was purged into the reaction mixture till the solution turned clear yellow and the whole solution was stirred for 1 hour. The reaction mixture was filtered and then concentrated under reduced pressure which gave bright yellow needle-shaped single crystals suitable for X-ray diffraction. Isolated yield 60% (35 mg). UV-Vis: λ_{max} = 392 nm; ε = 2.0 ×10^4 L mol^{-1} cm^{-1}; λ_{max} = 340 nm; ε = 5.42 × 10^4 L mol^{-1} cm^{-1}; λ_{max} = 250 nm; ε = 2.26 × 10^4 L mol^{-1} cm^{-1}; λ_{max} = 203 nm; ε =6.7 × 10^4 L mol^{-1} cm^{-1}. NMR (CD_3OD): δ ppm: ^{1}H: 2.64 (s,12H, –CH_3), 7.40–7.50 (m, 12H, Aromatic-CH), 7.83–7.96 (m, 4H, Aromatic-CH),8.13–8.35 (m,10H, aromatic –CH). IR (cm−1): 1552(s), 1586(m).

8·Y: A 25 mL Schlenk tube was charged with a magnetic stirring bar, followed by the addition of **5·Y** polymer (0.05 mmol ,28 mg) and 15 ml of degassed methanol. Carbon dioxide gas was purged into the reaction mixture till the solution turned clear yellow and the whole solution was stirred for 1 hour. The reaction mixture was filtered and then concentrated under reduced pressure which gave bright yellow needle-shaped single crystals suitable for X-ray diffraction. Isolated yield 58% (34 mg). UV-Vis: λ_{max} = 394 nm; ε = 1.83 ×10^4 L mol^{-1} cm^{-1}; λ_{max} = 344 nm; ε = 4.90 × 10^4 L mol^{-1} cm^{-1}; λ_{max} = 253 nm; ε = 2.3 × 10^4 L mol^{-1} cm^{-1}. NMR (CD_3OD): δ ppm: ^{1}H: 2.41 (s,12H, –CH_3), 2.62 (s,12H, –CH_3), 7.20–7.30 (m, 8H, Aromatic-CH), 7.68–

7.865 (br, 4H, Aromatic-CH), 7.98–8.22 (m,10H, aromatic –CH). IR (cm^{-1}): 1551 (m),1557(m), 1612(m), 1680(m).

9·La: A 25 mL Schlenk tube was charged with a magnetic stirring bar, followed by the addition of **5·La** polymer (0.05 mmol, 31 mg) and 15 ml of degassed methanol. Carbon dioxide gas was purged into the reaction mixture till the solution turned clear yellow and the whole solution was stirred for 1 hour. The reaction mixture was filtered and then concentrated under reduced pressure which gave yellow plate-shaped crystals suitable for X-ray diffraction.

Isolated yield 55% (31 mg). NMR (CD_3OD): δ ppm: ^1H: 2.33 (s,12H, –CH3), 2.49 (s,12H, –CH3), 7.03–7.13 (m, 8H, Aromatic-CH), 7.39–7.46 (m, 8H, Aromatic-CH), 8.06–8.13 (m,4H, aromatic –CH), 8.30–8.35 (m,2H, aromatic –CH).

10b·Y: A 25 mL Schlenk tube was equipped with a magnetic stirring bar to which a solution of 0.1 mmol of lanthanide salt (54 mg of $Y(OTf)_3$) in 5 ml of methanol (dried and degassed) was added to a slurry of 0.1 mmol of the ligand (40 mg of $\mathbf{H_2L^1}$) in 5 ml of methanol (dried and degassed). The mixture was stirred at room temperature for 30 minutes. The yellow precipitate was immediately visible after adding NEt_3 (0.60 mmol, 84 µL). After an additional 15 minutes of stirring at room temperature, CO_2 gas was purged into the reaction mixture until a clear yellow solution was obtained. The mixture was filtered and concentrated under reduced pressure, affording bright yellow needle-shaped and yellow rhomboidal crystals suitable for single-crystal X-ray diffraction. The needle-shaped crystals corresponded to the molecular structure of **7·Y**, while the rhomboidal crystals corresponded to **10b·Y.**

15·Y: 66 mg (0.165 mmol) of the organic ligand $\mathbf{H_2L^1}$ was suspended in 20 ml of EtOH and heated to 45°C. This white suspension was added dropwise to the preheated 5 ml normal degassed EtOH solution of $YCl_3.6H_2O$ (50 mg, 0.165 mmol). The whole reaction mixture was heated to 60°C for 1 hour upon stirring and cooled to room temperature to yield yellow clear solution. Et_3N (10 times diluted in EtOH; 0.459ml, 0.33 mmol) was added slowly to the cooled reaction mixture and stirred for 3 min to obtain dark yellow solution. The reaction mixture was filtered and concentrated to about 9 ml under reduced pressure and added excess of diethyl ether to yield yellow rod crystals after 4-5 days. The crystals were filtered and washed with diethylether and vacuum dried to obtain yellow crystalline solid.

Isolated yield 64% (75 mg). NMR (CD_3OD): δ ppm: ^1H: 2.73 (s,6H, –CH3), 7.42–7.53 (m, 6H, Aromatic-CH), 8.02–8.08 (m,2H, aromatic –CH), 8.26–8.34 (m,5H, aromatic –CH).

Supplementary Text:

Base Layering: A 25 mL Schlenk tube was charged with a magnetic stirring bar, followed by the addition of lanthanide salt (0.120 mmol of $Y(OTf)_3 \cdot xH_2O$/ $La(OTf)_3 \cdot xH_2O$) and ligand (0.25 mmol $\mathbf{H_2L^1}$/$\mathbf{H_2L^2}$). Subsequently, 5 mL of degassed methanol was introduced, and the resulting mixture was refluxed for 1 hour. The solution was then filtered into another Schlenk tube, to which Triethylamine (NEt_3, 0.360 mmol,) was added slowly in its diluted form (50 μL in 2ml methanol) leading to formation of two distinct layers. Crystals started to grew on the junction of two layers after few hours which were later taken for X-ray diffraction.

Scale of Reactions performed for the kinetics experiment:

Inside the glove box, 0.1 mg of **3·Ln** (2×10^{-4} mmol for **3·Y** and 1.8×10^{-4} mmol for **3·La**) was added to 4 ml of degassed methanol and the whole suspension was transferred to a cuvette equipped with a magnetic stirrer, The cuvette was properly sealed and taken out for the experiment. The measurements were performed with CO_2 gas being purged through the solution under stirring condition.

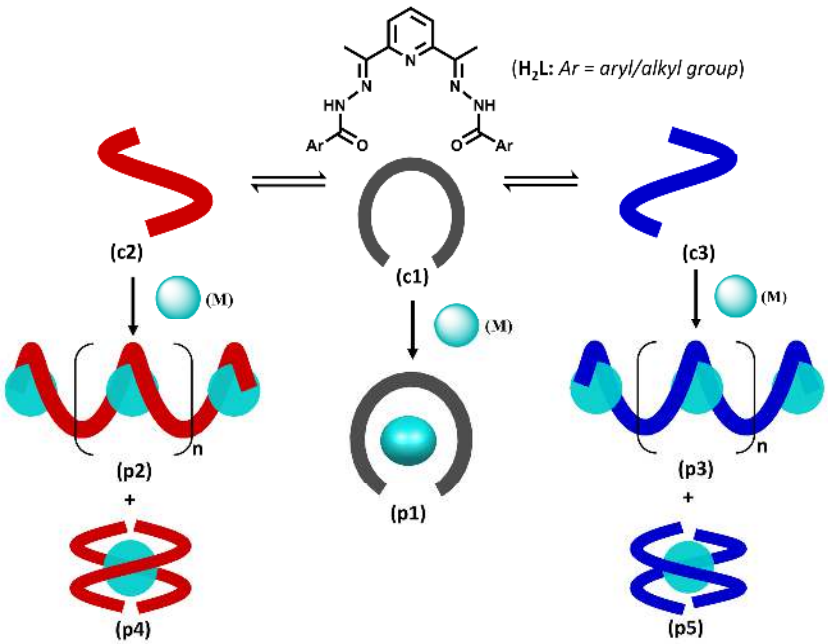

Scheme S1: The *ChemDraw* structure of the generalized pentadentate chelating ligands (**H_2L**) with *N_3O_2-pentadentate* chelating pockets and having aryl (Ar = aryl groups) or alkyl (Ar = alkyl groups) peripheral substituents; the diagrammatic representation for their planar conformations (**c1**), Δ-isomeric helical conformations (**c2**) and Λ-isomeric helical conformations (**c3**); the diagrammatic representation for their most probable self-sorting with metal ions (**M**) to form [1:1] metal-ligand self-assembled mononuclear complexes **p1**, [1:1] metal-ligand self-assembled 1D coordination polymers **p2** (having Δ-isomeric ligand conformations) and **p3** (having Λ-isomeric ligand conformations), [1:2] metal-ligand self-assembled mononuclear complexes **p4** (having Δ-isomeric ligand conformations) and **p5** (having Λ-isomeric ligand conformations).

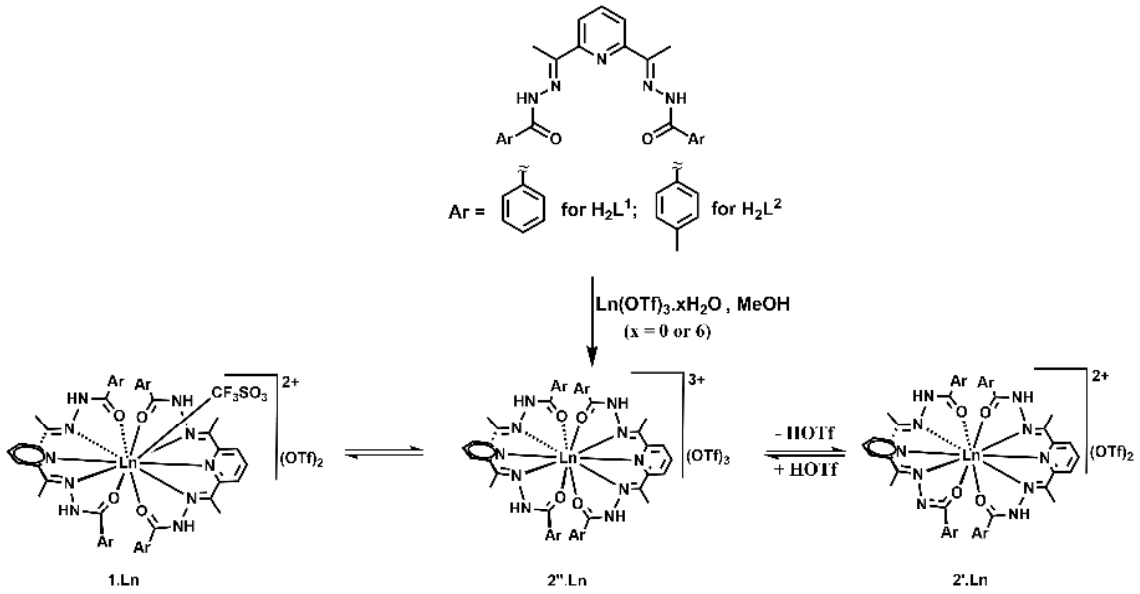

Scheme S2: Schematic representation for the formation of the mononuclear complexes **1·Ln**, **2′·Ln** and **2"·Ln** (Ln = Y and La).

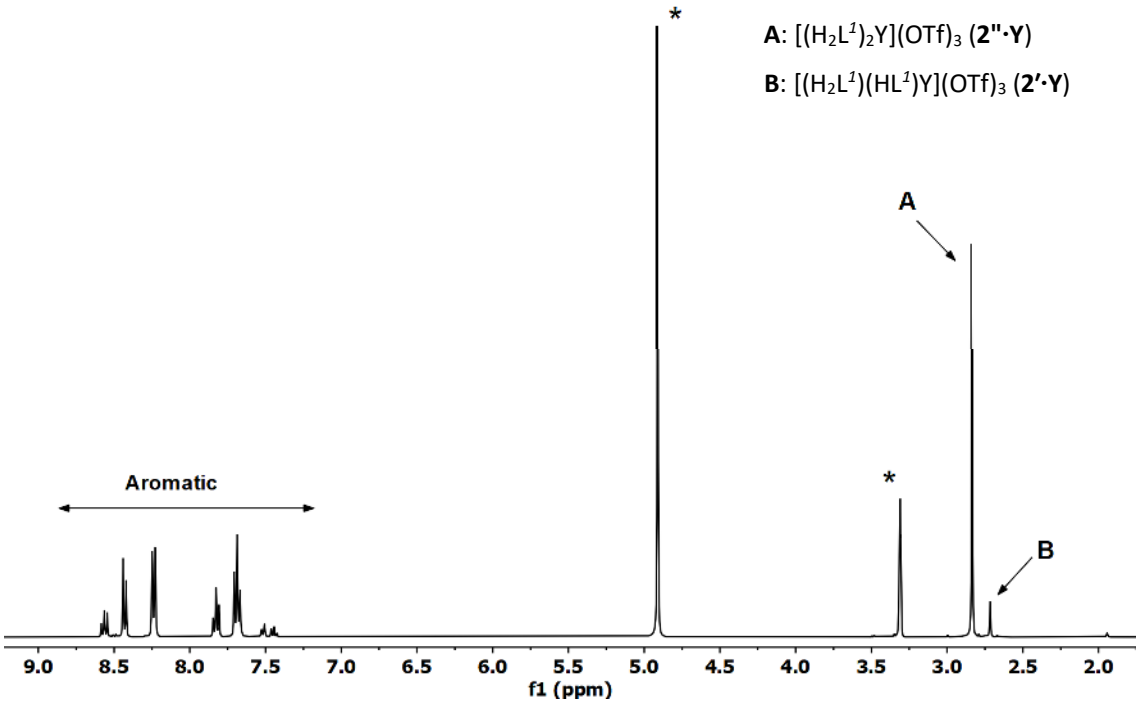

Fig. S1. The room temperature solution ^{1}H NMR spectrum of the reaction mixture which was obtained upon treatment of $Y(OTf)_3 \cdot xH_2O$ with $\mathbf{H_2L^1}$ in 1 : 1 molar ratio in CD_3OD solvent medium.[8] The signals corresponding to the residual solvent / grease are indicated by asterisks. The characteristic signals corresponding to the CH_3 moieties of the imine functionality of the ligand ($\delta_{CH_3}(imine$, ppm)) in the products **2′·Y** (2.71 ppm) and **2"·Y** (2.83 ppm) are labelled in the aliphatic region of the spectrum.

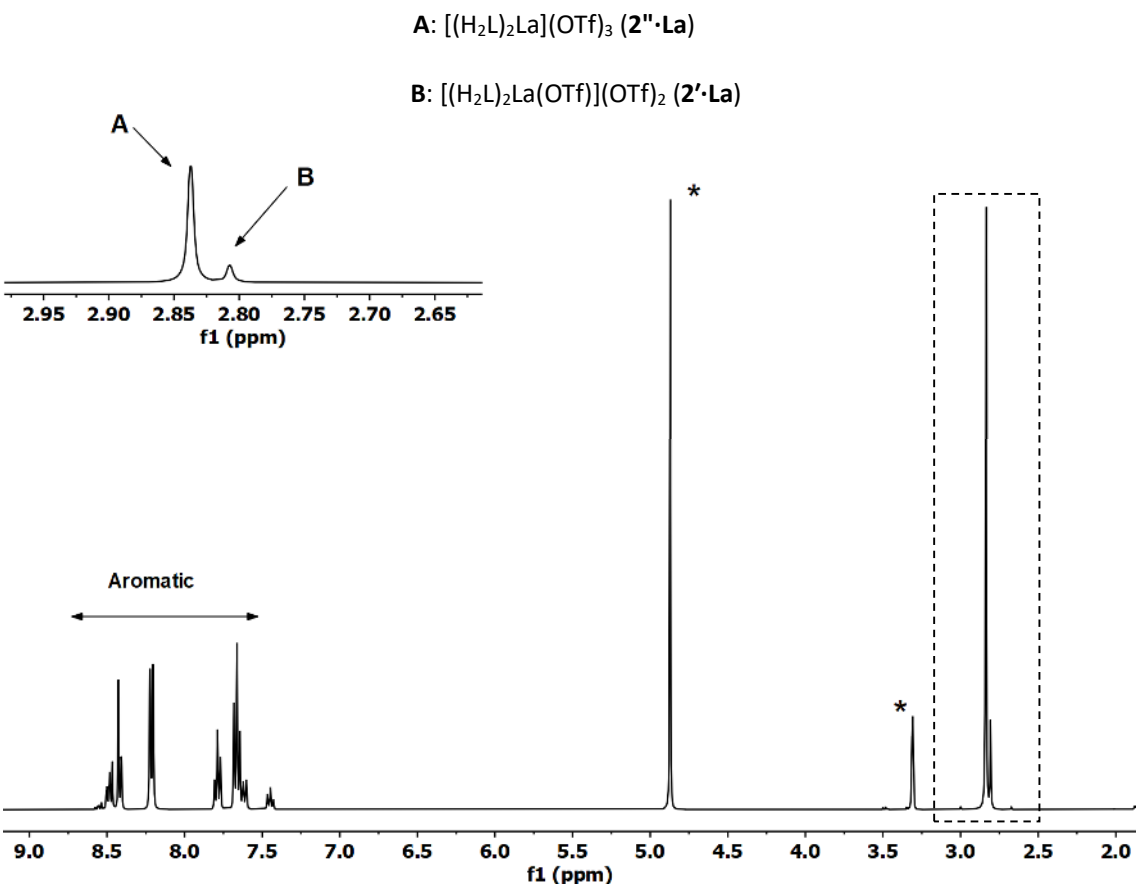

Fig. S2. The room temperature solution ^{1}H NMR spectrum of the reaction mixture which was obtained upon treatment of La(OTf)$_3$·xH$_2$O with $\mathbf{H_2L}^{I}$ in 1 : 1 molar ratio in CD$_3$OD solvent medium. The signals corresponding to the residual solvent / grease are indicated by asterisks. The characteristic signals corresponding to the CH$_3$ moieties of the imine functionality of the ligand ($\delta_{CH_3}(imine, \text{ppm})$) in the products **2′·La** (2.80 ppm) and **2"·La** (2.84 ppm) are labelled in the *inset*, which is a zoomed-in segment (highlighted with the dashed rectangle) of the aliphatic region of the spectrum.

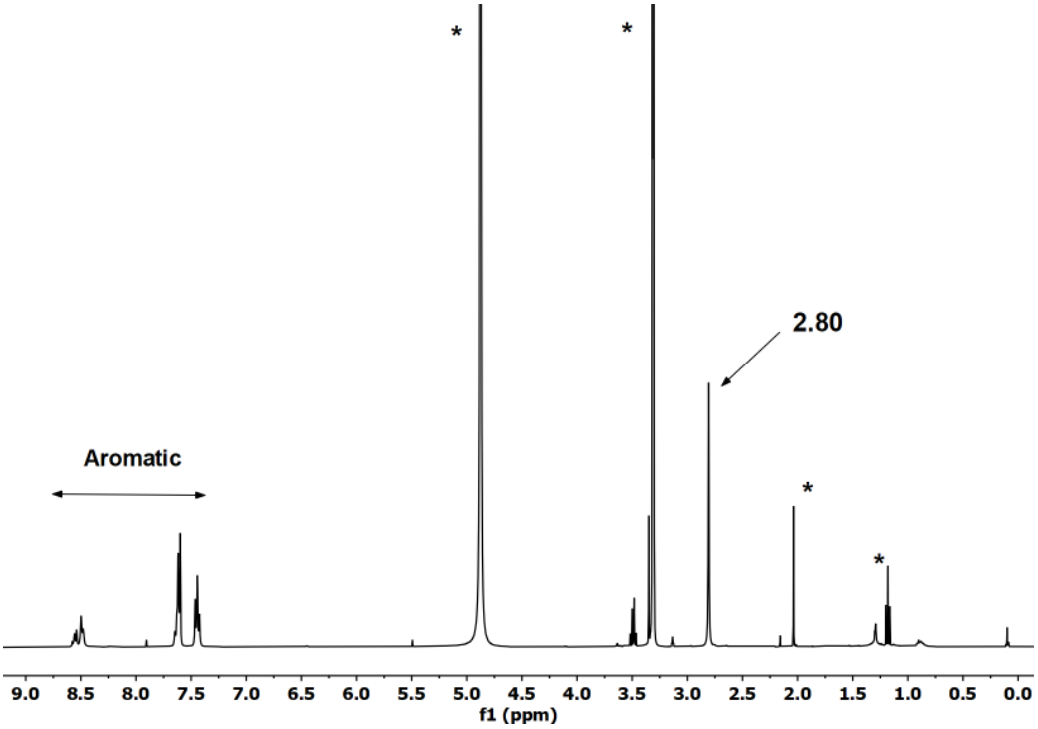

Fig. S3. The solution ^{1}H NMR spectrum of the isolated polycrystalline sample of **1·La**. The spectrum was recorded in CD_3OD at room temperature. The signals corresponding to the residual solvent / grease are indicated by asterisks. The characteristic signals corresponding to the CH_3 moieties of the imine functionality of the ligand ($\delta_{CH_3}(imine, \text{ppm})$) in **1·La** is labelled with the chemical shift value.

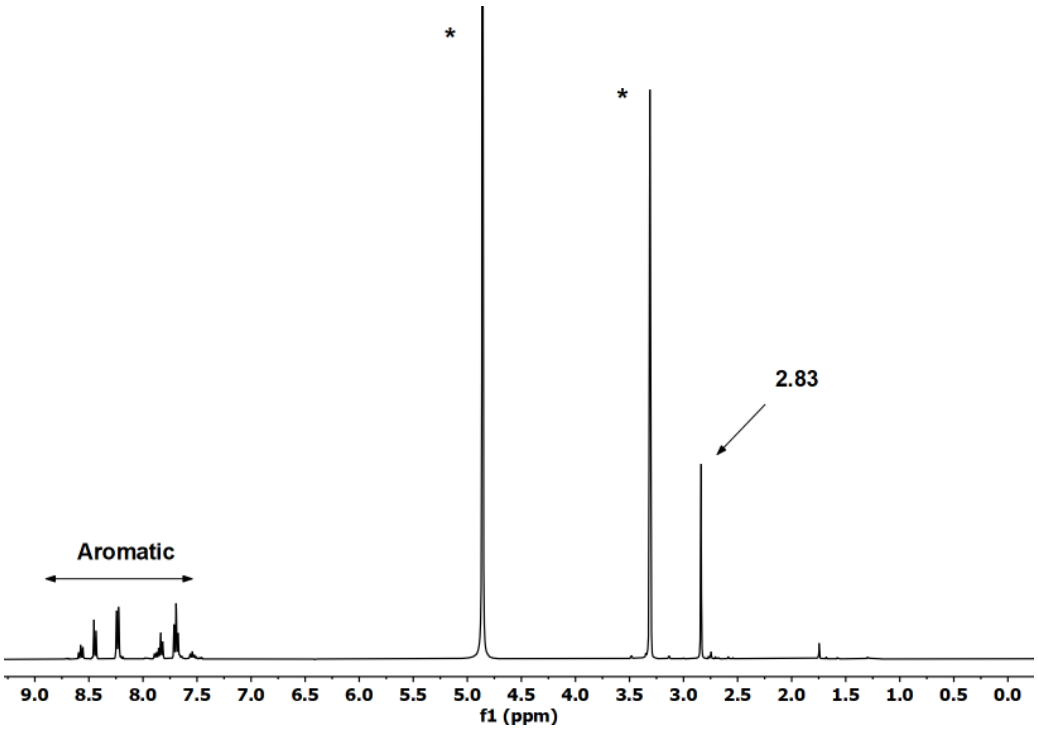

Fig. S4. The solution ^{1}H NMR spectrum of the isolated polycrystalline sample of **2′′·Y**. The spectrum was recorded in CD_3OD at room temperature. The signals corresponding to the residual solvent / grease are indicated by asterisks. The characteristic signals corresponding to the CH_3 moieties of the imine functionality of the ligand ($\delta_{CH_3}(imine, \text{ppm})$) in **2′′·Y** is labelled with the chemical shift value.

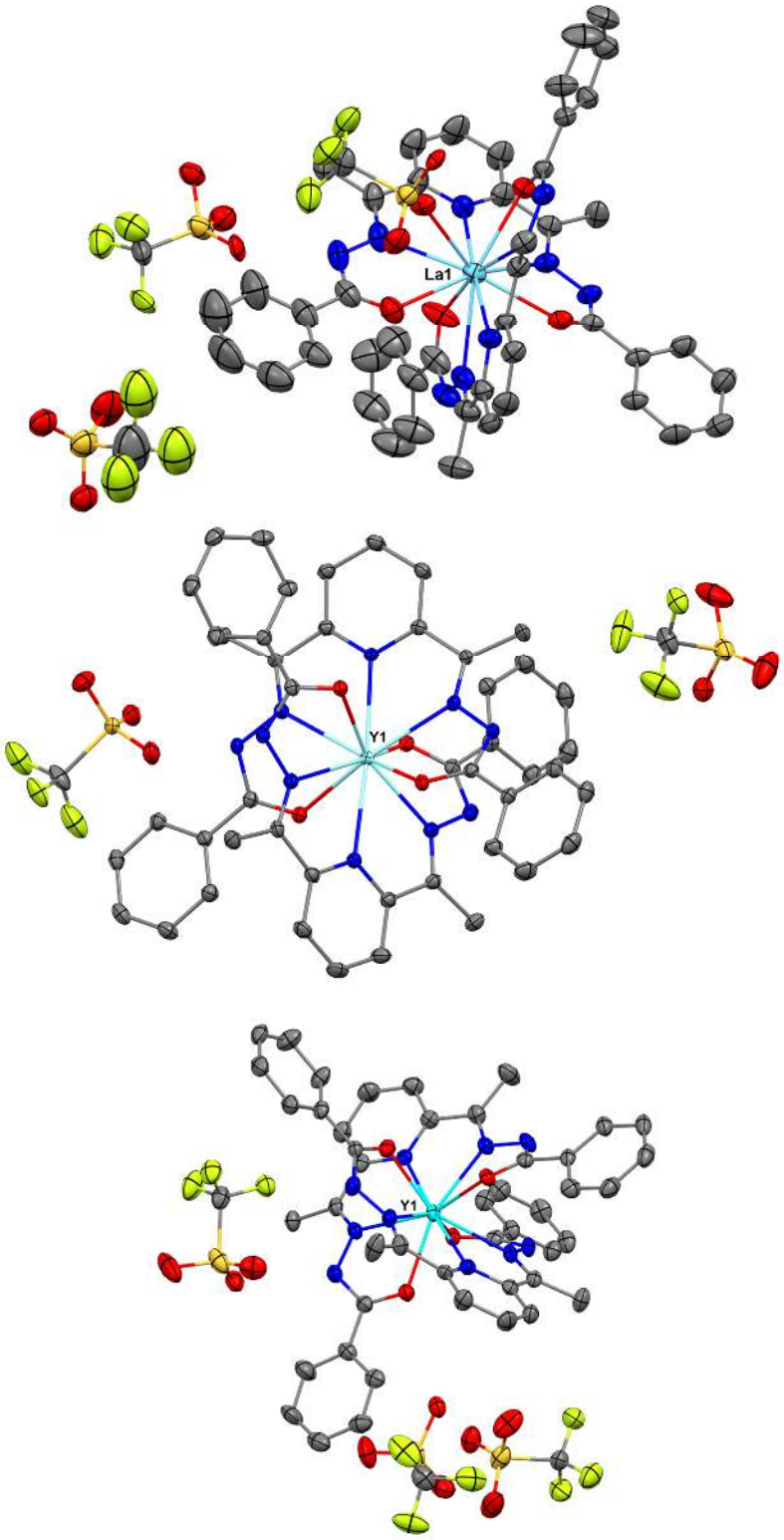

Fig. S5. ORTEP representations with 40% ellipsoid probability for the solid-state single crystal X-ray molecular structures of the ΛΛ-isomers (cf. Scheme 1, main text) of **1**·**La** (*top*), **2′**·**Y** (*middle*) and **2′′**·**Y** (*bottom*). The H atoms, thermally disordered atoms and the co-crystallized solvent molecules are omitted for clarity. Color codes: cyan, La and Y; yellow, S; green, F; red, O; blue, N; and grey, C.

Table S1. Selected crystallographic data and refinement parameters for **1·La, 2′·Y** and **2′′·Y**

	1·La	**2′·Y**	**2′′·Y**
Formula	$C_{50}H_{45}F_9LaN_{10}O_{14}S_3$	$C_{51}H_{53}F_6N_{10}O_{13}S_2Y$	$C_{49}H_{44}F_9N_{10}O_{14}S_3Y$
Mr (g mol^{-1})	1416.05	1281.06	1353.03
Crystal system	Monoclinic	Triclinic	Triclinic
Space group	C2/C	P-1	P-1
T (K)	100	150	100
a (Å)	16.2641(8)	11.2464(10)	11.7862(18)
b (Å)	16.0742(9)	13.0608(12)	13.673(2)
c (Å)	45.157(3)	20.3371(18)	19.090(3)
α (°)	90	95.964(3)	102.972(5)
β (°)	90.972(2)	104.907(3)	98.931(5)
γ (°)	90	101.751(3)	105.652(5)
V (Å^3)	11803.8(11)	2787.4(4)	2809.3(8)
Z	8	2	2
ρcalcd. (g cm^{-3})	1.594	1.526	1.600
μ (mm^{-1})	0.929	1.213	1.253
collected reflns	66350	49460	66441
unique reflns	12094	12855	11048
No. of parameters	830	790	818
Reflns for Refinement	66350	49460	66441
R ($I > 3\sigma(I)$)[a]	0.0846	0.0628	0.0832
wR ($I > 3\sigma(I)$)[b]	0.2545	0.1766	0.2474
GOF on *F*	1.057	1.037	1.060

[a] $R = \Sigma||F_o| - |F_c||/\Sigma|F_o|$, [b] $wR = [\Sigma(w(F_o^2 - F_c^2)^2)/\Sigma([w(F_o^2)^2]^{1/2}$ where $w = 1/(\sigma^2(F_o^2) + (aP)^2 + bP)$ with $P = (2F_c^2 + \max(F_o^2,0))/3$.

Table S2: Selected bond lengths (Å) and bond angles (°) of the complexes **1·La**, **2′·Y** and **2′′·Y**

Complex **1·La**

La1 O3 2.558(5)	La1 O2 2.566(6)	La1 O5 2.738(6)	La1 N7 2.724(6)
La1 N4 2.746(6)	La1 O1 2.534(6)	La1 O4 2.543(6)	La1 N8 2.814(6)
La1 N3 2.809(6)	La1 N9 2.791(7)	La1 N2 2.774(7)	O1 C17 1.230(12)
O4 C33 1.235(12)	O3 C40 1.231(9)	O2 C10 1.225(9)	N6 N4 1.379(9)
N6 C40 1.348(9)	N5 N7 1.388(9)	N2 N1 1.375(10)	N9 N10 1.381(10)
N10 C33 1.331(13)	N1 C17 1.354(14)	N5 C10 1.351(9)	

O1 La1 N2	58.9(2)	N2 La1 N3	57.6(2)	N7 La1 N3	56.73(19)
O2 La1 N7	58.75(17)	N2 N1 C17	116.7(8)	C10 N5 N7	116.2(6)
O3 La1 N4	58.99(16)	N7 La1 N8	56.97(17)	N9 La1 N8	57.35(19)
O4 La1 N9	58.1(2)	C40 N6 N4	116.1(6)	C33 N10 N9	117.3(7)

Complex **2′·Y**

Y1 O4	2.333(2)	Y1 O3	2.450(2)	Y1 O1	2.411(2)	Y1 O2	2.463(2)
Y1 N8	2.627(3)	Y1 N3	2.636(3)	Y1 N2	2.533(2)	Y1 N4	2.556(2)
Y1 N9	2.477(3)	Y1 N7	2.559(2)	O1 C17	1.240(4)	O4 C33	1.282(4)
O3 C40	1.244(4)	O2 C10	1.242(4)	N6 N7	1.384(3)	N6 C40	1.352(4)
N5 N4	1.388(3)	N2 N1	1.383(4)	N10 N9	1.390(4)	N10 C33	1.323(4)
N1 C17	1.350(4)	N5 C10	1.349(4)				

O1 Y1 N2	62.07(8)	N2 Y1 N3	60.70(8)	N4 Y1 N3	59.91(8)
O2 Y1 N4	61.36(8)	C17 N1 N2	113.4(3)	C10 N5 N4	114.1(3)
O3 Y1 N7	61.03(8)	N7 Y1 N8	59.82(9)	N9 Y1 N8	61.53(9)
O4 Y1 N9	63.14(9)	C40 N6 N7	114.3(3)	C33 N10 N9	108.7(3)

Complex **2″·Y**

Y1 O1	2.375(4)	Y1 O4	2.342(4)	Y1 O3	2.451(4)	Y1 O2	2.436(4)
Y1 N7	2.500(5)	Y1 N8	2.596(5)	Y1 N4	2.537(5)	Y1 N3	2.615(5)
Y1 N2	2.546(5)	Y1 N9	2.554(5)	O1 C17	1.247(7)	O4 C33	1.247(7)
O3 C40	1.231(7)	O2 C10	1.244(7)	N7 N6	1.380(7)	N6 C40	1.355(8)
N4 N5	1.391(7)	N2 N1	1.391(7)	N10 N9	1.388(7)	N10 C33	1.351(8)
N1 C17	1.344(8)	N5 C10	1.342(8)				

O1 Y1 N2	62.32(15)	N2 Y1 N3	60.97(15)	N4 Y1 N3	60.41(15)
O2 Y1 N4	61.21(15)	C17 N1 N2	114.3(5)	C10 N5 N4	114.3(5)
O3 Y1 N7	61.30(15)	N7 Y1 N8	61.70(16)	N9 Y1 N8	61.36(16)
O4 Y1 N9	62.06(16)	C40 N6 N7	113.5(5)	C33 N10 N9	114.0(5)

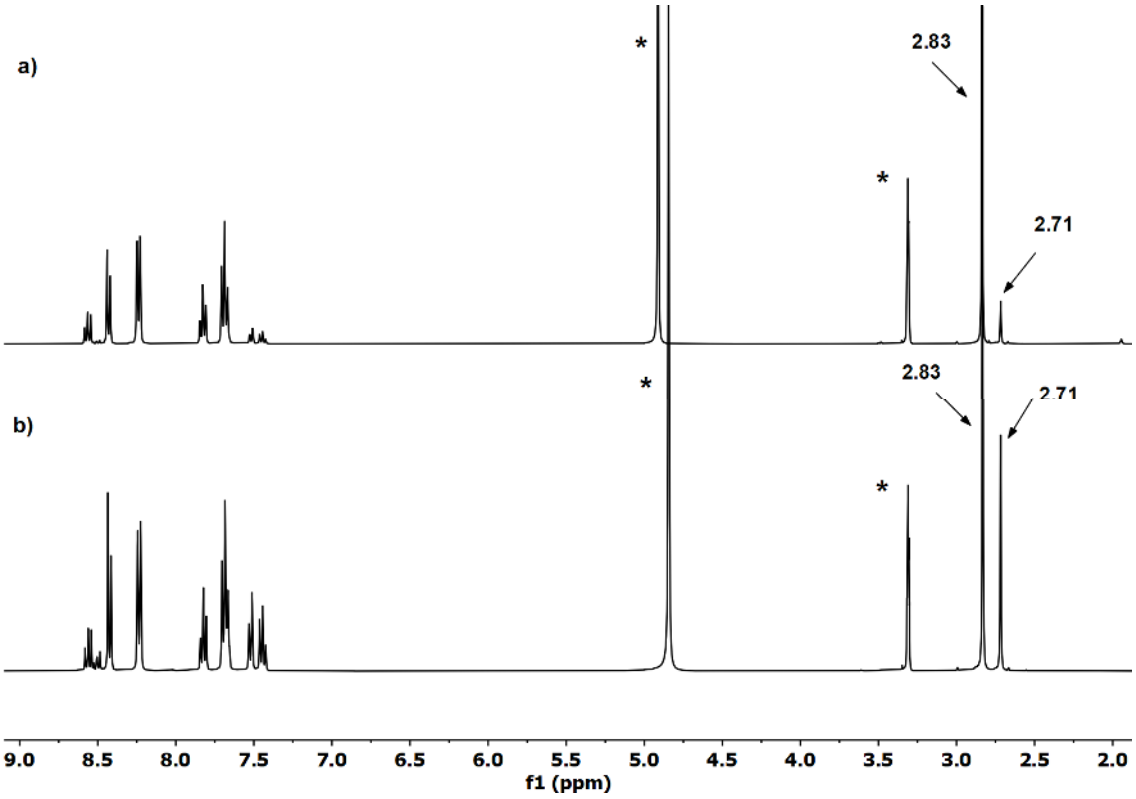

Fig. S6. The comparative solution ^{1}H NMR spectra recorded on the reaction mixtures that were obtained upon treatment of: ***a)*** $Y(OTf)_3 \cdot xH_2O$ with $\mathbf{H_2L^1}$ in 1 : 1 molar ratio in the absence of base under Ar atmosphere; ***b)*** $Y(OTf)_3$ with $\mathbf{H_2L^1}$ in 1 : 1 molar ratio in the absence of base under open atmospheric conditions followed by the treatment of the reaction mixture with excess of CO_2 gas. All the reactions were carried out in CD_3OD medium at room temperature. The signals corresponding to the residual solvent / grease are indicated by asterisks. The characteristic signals corresponding to the CH_3 moieties of the imine functionality of the ligand ($\delta_{CH_3}(imine, \text{ppm})$) in the products of the reactions are labelled with their chemical shift values. $\delta_{CH_3}(imine, \text{ppm})$ = 2.71 and 2.83 correspond to the products **2′·Y** and **2"·Y**, respectively.

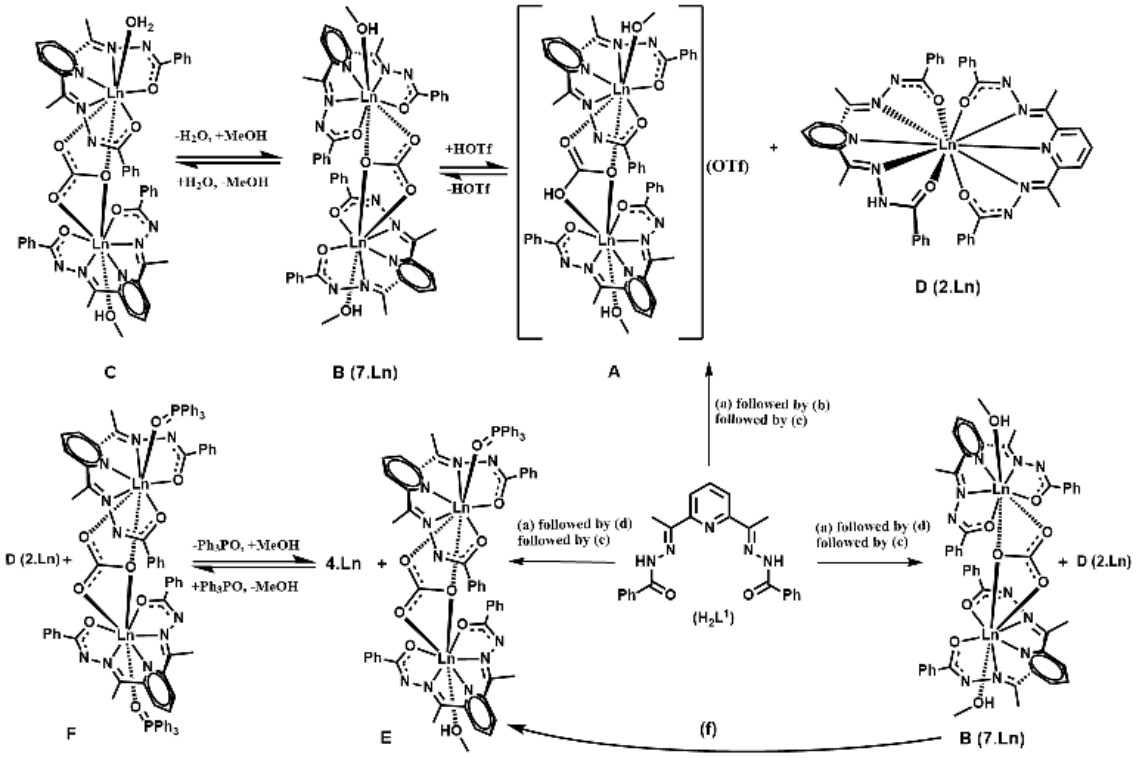

Scheme S3: Schematic illustration for the formation of various CO_3^{2-}-bridged dinuclear complexes (**A**-**C** and **E**-**F**) and the mononuclear decacoordinate complexes (**D**) under different reaction conditions.[8] The general reaction conditions are as follows: (a) H_2L^1 and $Y(OTf)_3 \cdot 6H_2O$ mixed in a 1:1 molar ratio in aqueous methanol, stirred for 5 minutes at room temperature; (b) addition of Et_3N (2 equivalents relative to H_2L^1) in situ, stirred for 5 minutes at room temperature; (c) purging with CO_2 gas, stirred for 5–10 minutes at room temperature; (d) addition of Et_3N (3 equivalents relative to H_2L^1) in situ, stirred for 5 minutes at room temperature; (e) addition of Ph_3PO in situ at room temperature; and (f) addition of Ph_3PO to the methanolic solutions of the isolated complexes **B** at room temperature. Ln = Y for **A** and **C**; Ln = Y and Er for **B** and **D**–**F**. The complexes **B** and **D** will be referred as **7·Ln** and **2·Ln**, respectively, here onwards in the current report.

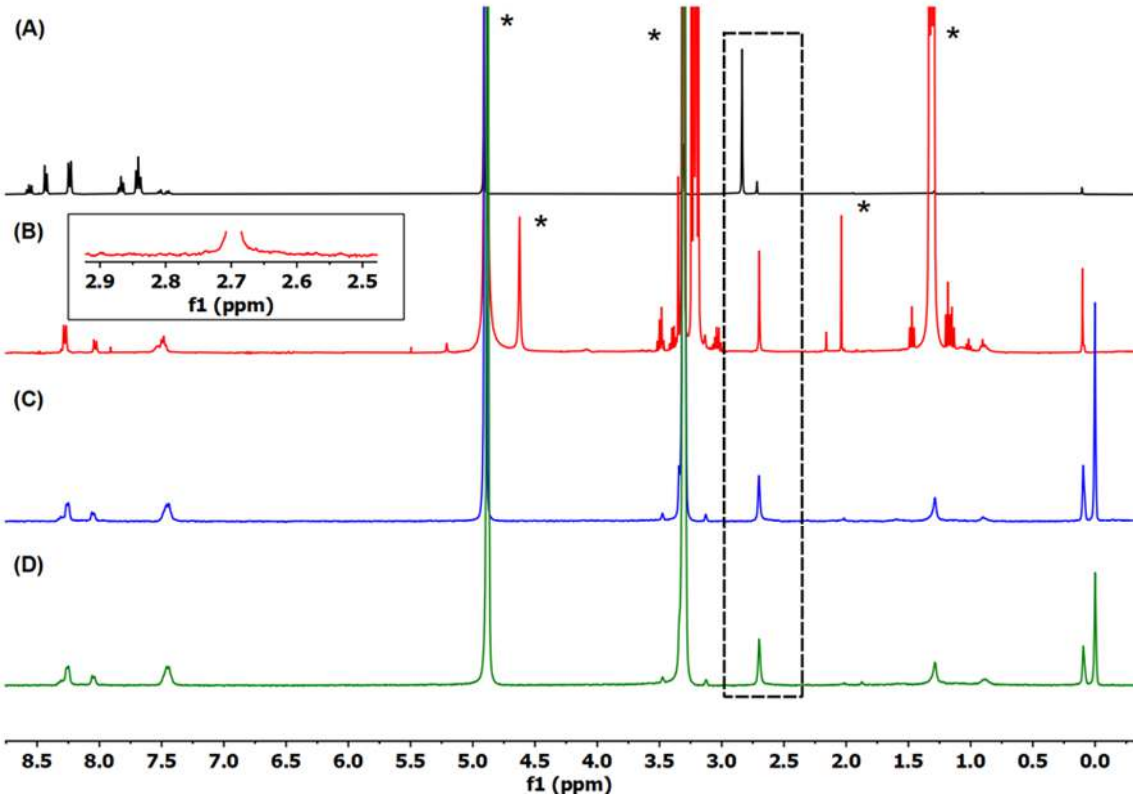

Fig. S7 The comparative solution ^{1}H NMR spectra of: **(A)** the reaction mixture before the addition of base; **(B)** the reaction mixture after addition of six equivalents of base (Et_3N) during the syntheses of **3·Y**; **(C)** the CD_3OD solution of the isolated polycrystalline sample of CP **3·Y**; and **(D)** the CD_3OD solution of the isolated polycrystalline sample of CP **4·Y**. All the spectra were recorded at room temperature under Ar atmospheres. The signals corresponding to the residual solvents / grease / Et_3N / Et_3NH^+ are indicated by asterisks. The characteristic signals corresponding to the CH_3 moieties of the imine functionality of the ligand in the complexes ($\delta_{CH_3}(imine, \text{ppm})$, see experimental section for details) are highlighted under the dashed-lined rectangle. The ^{1}H NMR spectra of the reaction mixture after addition of base was recorded with 1048 scans whereas the ^{1}H NMR spectra of the CPs were recorded with 512 scans and the reaction NMR of reaction mixture before addition of base was recorded with 16 scans. ***Inset:*** the inset is a zoomed-in section between 2.9 ppm – 2.5 ppm of the spectrum corresponding to the reaction mixture after addition of six equivalents of Et_3N, which confirmed the complete absence of the products of the reaction mixture before addition of any base.

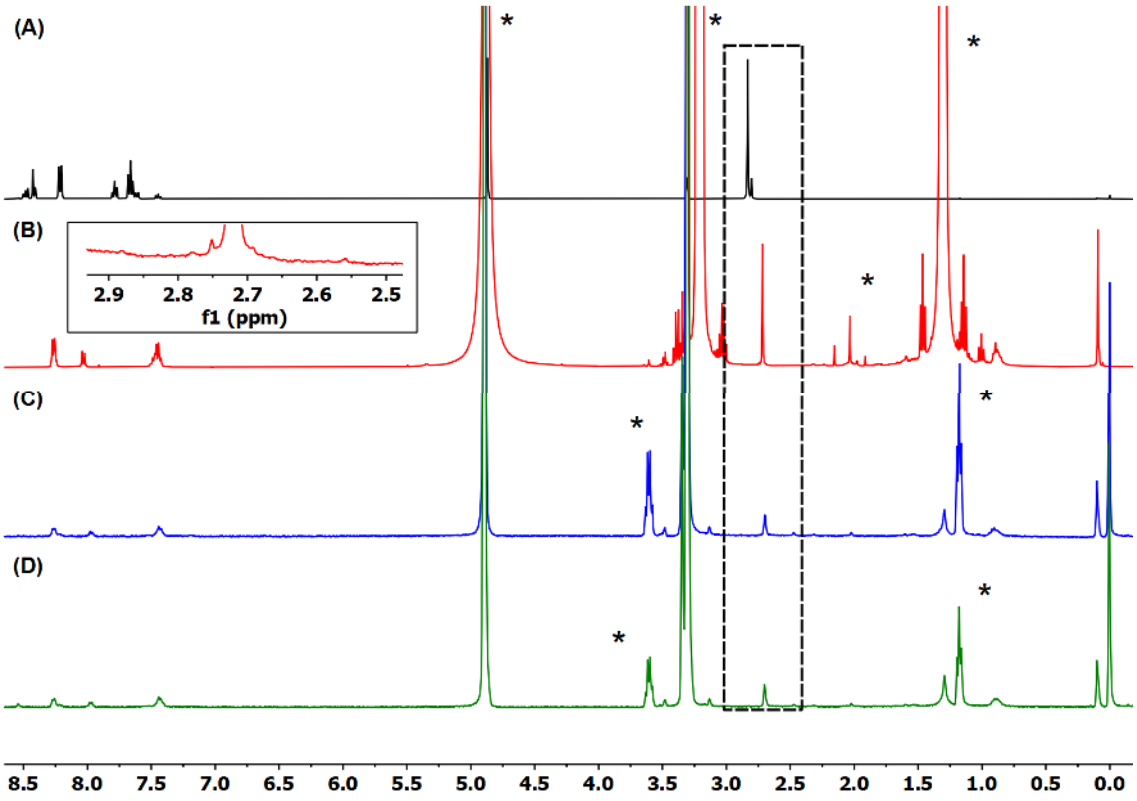

Fig. S8 The comparative solution ^{1}H NMR spectra of: **(A)** the reaction mixture before the addition of base; **(B)** the reaction mixture after addition of six equivalents of base (Et_3N) during the syntheses of **3·La**, **(C)** the CD_3OD solution of the isolated polycrystalline sample of CP **3·La**; and **(D)** the CD_3OD solution of the isolated polycrystalline sample of CP **4·La**. All the spectra were recorded at room temperature under Ar atmosphere. The signals corresponding to the residual solvents / grease / Et_3N / Et_3NH^+ are indicated by asterisks. The characteristic signals corresponding to the CH_3 moieties of the imine functionality of the ligand in the complexes ($\delta_{CH_3}(imine$, ppm), see experimental section for details) are highlighted under the dashed-lined rectangle. The ^{1}H NMR spectra of the reaction mixture after addition of base were recorded with 1048 scans whereas the ^{1}H NMR spectra of the CPs were recorded with 512 scans and the reaction NMR of reaction mixture before addition of base was recorded with 16 scans. ***Inset:*** the inset is a zoomed-in section between 2.9 ppm – 2.5 ppm of the spectrum corresponding to the reaction mixture after addition of six equivalents of Et_3N, which confirmed the complete absence of the products of the reaction mixture before addition of any base.

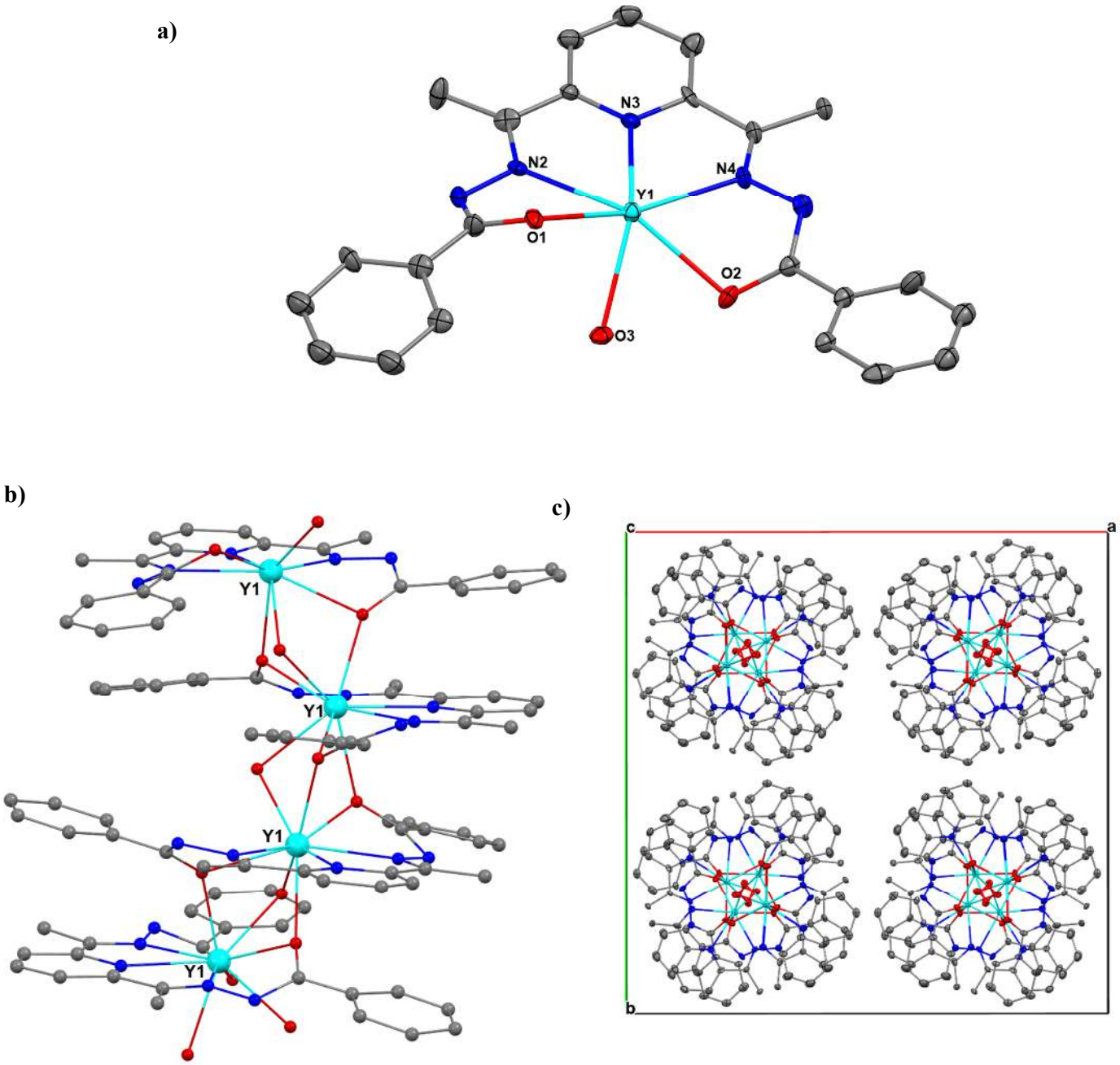

Fig. S9. Solid-state single crystal X-ray structures of **3·Y** (a) ORTEP representations with 40% ellipsoid probability for the asymmetric unit of the Δ-isomer, (b) polymeric growth along the crystallographic *c* axis up to the one-unit cell length for the Δ-isomer, and c) unit cell packing for both the Δ- and Λ-isomers. The H atoms and the co-crystallized solvent molecules are omitted for clarity. Color codes: cyan, Y; red, O; blue, N; and grey, C.

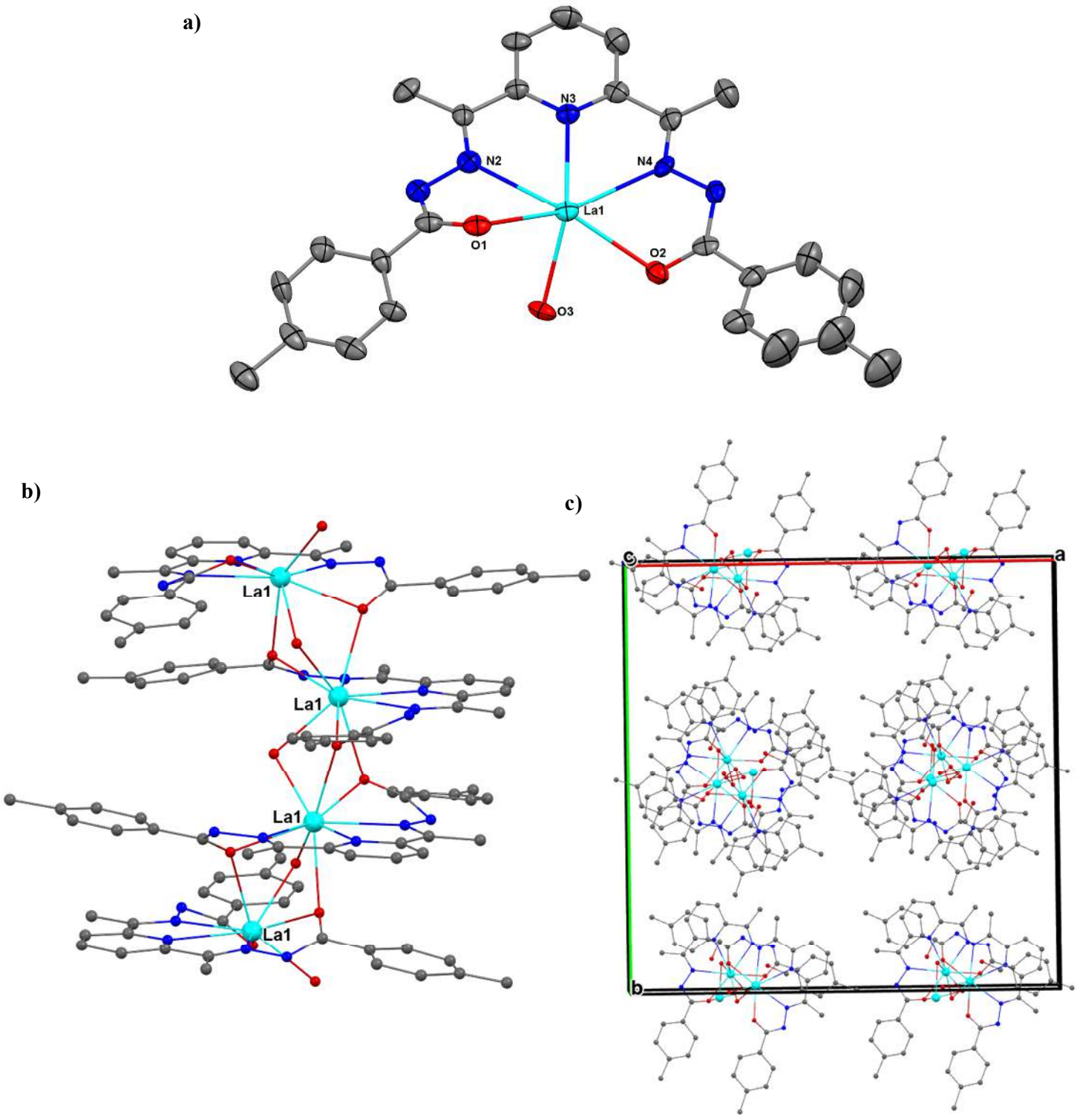

Fig. S10. Solid-state single crystal X-ray structures of **5·La** (a) ORTEP representations with 40% ellipsoid probability for the asymmetric unit of the Δ-isomer, (b) polymeric growth along the crystallographic *c* axis up to the one-unit cell length for the Δ-isomer, and c) unit cell packing for both the Δ- and Λ-isomers. The H atoms and the co-crystallized solvent molecules are omitted for clarity. Color codes: cyan, La; red, O; blue, N; and grey, C.

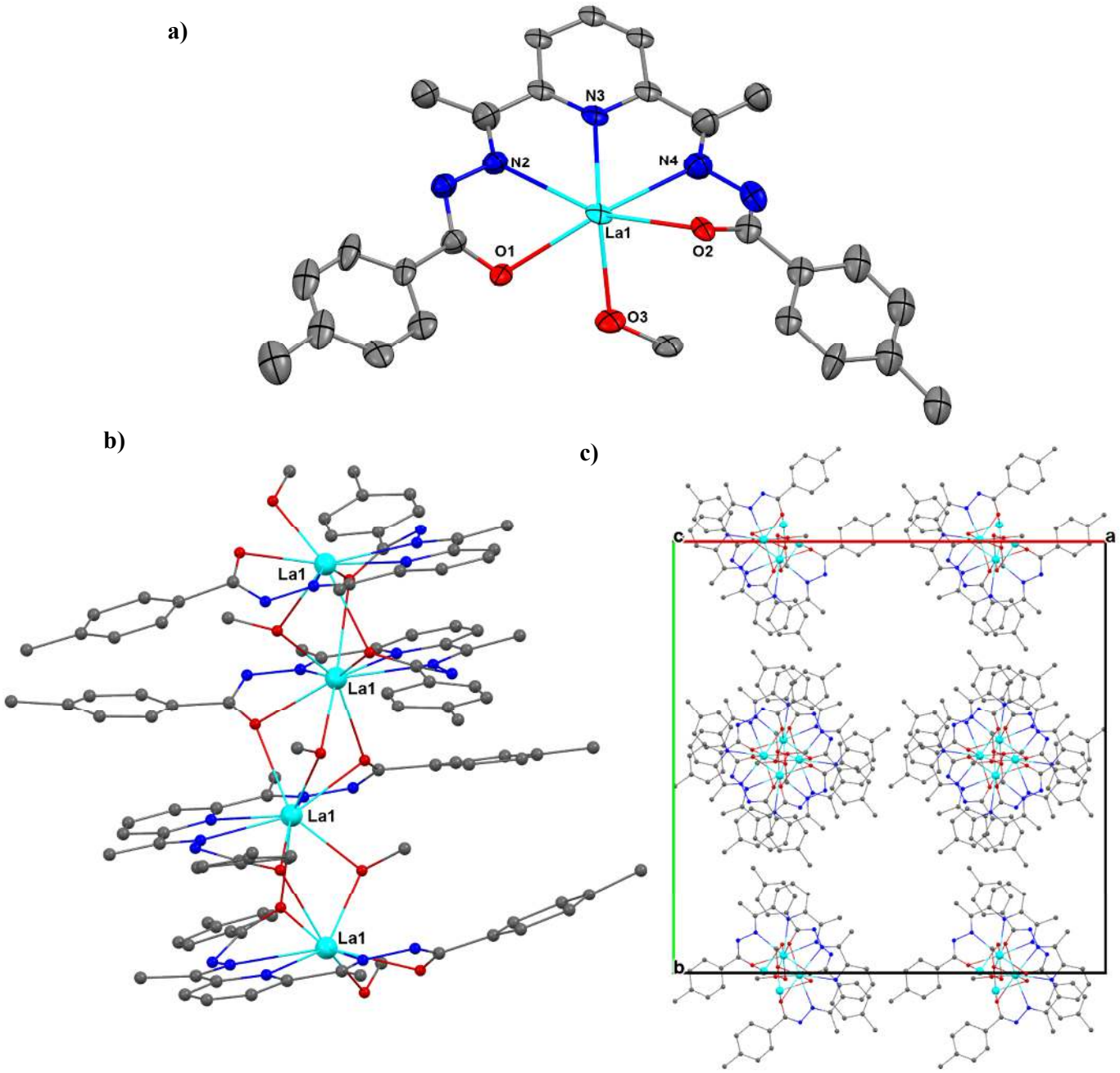

Fig. S11. Solid-state single crystal X-ray structures of **6·La** (a) ORTEP representations with 40% ellipsoid probability for the asymmetric unit of the Δ-isomer, (b) polymeric growth along the crystallographic *c* axis up to the one-unit cell length for the Δ-isomer, and c) unit cell packing for both the Δ- and Λ-isomers. The H atoms and the co-crystallized solvent molecules are omitted for clarity. Color codes: cyan, La; red, O; blue, N; and grey, C.

Table S3. Selected crystallographic data and refinement parameters for **3·Y, 3·La**, **4·La, 5·La and 6·La**

	3·Y	**3·La**	**4·La**
Formula*	$C_{24}H_{28}N_5O_6Y$	$C_{24.5}H_{26}N_5O_{4.5}La$	$C_{26.34}H_{31.37}N_5O_{5.34}La$
Mr (g mol^{-1})*	571.42	601.41	642.36
crystal system	Tetragonal	Tetragonal	Tetragonal
space group	$I4_1cd$	$I4_1/a$	$I4_1/a$
T (K)	150	100	100
a (Å)	28.203(4)	28.803(3)	29.1452(19)
b (Å)	28.203(4)	28.803(3)	29.1452(19)
c (Å)	12.5662(19)	13.3477(19)	13.6547(7)
α (°)	90	90	90
β (°)	90	90	90
γ (°)	90	90	90
V (Å^3)	9995(3)	11073(3)	11598.9(17)
Z	16	16	16
$\rho_{calcd.}$ (g cm^{-3})	1.519	1.443	1.471
μ (mm^{-1})	2.383	1.581	1.517
collected reflns	36396	35596	73476
unique reflns	4413	4892	5207
No. of parameters	320	296	352
Reflns for Refinement	36396	35596	73476
R (I > 3σ(I))[a]	0.0584	0.0837	0.0687
wR (I > 3σ(I))[b]	0.1576	0.2439	0.1840
GOF on *F*	1.048	1.036	1.122

	5·La	**6·La**
Formula*	$C_{26}H_{30}N_5O_5La$	$C_{29}H_{38}N_5O_6La$
Mr (g mol^{-1})*	631.46	691.55
crystal system	Tetragonal	Tetragonal
space group	$I4_1/a$	$I4_1/a$
T (K)	100	100
a (Å)	29.6675(16)	31.8689(16)
b (Å)	29.6675(16)	31.8689(16)
c (Å)	13.3788(10)	13.5485(8)
α (°)	90	90
β (°)	90	90
γ (°)	90	90
V (Å^3)	11775.5(15)	13760.2(16)
Z	16	16
$\rho_{calcd.}$ (g cm^{-3})	1.425	1.335
μ (mm^{-1})	1.492	1.285
collected reflns	63673	47046
unique reflns	5198	6106
No. of parameters	313	322
Reflns for Refinement	63673	47046
R (I > 3σ(I))[a]	0.0995	0.1013
wR (I > 3σ(I))[b]	0.2618	0.2508

GOF on F	1.114	1.100

[a] $R = \Sigma||F_o| - |F_c||/\Sigma|F_o|$, [b] $wR = [\Sigma(w(F_o^2 - F_c^2)^2)/\Sigma([w(F_o^2)^2]^{1/2}$ where $w = 1/(\sigma^2(F_o^2) + (aP)^2 + bP)$ with $P = (2F_c^2 + \max(F_o^2,0))/3$.
*Including the squeezed-out solvents

Table S4. Selected bond lengths (Å) and bond angles (°) of the complexes **3·Y, 3·La, 4·La, 5·La and 6·La**

Complex **3·Y**

Y1 Y1[1] 3.6783(9)	Y1 Y1[2] 3.6783(9)	Y1 O1[3] 2.412(7)	Y1 O3 2.385(8)
Y1 O3[2] 2.433(7)	Y1 N4[2] 2.485(8)	Y1 N3[2] 2.573(8)	Y1 O2[2] 2.466(8)
Y1 O2 2.368(8)	Y1 N2[2] 2.481(9)	O1 C17 1.266(14)	N4 N5 1.397(13)
N2 N1 1.409(13)	N1 C17 1.348(16)	N5 C10 1.290(14)	O2 C10 1.317(14)
Y1 O1[2] 2.461(8)			

[1]1-Y,1/2+X,1/4+Z; [2]-1/2+Y,1-X,-1/4+Z; [3]1/2-X,3/2-Y,-1/2+Z

Y1[1] Y1 Y1[2]	136.84(3)	Y1[4] O1 Y1[2]	98.0(3)	O1[3] Y1 Y1[2]	41.5(2)
C17 O1 Y1[1]	113.9(7)	O1[3] Y1 Y1[1]	160.2(2)	C17 O1 Y1[4]	133.2(8)
O1[2] Y1 Y1[1]	40.50(17)	Y1 O3 Y1[1]	99.5(3)	O1[2] Y1 Y1[2]	113.56(18)
N5 N4 Y1[1]	115.5(6)	O1[3] Y1 O1[2]	119.8(3)	C8 N4 Y1[1]	127.4(7)
O1[3] Y1 O3[2]	65.1(3)	C8 N4 N5	117.0(8)	O1[3] Y1 N4[2]	81.7(3)
C3 N3 Y1[1]	120.3(7)	O1[2] Y1 N4[2]	158.3(3)	C7 N3 Y1[1]	120.3(7)
O1[2] Y1 N3[2]	119.0(3)	C7 N3 C3	118.6(9)	O1[3] Y1 N3[2]	74.1(3)
Y1 O2 Y1[1]	99.1(3)	O1[3] Y1 O2[2]	74.6(3)	C10 O2 Y1[1]	111.7(7)
O1[2]Y1 O2[2]	122.4(3)	C10 O2 Y1	134.6(7)	O1[2] Y1 N2[2]	61.7(3)
O1[3] Y1 N2[2]	83.4(3)	C2 N2 Y1[1]	126.8(7)	O3 Y1 Y1[2]	102.79(18)
O3 Y1 Y1[1]	39.74(19)	C17 N1 N2	107.6(9)	O3[2] Y1 Y1[2]	39.74(19)
C10 N5 N4	111.6(9)	O3[2] Y1 Y1[1]	102.77(18)	O3[2] Y1 O1[2]	73.9(3)
O3 Y1 O1[3]	144.2(3)	O3 Y1 O1[2]	65.1(3)	O3 Y1 O3[2]	84.98(12)
O3[2] Y1 N4[2]	121.7(3)	O3 Y1 N4[2]	99.3(3)	O3[2] Y1 N3[2]	137.2(3)
O3 Y1 N3[2]	137.8(3)	O3[2] Y1 O2[2]	63.1(3)	O3 Y1 O2[2]	74.4(3)
O3 Y1 N2[2]	122.6(3)	O3[2] Y1 N2[2]	99.6(3)	N4[2] Y1 Y1[1]	117.9(2)
N4[2] Y1 Y1[2]	83.7(2)	N4[2] Y1 N3[2]	61.6(3)	N4[2] Y1 N2[2]	123.6(3)
N3[2] Y1 Y1[2]	111.1(2)	N3[2] Y1 Y1[1]	112.0(2)	O2[2] Y1 Y1[2]	39.5(2)
O2[2] Y1 Y1[1]	115.11(19)	O2 Y1 Y1[2]	161.4(2)	O2 Y1 Y1[1]	41.5(2)
O2 Y1 O1[3]	149.3(2)	O2 Y1 O1[2]	75.5(3)	O2 Y1 O3[2]	144.1(3)
O2 Y1 O3	65.3(3)	O2[2] Y1 N4[2]	62.5(3)	O2 Y1 N4[2]	84.4(3)
O2 Y1 N3[2]	75.1(3)	O2[2] Y1 N3[2]	118.5(3)	O2 Y1 O2[2]	122.0(3)
O2 Y1 N2[2]	81.7(3)	O2[2] Y1 N2[2]	156.2(3)	N2[2] Y1 Y1[2]	116.8(2)
N2[2] Y1 Y1[1]	83.5(2)	N2[2].Y1 N3[2]	62.0(3)		

[1]1-Y,1/2+X,1/4+Z; [2]-1/2+Y,1-X,-1/4+Z; [3]1/2-X,3/2-Y,-1/2+Z; [4]1/2-X,3/2-Y,1/2+Z

Complex **3·La**

La1	La1[1]	3.8191(6)	La1	La1[2]	3.8192(6)	La1	O2	2.571(8)	La1	O2[1]	2.585(10)
La1	O1	2.571(9)	La1	O1[2]	2.591(9)	La1	N2	2.643(10)	La1	N4	2.619(11)
La1	O3[1]	2.418(8)	La1	O3	2.460(9)	La1	N3	2.730(11)	O2	C10	1.279(15)
O1	C17	1.295(15)	N2	N1	1.430(14)	N4	N5	1.412(14)	N5	C10	1.334(16)
N1	C17	1.286(17)									

[1]3/4-Y,1/4+X,1/4+Z; [2]-1/4+Y,3/4-X,-1/4+Z

La1[1] La1 La1[2]	139.767(18)	La1 O2 La1[2]	95.6(3)	O2[1] La1 La1[1]	42.06(17)
C10 O2 La1[2]	135.8(8)	O2 La1 La1[1]	116.1(2)	C10 O2 La1	114.1(8)
O2 La1 La1[2]	42.3(2)	La1 O1 La1[1]	95.4(3)	O2[1] La1 La1[2]	164.02(18)
C17 O1 La1[1]	135.9(8)	O2 La1 O2[1]	122.0(3)	C17 O1 La1	114.2(8)
O2 La1 O1[2]	74.2(3)	N1 N2 La1	116.0(7)	O2[1] La1 O1[2]	142.0(3)
C2 N2 La1	127.2(8)	O2 La1 N2	160.0(3)	O2[1] La1 N2	75.8(3)
N5 N4 La1	117.6(7)	O2 La1 N4	59.5(3)	C8 N4 La1	126.6(9)
O2[1] La1 N4	84.4(3)	O2[1] La1 N3	70.7(3)	C10 N5 N4	109.0(10)
O2 La1 N3	115.3(3)	C17 N1 N2	110.2(10)	O1[2] La1 La1[2]	42.08(19)
La1[2] O3 La1	103.0(3)	O1[2] La1 La1[1]	166.04(19)	C7 N3 La1	119.5(8)
O1 La1 La1[1]	42.5(2)	C3 N3 La1	121.0(9)	O1 La1 La1[2]	117.5(2)
C3 N3 C7	119.4(11)	O1 La1 O2	130.7(3)	O1 La1 O2[1]	74.3(3)
O1 La1 O1[2]	123.8(3)	O1[2] La1 N2	86.1(3)	O1 La1 N2	59.1(3)
O1[2] La1 N4	75.5(3)	O1 La1 N4	158.5(3)	O1 La1 N3	114.0(3)
O1[2] La1 N3	71.4(3)	N2 La1 La1[1]	82.9(2)	N2 La1 La1[2]	119.0(3)
N2 La1 N3	59.1(3)	N4 La1 La1[2]	82.9(2)	N4 La1 La1[1]	117.5(2)
N4 La1 N2	118.5(3)	N4 La1 N3	59.5(3)	O3[1] La1 La1[1]	39.0(2)
O3[1] La1 La1[2]	106.9(2)	O3 La1 La1[1]	107.4(2)	O3 La1 La1[2]	38.08(19)
O3[1] La1 O2	77.4(3)	O3 La1 O2[1]	149.4(3)	O3[1] La1 O2[1]	66.0(3)
O3 La1 O2	65.7(3)	O3[1] La1 O1[2]	148.8(3)	O3 La1 O1	79.7(3)
O3 La1 O1[2]	65.7(3)	O3[1] La1 O1	68.0(3)	O3 La1 N2	104.2(3)
O3[1] La1 N2	121.0(3)	O3 La1 N4	119.7(3)	O3[1] La1 N4	100.8(3)
O3[1] La1 O3	89.66(15)	O3[1] La1 N3	134.1(4)	O3 La1 N3	136.2(4)
N3 La1 La1[1]	109.6(2)	N3 La1 La1[2]	110.6(2)		

[1]3/4-Y,1/4+X,1/4+Z; [2]-1/4+Y,3/4-X,-1/4+Z

Complex **4·La**

La1	La1[1]	3.8901(4)	La1	La1[2]	3.8901(4)	La1	O1	2.610(6)	La1	O1[1]	2.642(7)
La1	O2	2.605(6)	La1	O2[2]	2.661(6)	La1	O3	2.433(6)	La1	O3[1]	2.418(7)

La1	N3	2.749(8)	La1	N2	2.651(9)	La1	N4	2.679(8)	O1	C17	1.314(12)
O2	C10	1.284(12)	O3	C24B	1.46(2)	O3	C24A	1.42(3)	N2	N1	1.409(12)
N4	N5	1.397(12)	N1	C17	1.310(13)	N5	C10	1.309(13)			

[1]5/4-Y,-1/4+X,-1/4+Z; [2]1/4+Y,5/4-X,1/4+Z

La1[1] La1 La1[2]	140.360(13)	C17 O1 La1[1]	135.3(6)	O1 La1 La1[2]	42.52(14)
La1 O2 La1[2]	95.2(2)	O1[2] La1 La1[1]	165.54(14)	C10 O2 La1	116.5(6)
O1 La1 La1[2]	117.37(14)	C10 O2 La1[2]	133.7(6)	O1[2] La1 La1[2]	41.90(14)
La1[1] O3 La1	106.6(2)	O1 La1 O1[2]	123.41(19)	C24B O3 La1	121.6(9)
O1 La1 O2	132.5(2)	C24B O3 La1[1]	116.0(9)	O1 La1 O2[1]	73.25(19)
C24A O3 La1[1]	120.7(12)	O1[2] La1 O2[1]	141.21(19)	C24A O3 La1	116.6(11)
O1[2] La1 N3	70.3(2)	C3 N3 La1	119.9(6)	O1 La1 N3	114.6(2)
C7 N3 La1	121.3(7)	O1[2] La1 N2	85.0(2)	C7 N3 C3	118.8(9)
O1 La1 N2	59.2(2)	N1 N2 La1	116.8(6)	O1 La1 N4	158.4(2)
C2 N2 La1	126.8(7)	O1[2] La1 N4	75.5(2)	O2[1] La1 La1[2]	166.25(14)
O2[1] La1 La1[1]	42.94(14)	N5 N4 La1	115.4(6)	O2 La1 O1[2]	73.64(19)
C8 N4 La1	126.0(7)	O2 La1 La1[1]	117.58(14)	O2 La1 N3	112.9(2)
O2 La1 La1[2]	42.94(14)	C17 N1 N2	111.7(8)	O2[1] La1 N3	70.9(2)
C10 N5 N4	113.1(8)	O2 La1 O2[1]	123.67(18)	O2 La1 N2	158.5(2)
O2 La1 N4	58.7(2)	O3[2] La1 O1	80.8(2)	O3[2] La1 La1[2]	36.81(14)
O3 La1 La1[2]	36.81(14)	O3[2] La1 La1[1]	109.01(14)	O3 La1 La1[2]	109.65(15)
O3 La1 O1[2]	151.4(2)	O3[2] La1 O1[2]	65.7(2)	O3 La1 O1	66.1(2)
O3[2] La1 O2	66.4(2)	O3 La1 O2	81.2(2)	O3[2] La1 O2[1]	150.7(2)
O3 La1 O2[1]	65.3(2)	O3[2] La1 O3	92.05(13)	O3 La1 N3	133.8(2)
O3[2] La1 N3	134.2(2)	O3[2] La1 N2	103.3(2)	O3 La1 N2	119.0(2)
O3[2] La1 N4	119.2(2)	O3 La1 N4	102.9(2)	N3 La1 La1[1]	110.29(17)
N3 La1 La1[2]	109.35(17)	N2 La1 La1[2]	117.64(18)	N2 La1 La1[1]	83.25(18)
N2 La1 O2[1]	74.8(2)	N2 La1 N3	59.7(3)	N2 La1 N4	118.2(3)
N4 La1 La1[1]	117.68(18)	N4 La1 La1[2]	83.45(18)	N4 La1 N3	58.5(2)
La1 O1 La1[1]	95.6(2)	C17 O1 La1	114.3(6)		

[1]1/4+Y,5/4-X,1/4+Z; [2]5/4-Y,-1/4+X,-1/4+Z

Complex **5·La**

La1	La1[1]	3.8205(5)	La1	La1[2]	3.8204(5)	La1	N3	2.728(10)	La1	O2[1]	2.586(9)
La1	O2	2.568(9)	La1	O3[2]	2.438(8)	La1	O3	2.457(9)	La1	N4	2.626(10)
La1	N2	2.651(11)	La1	O1[2]	2.584(9)	O1	C18	1.323(16)	La1	O1	2.556(9)
N4	N5	1.433(15)	N2	N1	1.392(15)	N5	C10	1.316(17)	N1	C18	1.315(17)
O2	C10	1.312(16)									

[1]5/4-Y,-1/4+X,-1/4+Z; [2]1/4+Y,5/4-X, 1/4+Z

La1[1] La1 La1[2] 140.037(18)	C3 N3 La1 120.0(8)	N3 La1 La1[2] 109.4(2)
La1 O2 La1[1] 95.7(3)	N3 La1 La1[1] 110.5(2)	C10 O2 La1[1] 136.1(8)
O2 La1 La1[2] 118.1(2)	C10 O2 La1 113.5(8)	O2 La1 La1[2] 42.0(2)
La1[1] O3 La1 102.6(3)	O2[2] La1 La1[2] 42.0(2)	N5 N4 La1 117.0(7)
O2[2] La1 La1[1] 166.62(19)	C8 N4 La1 127.0(8)	O2[2] La1 N3 70.6(3)
C8 N4 N5 115.6(10)	O2 La1 N3 115.5(3)	N1 N2 La1 117.7(7)
O2 La1 O2[2] 124.6(3)	C2 N2 La1 126.2(8)	O2 La1 N4 59.7(3)
C2 N2 N1 115.9(11)	O2[2] La1 N4 85.6(3)	C10 N5 N4 108.2(10)
O2 La1 N2 158.2(3)	C18 N1 N2 110.5(11)	O2[2] La1 N2 75.5(3)
O3 La1 N2 104.4(3)	O2 La1 O1 129.7(3)	N2 C2 C1 123.4(11)
O2 La1 O1[1] 74.4(3)	O3[2] La1 La1[2] 38.88(19)	O3 La1 La1[2] 105.24(19)
O3 La1 La1[1] 38.53(18)	O3[2] La1 La1[1] 109.64(19)	C20 C19 C18 125.3(14)
O3[2] La1 N3 131.7(3)	O3 La1 N3 138.4(3)	O3 La1 O2[2] 147.2(3)
O3 La1 O2 64.2(3)	O3[2] La1 O2[2] 64.2(3)	O3[2] La1 O2 79.3(3)
O3[2] La1 O3 89.93(13)	La1 O1 La1[2] 96.0(3)	O3 La1 N4 119.9(3)
C18 O1 La1 115.6(8)	O3 La1 N4 119.9(3)	C18 O1 La1[2] 131.3(8)
O3[2] La1 N2 120.7(3)	O3[2] La1 O1 68.9(3)	O3 La1 O1 77.5(3)
O3 La1 O1[1] 68.2(3)	O3[2] La1 O1[1] 151.2(3)	N4 La1 La1[2] 118.6(2)
N4 La1 La1[1] 83.7(2)	N4 La1 N3 60.2(3)	N4 La1 N2 119.7(3)
N2 La1 La1[2] 82.1(2)	N2 La1 La1[1] 117.0(2)	N2 La1 N3 59.5(3)
O1[1] La1 La1[1] 41.72(19)	O1 La1 La1[2] 42.3(2)	O1 La1 La1[1] 115.3(2)
O1[1] La1 La1[2] 162.7(2)	O1[1] La1 N3 71.9(3)	O1 La1 N3 114.8(3)
O1 La1 O2[2] 74.6(3)	O1[1] La1 O2[2] 142.5(3)	O1[1] La1 N4 77.6(3)
O1 La1 N4 159.8(3)	O1 La1 N2 59.3(3)	C15 C14 C17 120.9(15)
O1[1] La1 N2 84.1(3)	O1 La1 O1[1] 120.8(3)	C7 N3 La1 119.6(9)

[1]3/4-Y,1/4+X,1/4+Z; [2]-1/4+Y,3/4-X,-1/4+Z

Complex **6·La**

La1 La1[1] 3.8618(5)	La1 La1[2] 3.8619(5)	La1 O2 2.597(9)	La1 O2[2] 2.615(8)
La1 O1 2.558(9)	La1 O1[1] 2.613(9)	La1 O3 2.414(8)	La1 O3[1] 2.424(9)
La1 N2 2.620(12)	La1 N4 2.654(13)	La1 N3 2.705(11)	O2 C10 1.297(15)
O1 C18 1.308(14)	N2 N1 1.420(17)	N5 N4 1.431(17)	N5 C10 1.320(18)
N1 C18 1.285(18)			

[1]1/4+Y,5/4-X,1/4+Z; [2]5/4-Y,-1/4+X,-1/4+Z

La1[1] La1 La1[2] 140.288(19)	La1 O1 La1[2] 96.6(3)	O2 La1 La1[2] 119.06(18)

C18 O1 La1	114.6(8)	O2[2] La1 La1[2]	42.0(2)	C18 O1 La1[2]	131.7(7)
O2 La1 La1[1]	42.37(17)	La1[2] O3 La1	105.9(3)	O2[2] La1 La1[1]	167.68(19)
C26 O3 La1[2]	117.5(9)	O2 La1 O2[2]	125.6(3)	C26 O3 La1	122.6(10)
O2 La1 O1[1]	73.0(3)	N1 N2 La1	117.2(8)	O2 La1 N2	156.9(3)
C2 N2 La1	126.5(10)	O2[2] La1 N2	74.8(3)	O2[2] La1 N4	86.6(3)
C10 N5 N4	109.6(11)	O2 La1 N4	58.9(3)	C18 N1 N2	108.9(11)
O2[2] La1 N3	70.3(3)	N5 N4 La1	116.7(9)	O2 La1 N3	112.8(3)
C8 N4 La1	129.6(11)	O1[1] La1 La1[2]	163.6(2)	C8 N4 N5	113.4(13)
O1 La1 La1[1]	116.0(2)	O1 La1 La1[2]	42.2(2)	O1[1] La1 La1[1]	41.14(19)
O1 La1 O2[2]	73.6(3)	O1[1] La1 O2[2]	142.0(3)	N2 C2 C3	114.9(13)
O1 La1 O2	131.7(3)	O1 La1 O1[1]	121.7(3)	O1 La1 N2	59.5(3)
O1[1] La1 N2	84.1(3)	O1 La1 N4	159.9(4)	O1[1] La1 N4	76.1(4)
O1 La1 N3	115.5(3)	O1[1] La1 N3	71.9(3)	C11 C17 C16	118.2(14)
O3[1] La1 La1[2]	108.2(2)	O3 La1 La1[2]	37.1(2)	O3[1] La1 La1[1]	36.95(19)
O3 La1 La1[1]	109.8(2)	O3 La1 O2	82.0(3)	O3 La1 O2[2]	65.8(3)
O3[1] La1 O2[2]	150.0(3)	O3[1] La1 O2	66.0(3)	O3 La1 O1	65.9(3)
O3[1] La1 O1[1]	64.9(3)	O3 La1 O1[1]	150.9(3)	O3[1] La1 O1	79.3(3)
O3[1] La1 O3	91.65(2)	O3[1] La1 N2	102.2(3)	O3 La1 N2	119.2(4)
O3[1] La1 N4	119.2(3)	O3 La1 N4	103.7(3)	O3 La1 N3	133.3(3)
O3[1] La1 N3	135.0(3)	N2 La1 La1[2]	83.0(2)	N2 La1 La1[1]	116.4(3)
N2 La1 N4	118.5(4)	N2 La1 N3	60.4(4)	N4 La1 La1[2]	119.2(2)
N4 La1 La1[1]	83.3(3)	N4 La1 N3	58.1(4)	N3 La1 La1[2]	109.8(2)
N3 La1 La1[1]	109.8(2)	La1 O2 La1[1]	95.6(3)	C10 O2 La1[1]	136.4(7)
C10 O2 La1	114.6(8)				

[1]1/4+Y,5/4-X,1/4+Z; [2]5/4-Y,-1/4+X,-1/4+Z

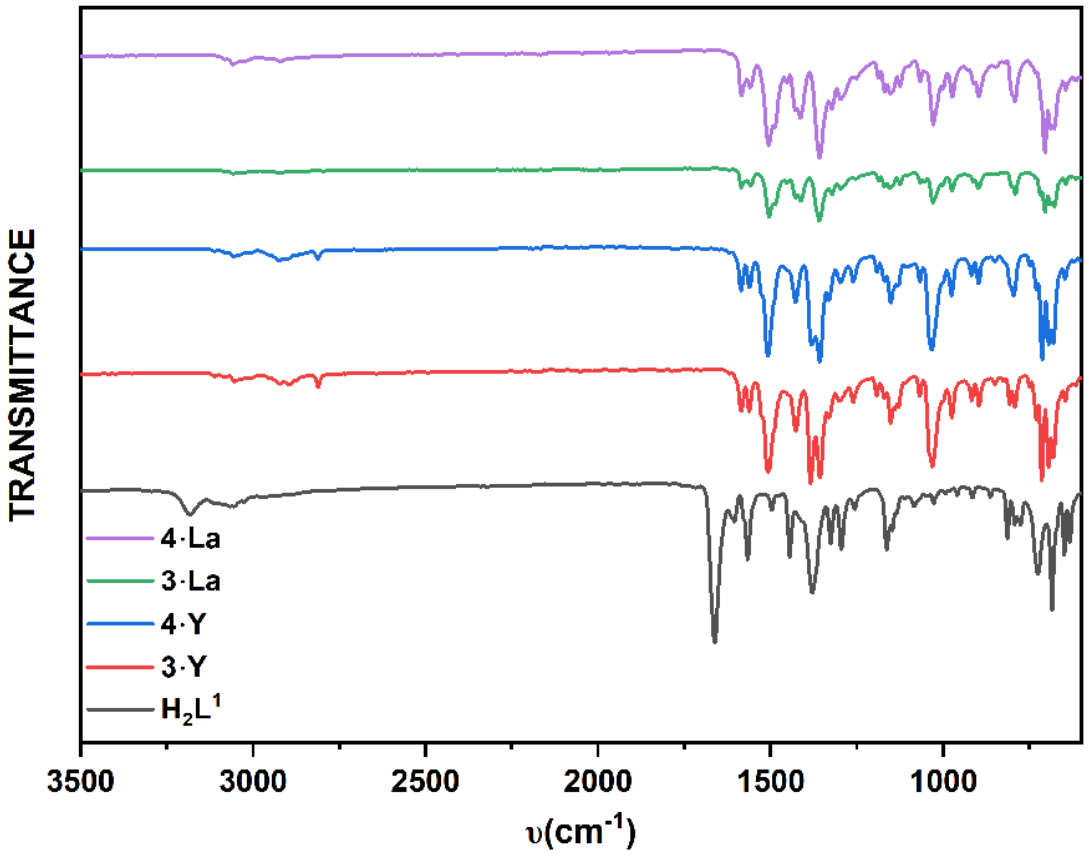

Fig. S12. The comparative FT-IR spectra: the solid-state FT-IR spectra recorded on the *as-synthesized* solid sample of the ligand $\mathbf{H_2L^1}$ (*solid black line*), and the coordination polymers **3·Y** (*solid red line*), **4·Y** (*solid blue line*), **3·La** (*solid green line*) and **4·La** (*solid purple line*). The FT-IR spectrum was recorded under ambient atmospheric conditions for $\mathbf{H_2L^1}$, while the sample manipulation and spectral studies were carried out under Ar atmosphere for all the coordination polymers **3·Ln** - **4·Ln** (Ln = Y and La).

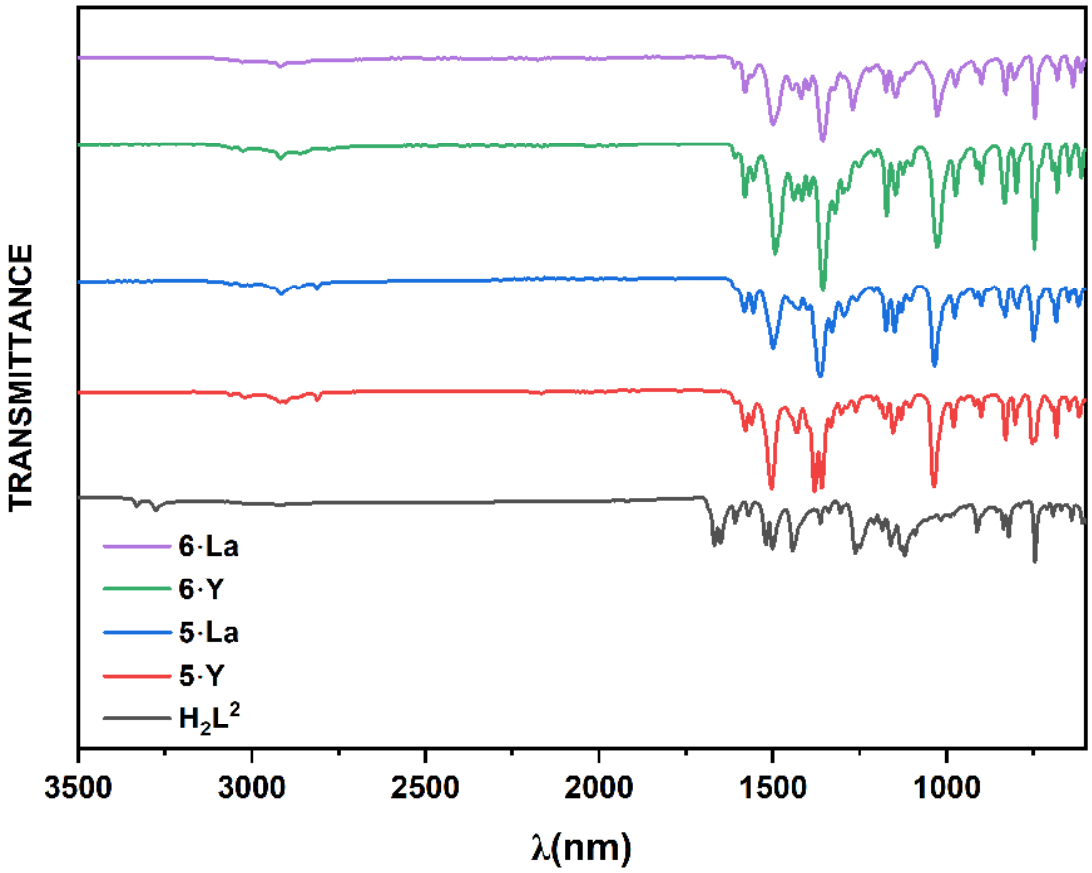

Fig. S13. The comparative FT-IR spectra: the solid-state FT-IR spectra recorded on the *as-synthesized* solid sample of the ligand $\mathbf{H_2L^2}$ (*solid black line*), and the coordination polymers **5·Y** (*solid red line*), **5·La** (*solid blue line*), **6·Y** (*solid green line*) and **6·La** (*solid purple line*). The FT-IR spectrum was recorded under ambient atmospheric conditions for $\mathbf{H_2L^2}$, while the sample manipulation and spectral studies were carried out under Ar atmosphere for all the coordination polymers **5·Ln** - **6·Ln** (Ln = Y and La).

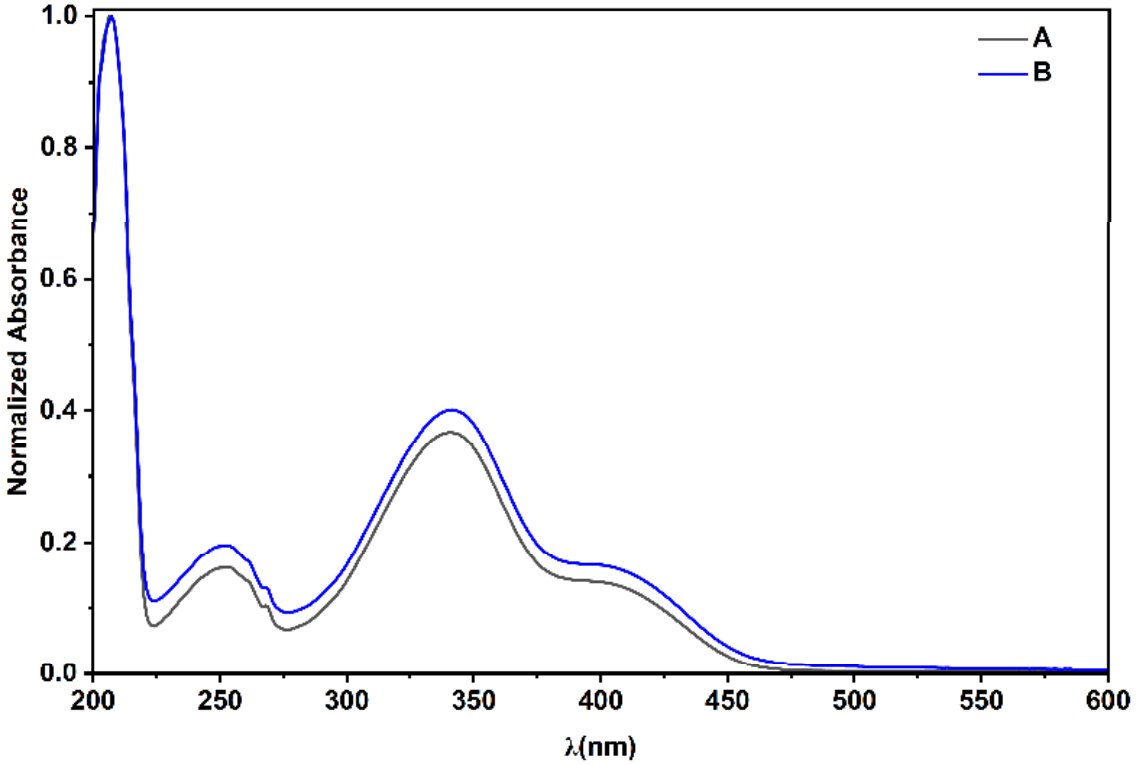

Fig. S14. The normalized comparative UV-vis spectra: ***A, solid black line*** – the UV-vis spectrum recorded on the methanolic solution of the *as-synthesized* solid sample of **3**·**Y**; ***B, solid blue line*** – the UV-vis spectrum recorded on the methanolic solution of the isolated single-crystals of **3**·**Y**. All the sample manipulation and spectral studies were carried out at room temperature under Ar atmospheres.

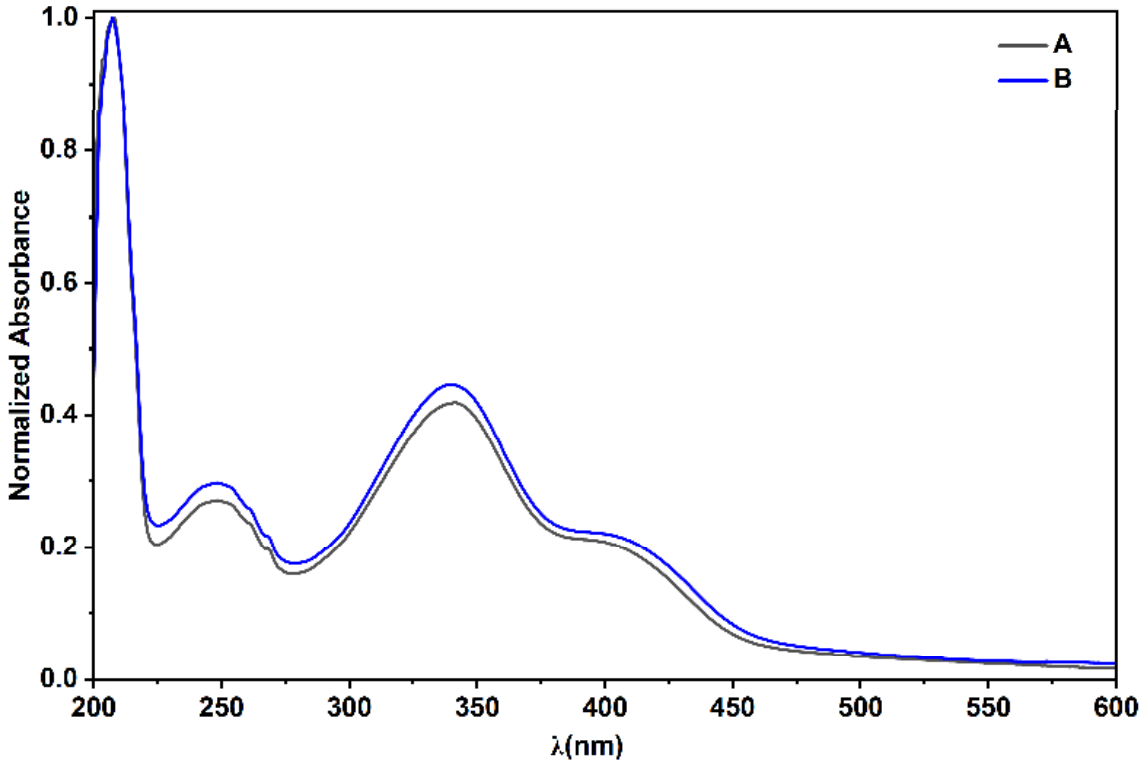

Fig. S15. The normalized comparative UV-vis spectra: ***A, solid black line*** – the UV-vis spectrum recorded on the methanolic solution of the *as-synthesized* solid sample of **4·Y**; ***B, solid blue line*** – the UV-vis spectrum recorded on the methanolic solution of the isolated single-crystals of **4·Y**. All the sample manipulation and spectral studies were carried out at room temperature under Ar atmospheres.

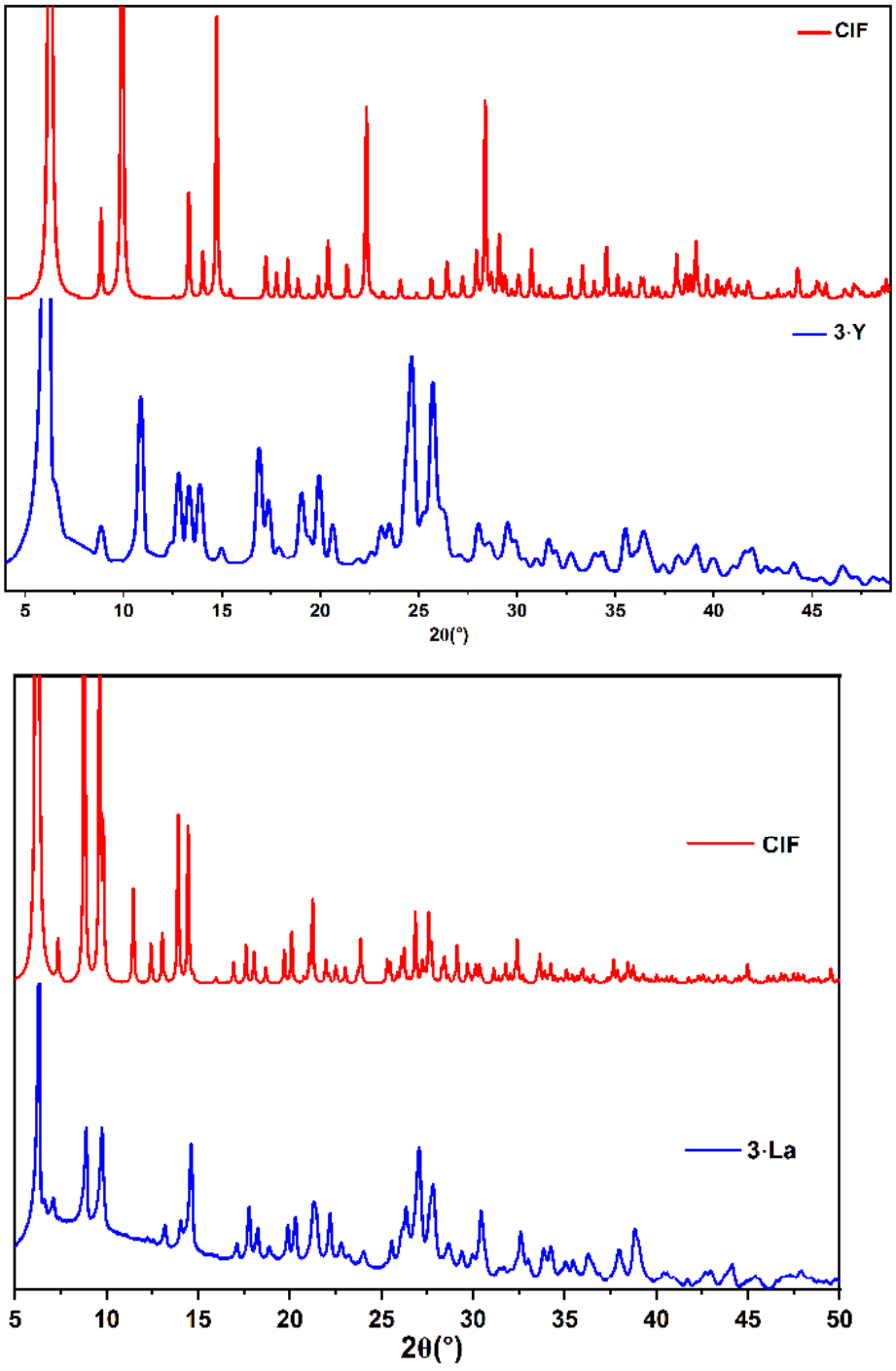

Fig. S16. The powder X-ray diffractograms of the *as-synthesized* solid sample (*solid blue line*) and the simulated pattern of the single-crystal X-ray molecular structure (*solid red line*) of the coordination polymers **3·Y** (*top*) and **3·La** (*bottom*).

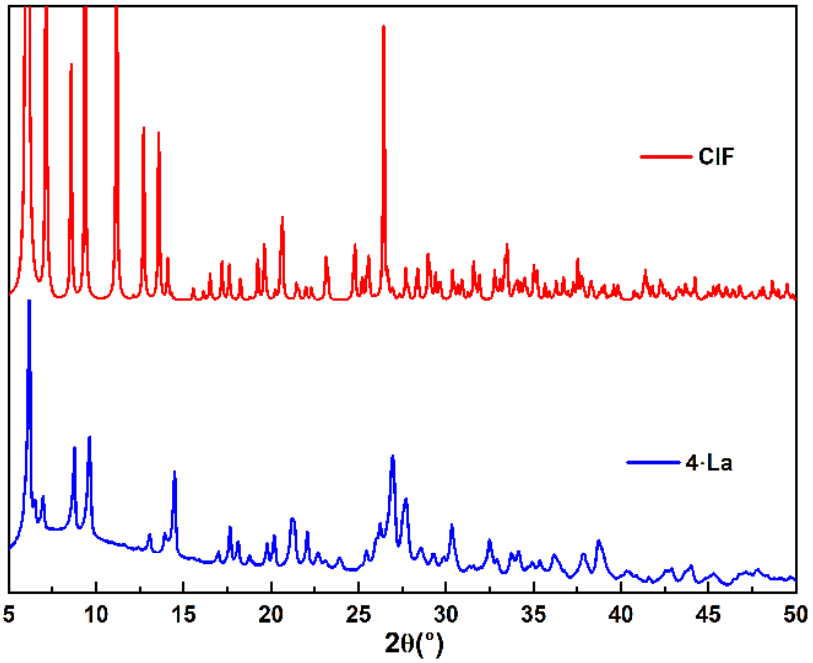

Fig. S17. The powder X-ray diffractograms of the *as-synthesized* solid sample (*solid blue line*) and the simulated pattern of the single-crystal X-ray molecular structure (*solid red line*) of the coordination polymer **4·La**.

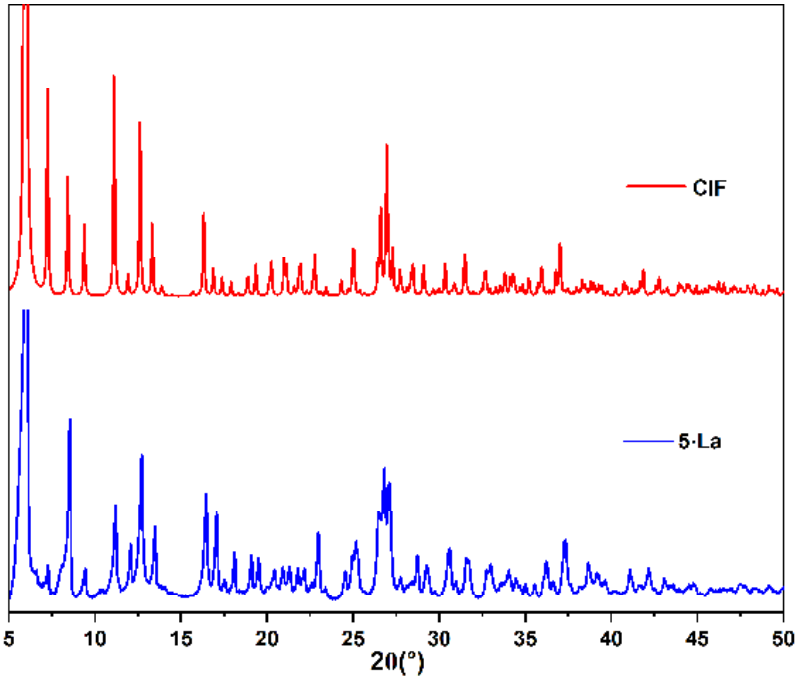

Fig. S18. The powder X-ray diffractograms of the *as-synthesized* solid sample (*solid blue line*) and the simulated pattern of the single-crystal X-ray molecular structure (*solid red line*) of the coordination polymer **5·La**.

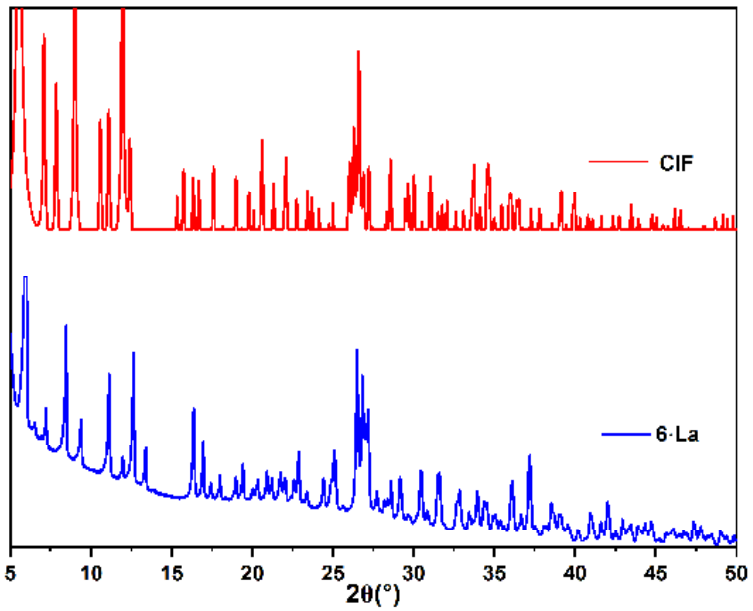

Fig. S19. The powder X-ray diffractograms of the *as-synthesized* solid sample (*solid blue line*) and the simulated pattern of the single-crystal X-ray molecular structure (*solid red line*) of the coordination polymer **6·La**.

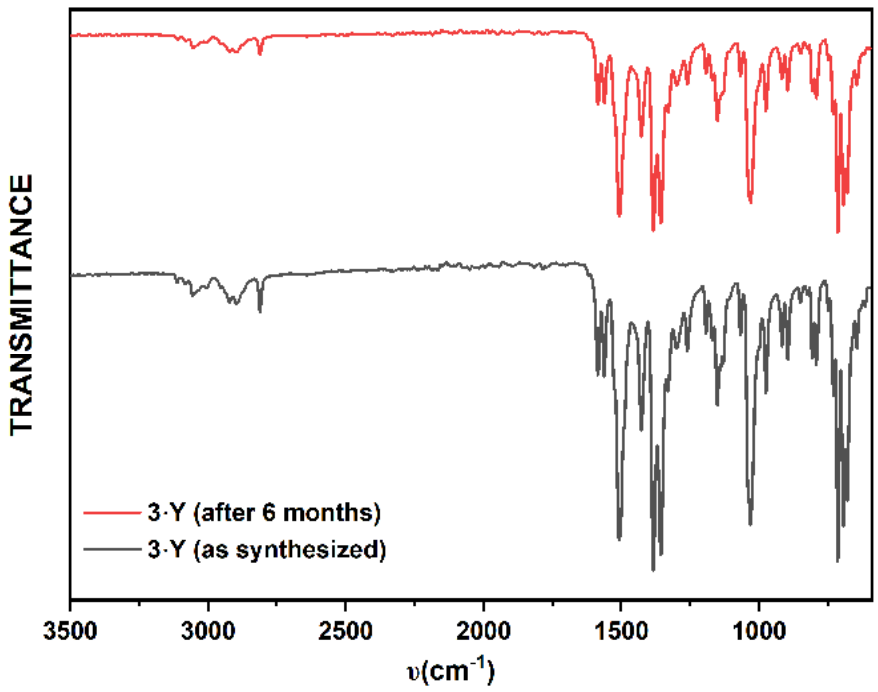

Fig. S20. Comparative FT-IR spectra: ***solid black line*** – the FT-IR spectrum recorded on the freshly synthesized solid sample of the polymer **3·Y**; and ***solid red line*** – the FT-IR spectrum recorded on the solid sample of the polymer **3·Y** after storing it under dry and inert conditions for 6 months.

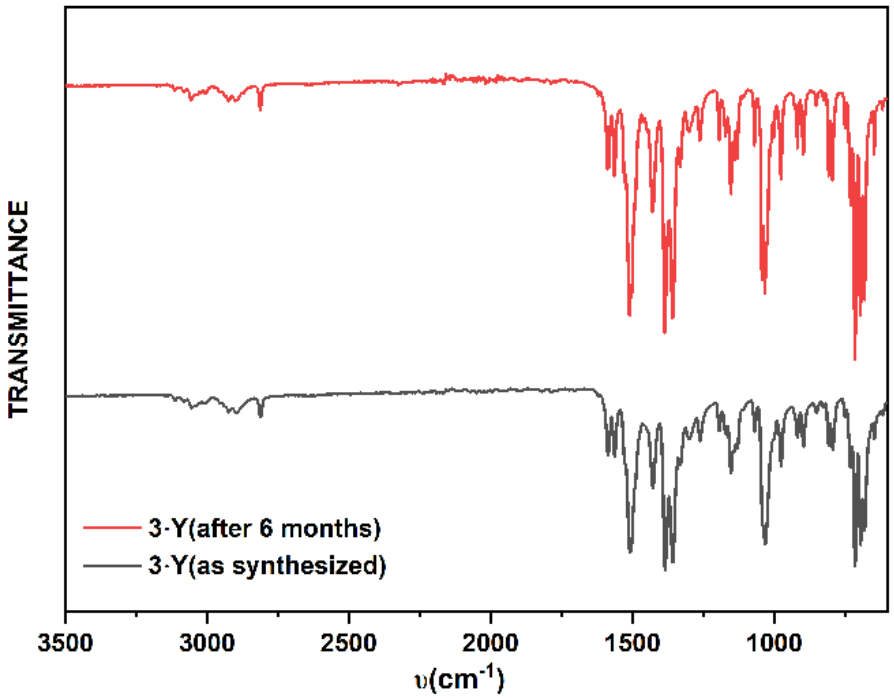

Fig. S21. Comparative FT-IR spectra: ***solid black line*** – the FT-IR spectrum recorded on the freshly synthesized solid sample of the polymer **3·Y**; and ***solid red line*** – the FT-IR spectrum recorded on the solid sample of the polymer **3·Y** after storing it under dry environment of CO_2 and O_2 for 6 months.

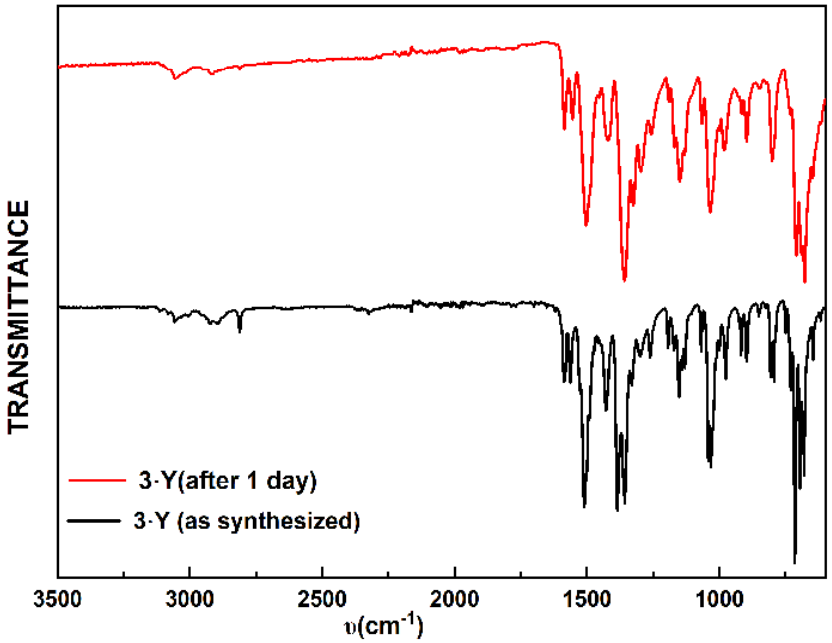

Fig. S22. Comparative FT-IR spectra: ***solid black line*** – the FT-IR spectrum recorded on the freshly synthesized solid sample of the polymer **3·Y**; and ***solid red line*** – the FT-IR spectrum recorded on the solid sample of the polymer **3·Y** after storing it in commercially available MeOH under Ar atmosphere for one day.

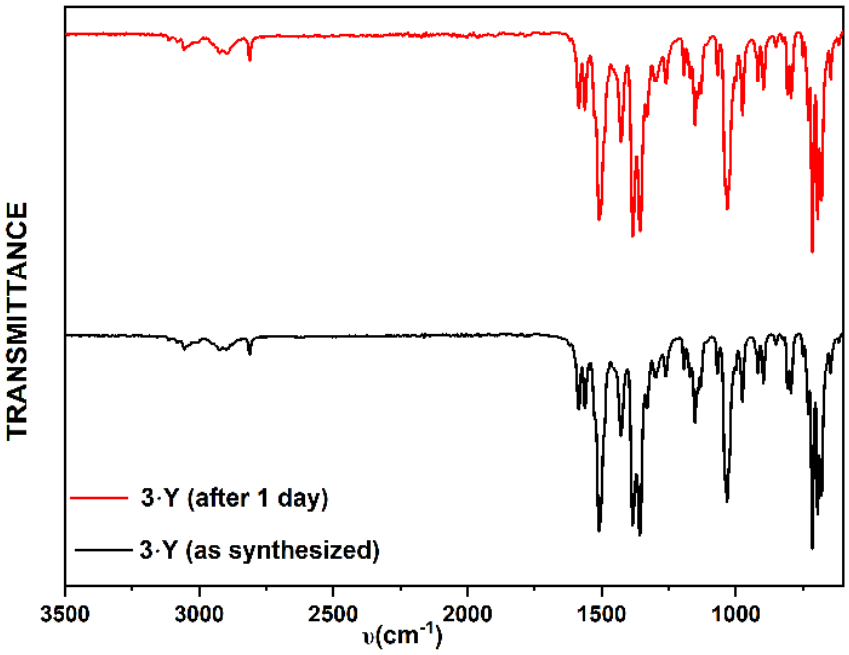

Fig. S23. Comparative FT-IR spectra: ***solid black line*** – the FT-IR spectrum recorded on the freshly synthesized solid sample of the polymer **3·Y**; and ***solid red line*** – the FT-IR spectrum recorded on the solid sample of the polymer **3·Y** after storing it in distilled water under Ar atmosphere for one day.

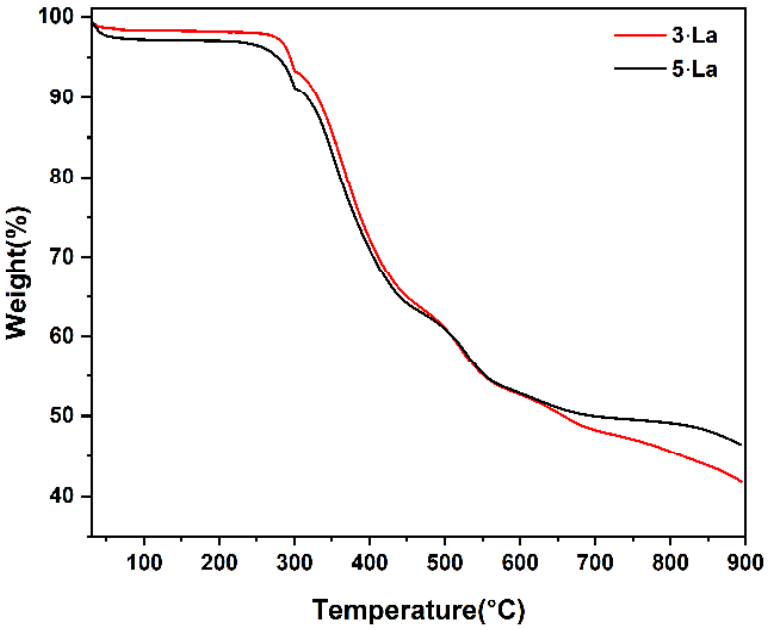

Fig. S24. Comparative thermo-gravimetric analysis (TGA) thermograms recorded on the as-synthesized solid samples of **3·La** (*red*) and **5·La** (*black*). The studies were carried out between the temperature 30-900 °C.

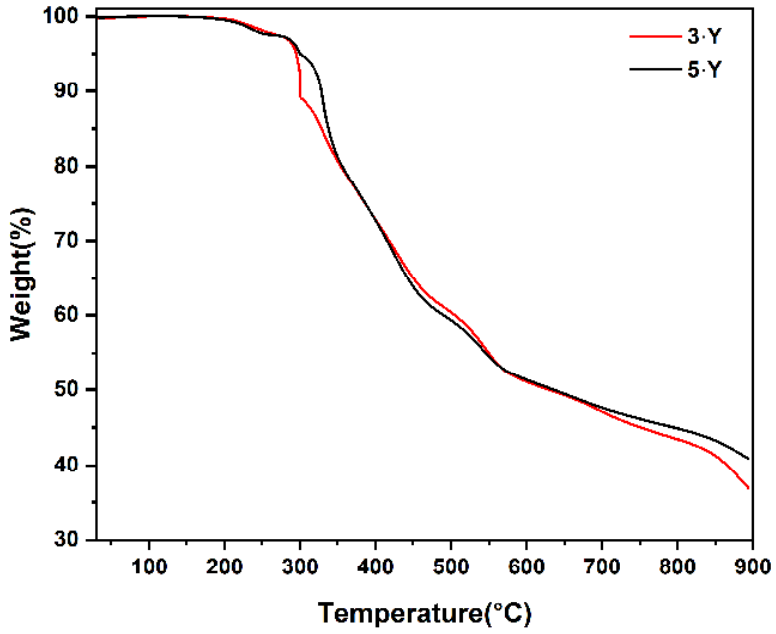

Fig. S25: Comparative thermo-gravimetric analysis (TGA) thermograms recorded on the as-synthesized solid samples of **3·Y** (*red*) and **5·Y** (*black*). The studies were carried out between the temperature 30-900 °C.

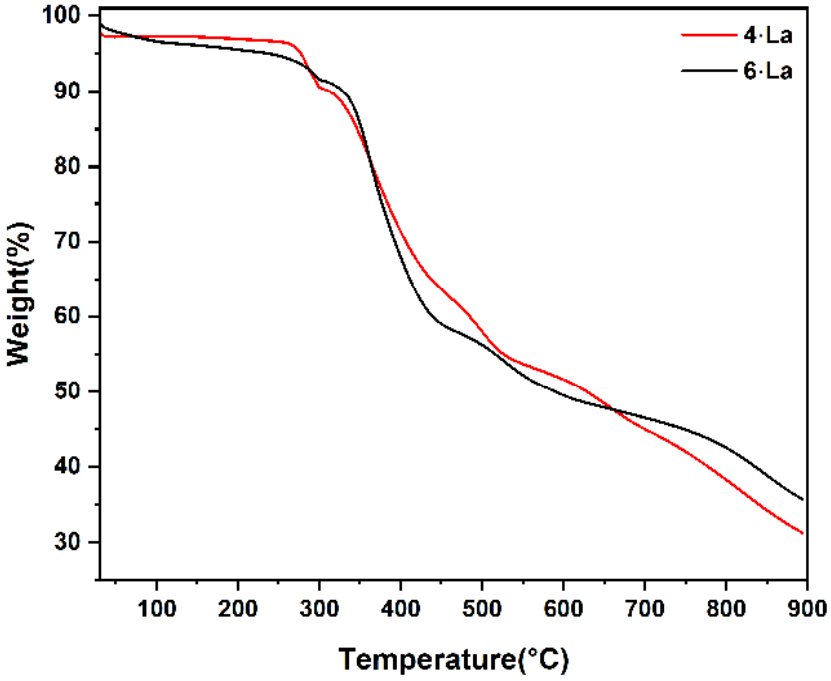

Fig. S26. Comparative thermo-gravimetric analysis (TGA) thermograms recorded on the as-synthesized solid samples of **4·La** (*red*) and **6·La** (*black*). The studies were carried out between the temperature 30-900 °C.

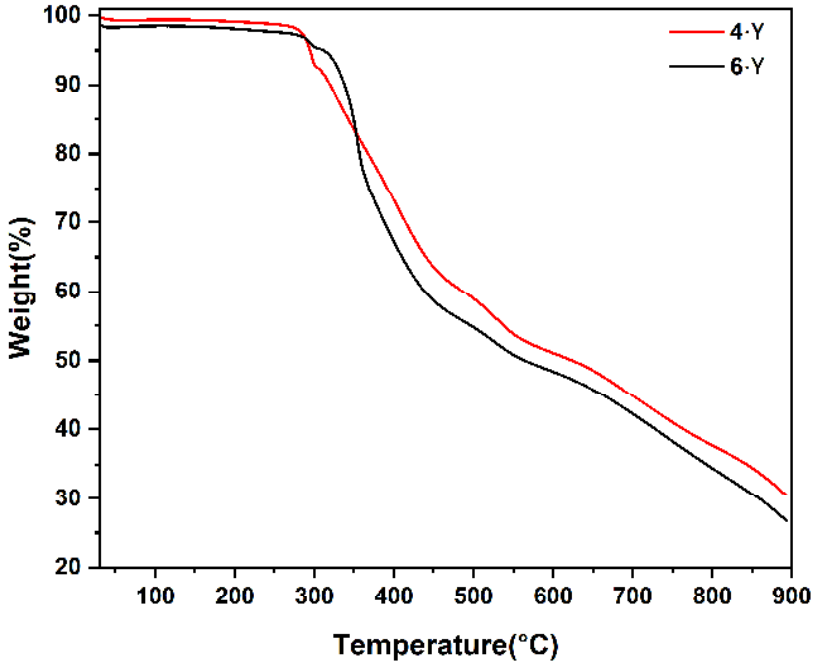

Fig. S27. Comparative thermo-gravimetric analysis (TGA) thermograms recorded on the as-synthesized solid samples of **4·Y** (*red*) and **6·Y** (*black*). The studies were carried out between the temperature 30-900 °C.

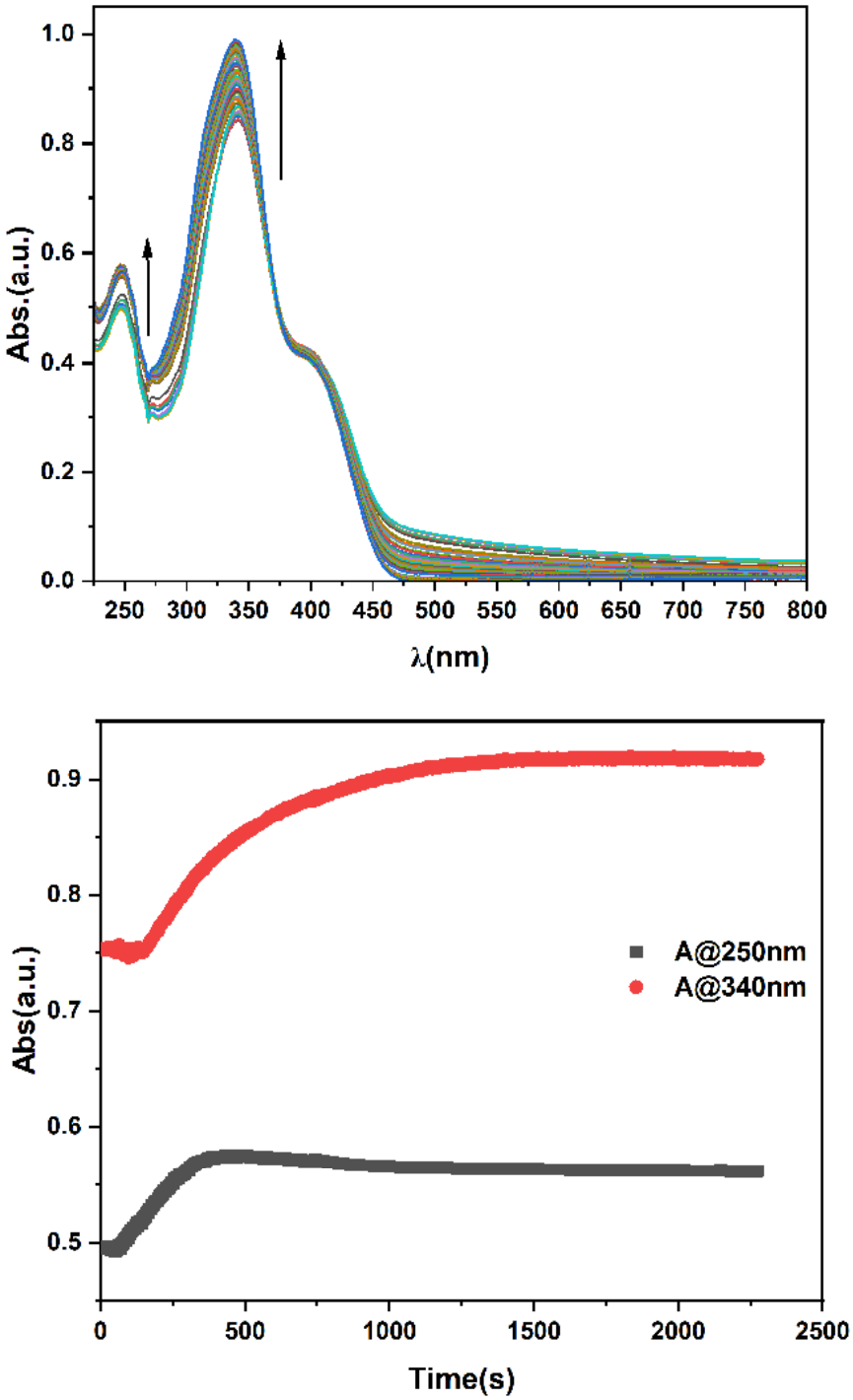

Fig. S28. Time-dependent UV-Vis absorption studies on the reaction between **3·Y** and CO_2 in methanol at room temperature under Ar atmosphere: ***Top*** – the time-dependent UV-vis spectral change between 0 to 40 minutes; and ***Bottom*** - the time-dependent changes in absorptions at the absorption maxima 250 nm (*solid black squares*) and 340 nm (*solid red circles*).

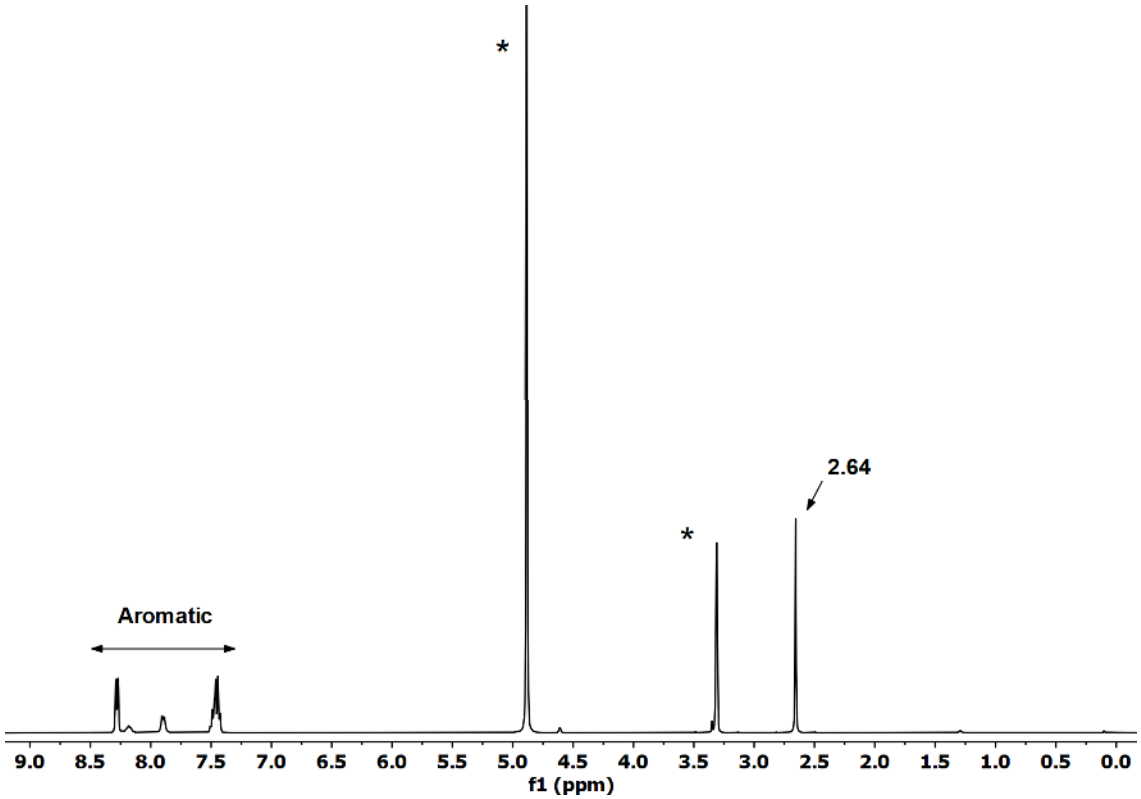

Fig. S29. The room temperature solution ^{1}H NMR spectrum recorded on the reaction mixture after treatment of **3·Y** with CO_2 gas in CD_3OD at room temperature under Ar atmosphere. The signals corresponding to the residual solvent / grease are indicated by asterisks. The characteristic signals corresponding to the CH_3 moieties of the imine functionality of the ligand ($\delta_{CH_3}(imine$, ppm)) in the product of the reaction is labelled with their chemical shift value. $\delta_{CH_3}(imine$, ppm) = 2.64 corresponds to the CO_3^{2-}-bridged dinuclear complex **7·Y**.

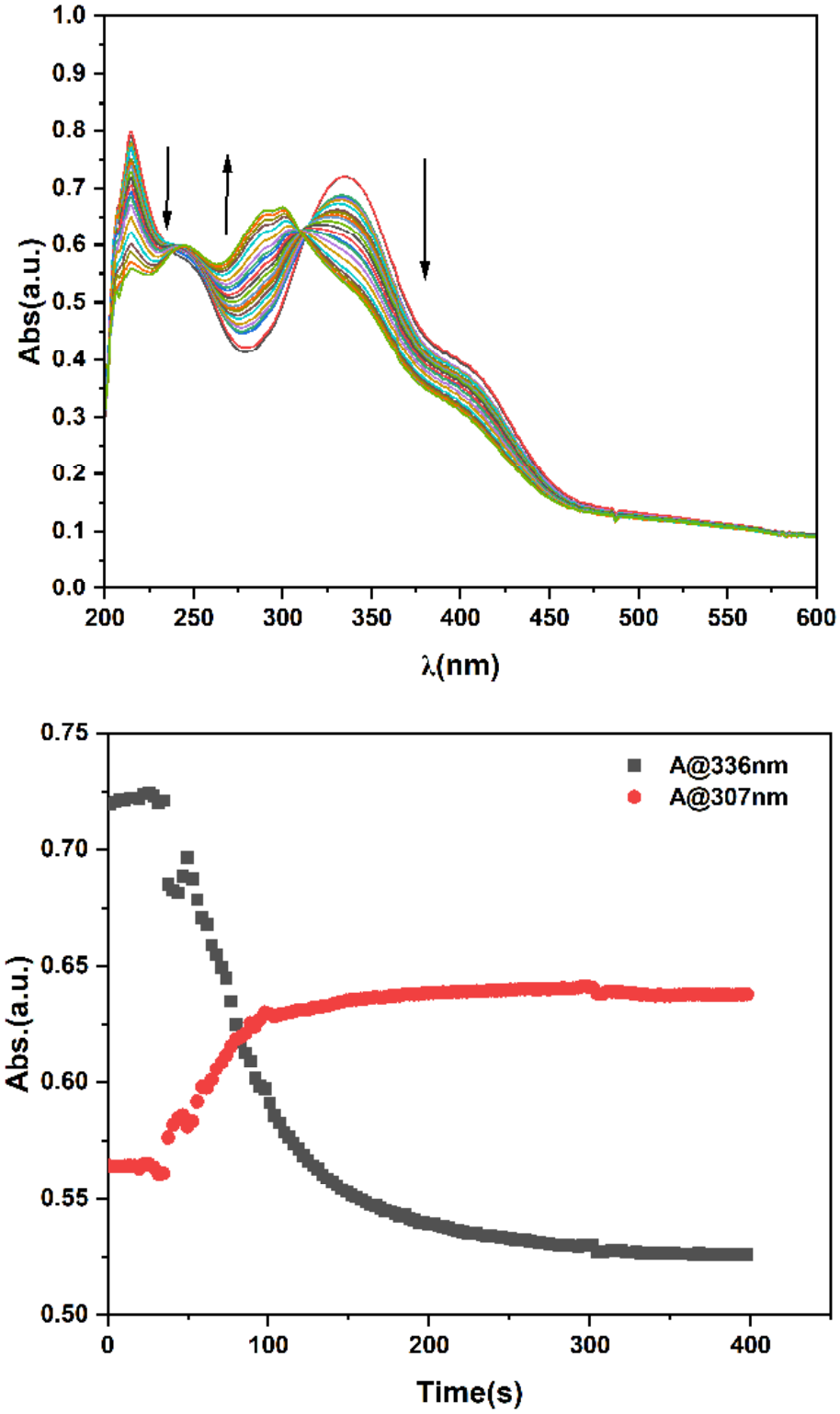

Fig. S30. Time-dependent UV-Vis absorption studies on the reaction between **3·La** and CO_2 in methanol at room temperature under Ar atmosphere: ***Top*** – the time-dependent UV-vis spectral change between 0 to 7 minutes; and ***Bottom*** - the time-dependent changes in absorptions at the absorption maxima 336 nm (*solid black squares*) and 307 nm (*solid red circles*).

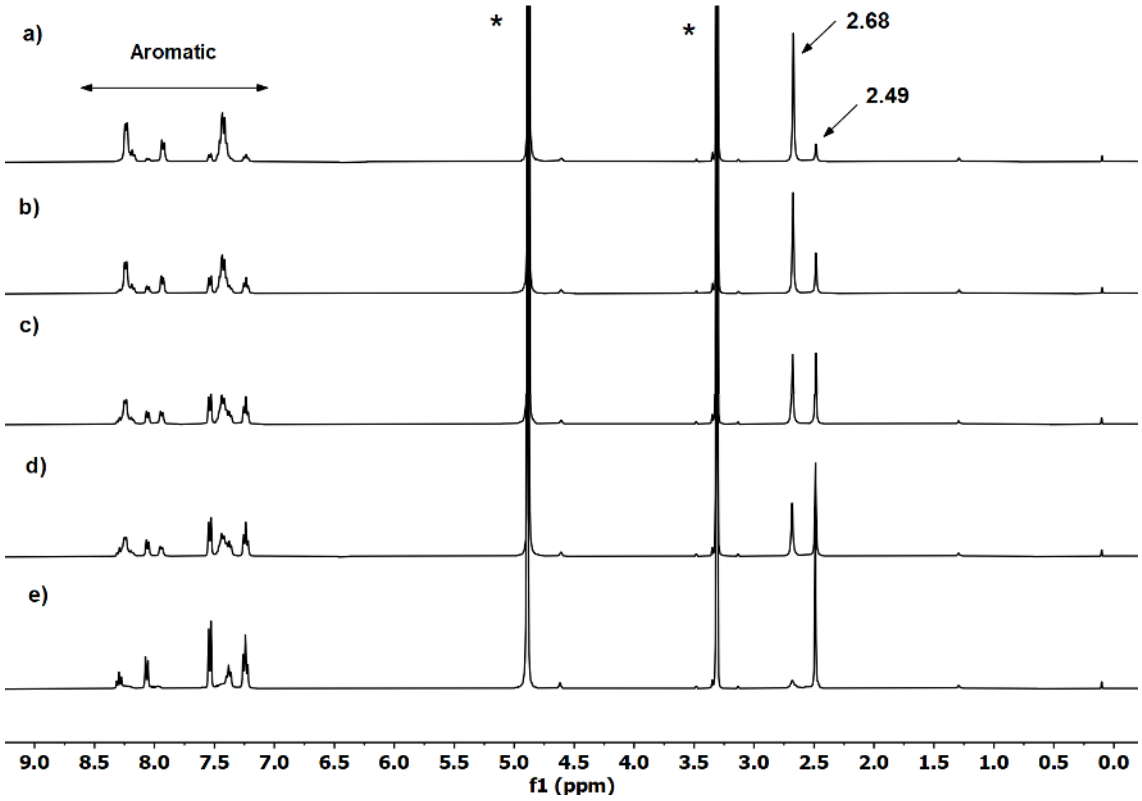

Fig. S31. The time-dependent solution ^{1}H NMR spectra of the reaction mixture upon treatment of **3·La** with CO_2 gas in CD_3OD at room temperature recorded under Ar atmosphere. The ^{1}H NMR spectra were recorded after the time periods of 30 minute (*a*), 1 hour (*b*), 2 hours (c), 4 hours (d) and 24 hours (*e*) during the progress of the reaction since the start of the reaction**.** The signals corresponding to the residual solvent / grease are indicated by asterisks. The characteristic signals corresponding to the CH_3 moieties of the imine functionality of the ligand ($\delta_{CH_3}(imine$, ppm)) in the products of the reaction are labelled with their chemical shift values. $\delta_{CH_3}(imine$, ppm) = 2.68 and 2.49 correspond to the CO_3^{2-}-bridged dinuclear complex **7·La** and the mononuclear decacoordinate neutral complex **2·La**, respectively. The gradual decrement of the signal at $\delta_{CH_3}(imine$, ppm) = 2.68 and the concomitant enhancement of the signal at $\delta_{CH_3}(imine$, ppm) = 2.49 implied the conversion of **7·La** into **2·La** during the course of the reaction.

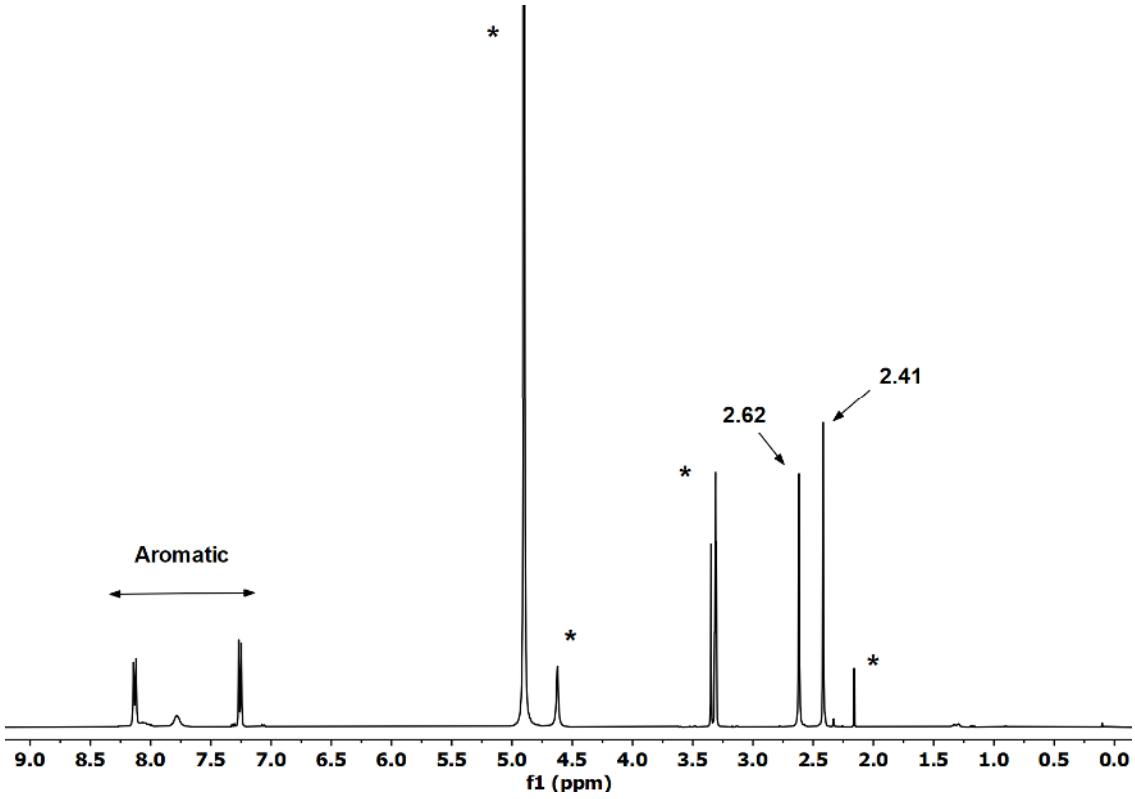

Fig. S32. The room temperature solution ^{1}H NMR spectrum recorded on the reaction mixture after treatment of **5·Y** with CO_2 gas in CD_3OD at room temperature under Ar atmosphere. The signals corresponding to the residual solvent / grease are indicated by asterisks. The characteristic signal corresponding to the CH_3 moiety of the imine functionality of the ligand ($\delta_{CH_3}(imine$, ppm)) and the characteristic signal corresponding to the CH_3 moiety of the toluene substituent of the ligand ($\delta_{CH_3}(toluene$, ppm)) the in the product of the reaction are labelled with their chemical shift values. $\delta_{CH_3}(imine$, ppm) = 2.62 corresponds to the CO_3^{2-}-bridged dinuclear complex **8·Y**. The chemical shift at 2.41 ppm in the spectrum corresponds to the CH_3 moiety of the toluene substituent of the ligand ($\delta_{CH_3}(toluene)$) in **8·Y**.

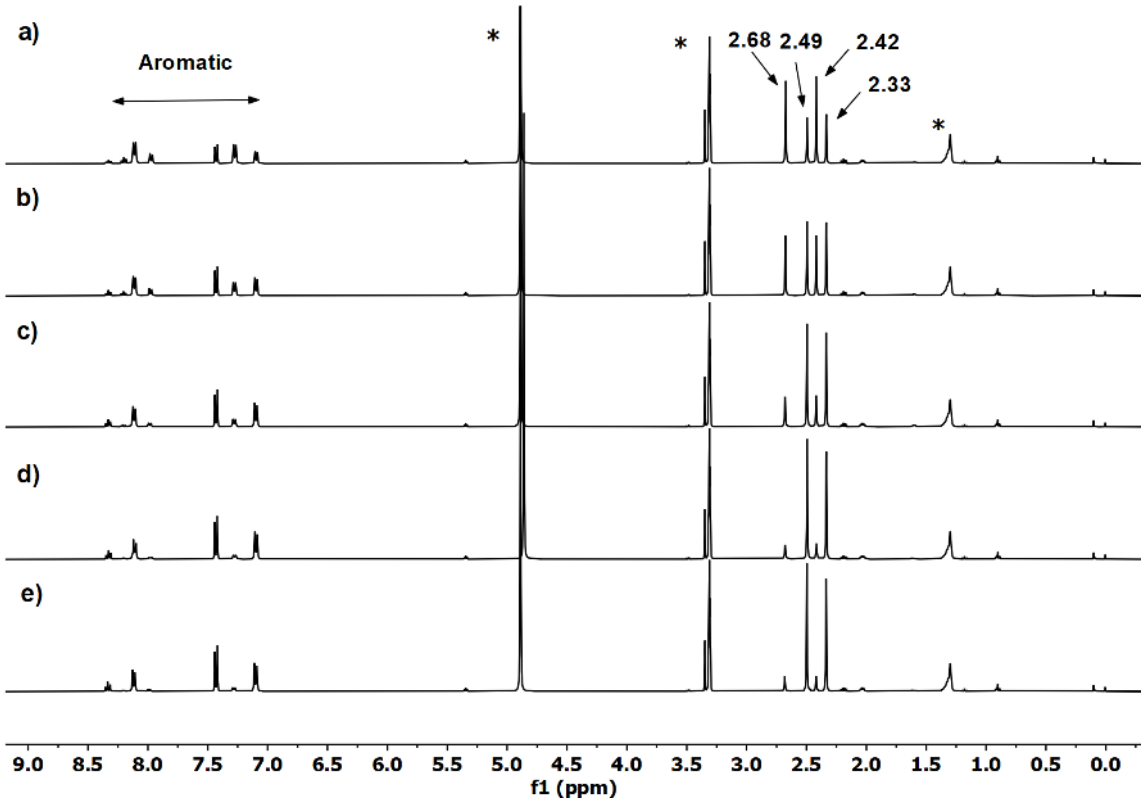

Fig. S33. The time-dependent solution ^{1}H NMR spectra of the reaction mixture upon treatment of **5·La** with CO_2 gas in CD_3OD at room temperature recorded under Ar atmosphere. The ^{1}H NMR spectra were recorded after the time periods of 30 minute (*a*), 2 hour (*b*), 4 hours (c), 8 hours (d) and 24 hours (*e*) during the progress of the reaction since the start of the reaction. The signals corresponding to the residual solvent / grease are indicated by asterisks. The characteristic signals corresponding to the CH_3 moiety of the imine functionality ($\delta_{CH_3}(imine$, ppm)) and the CH_3 moiety of the toluene substituent ($\delta_{CH_3}(toluene$, ppm)) of the ligand in the products of the reaction are labelled with their chemical shift values. $\delta_{CH_3}(imine$, ppm) = 2.68 and 2.49 correspond to the CO_3^{2-}-bridged dinuclear complex **8·La** and the mononuclear decacoordinate neutral complex **9·La**, respectively. The gradual decrement of the signal at $\delta_{CH_3}(imine$, ppm) = 2.68 and the concomitant enhancement of the signal at $\delta_{CH_3}(imine$, ppm) = 2.49 implied the conversion of **8·La** into **9·La** during the course of the reaction. The chemical shifts at 2.42 ppm and 2.33 ppm in the spectra correspond to the CH_3 moieties of the toluene substituent of the ligand ($\delta_{CH_3}(toluene)$) in **8·La** and **9·La**, respectively.

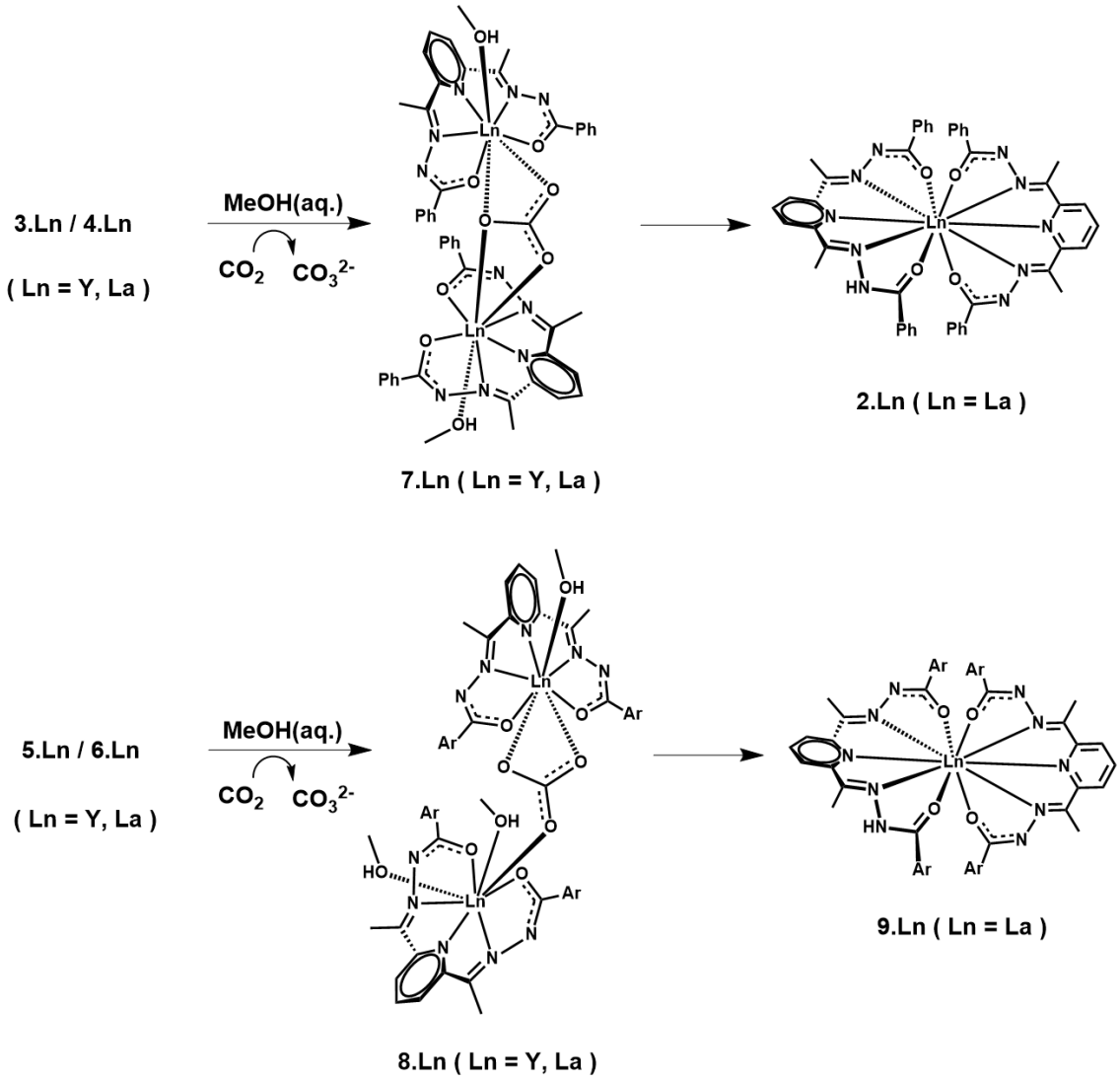

Scheme S4: Schematic representations for the reactions of the CPs **3·Ln - 6·Ln** with CO_2 in aqueous MeOH medium and the formation of the CO_3^{2-}-bridged dinuclear complexes **7·Ln - 8·Ln** as well as the formation of the mononuclear decacoordinate complexes **8·Ln - 9·Ln**.

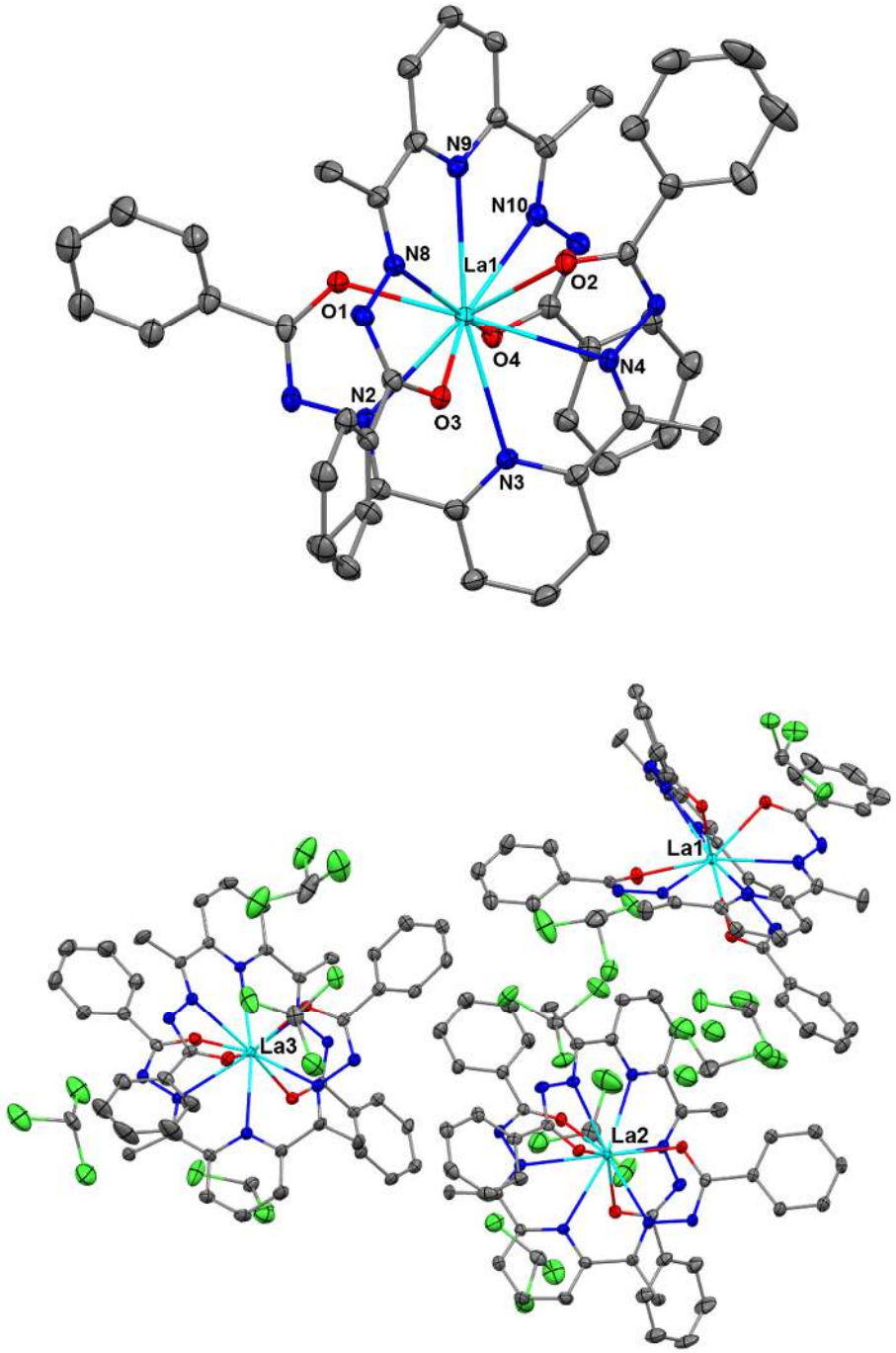

Fig. S34. ORTEP representations with 40% ellipsoid probability for the solid-state single crystal X-ray molecular structure of the ΔΔ-isomer of **2·La** (*top*) and the content of the asymmetric unit of the solid-state packing of **2·La** (*bottom*). The H atoms and thermally disordered atoms are omitted for clarity. Color codes: cyan, La; green, Cl; red, O; blue, N; and grey, C.

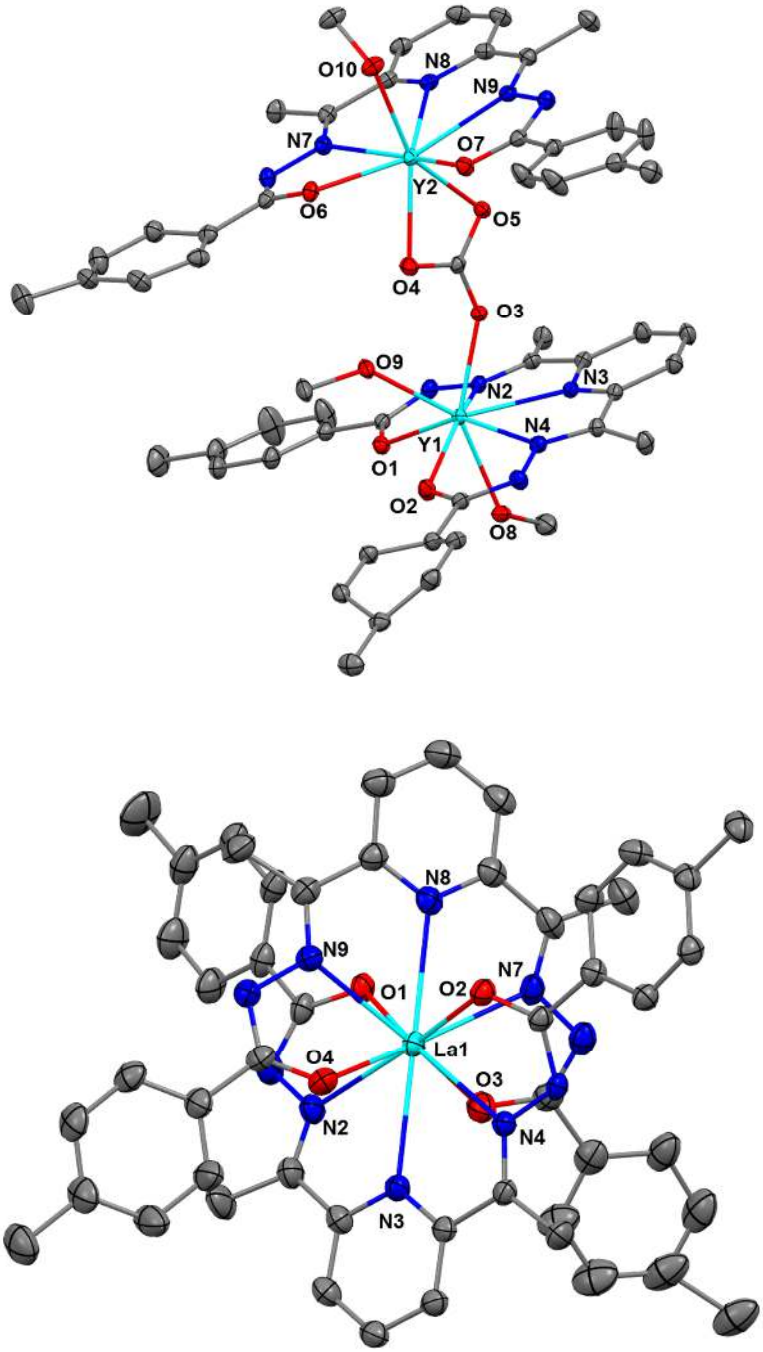

Fig. S35. ORTEP representations with 40% ellipsoid probability for the solid-state single crystal X-ray molecular structures of **8·Y** (*top*) and the ΔΔ-isomer of **9·La** (*bottom*). The H atoms, thermally disordered atoms and the co-crystallized solvent molecules are omitted for clarity. Color codes: cyan, La and Y; red, O; blue, N; and grey, C.

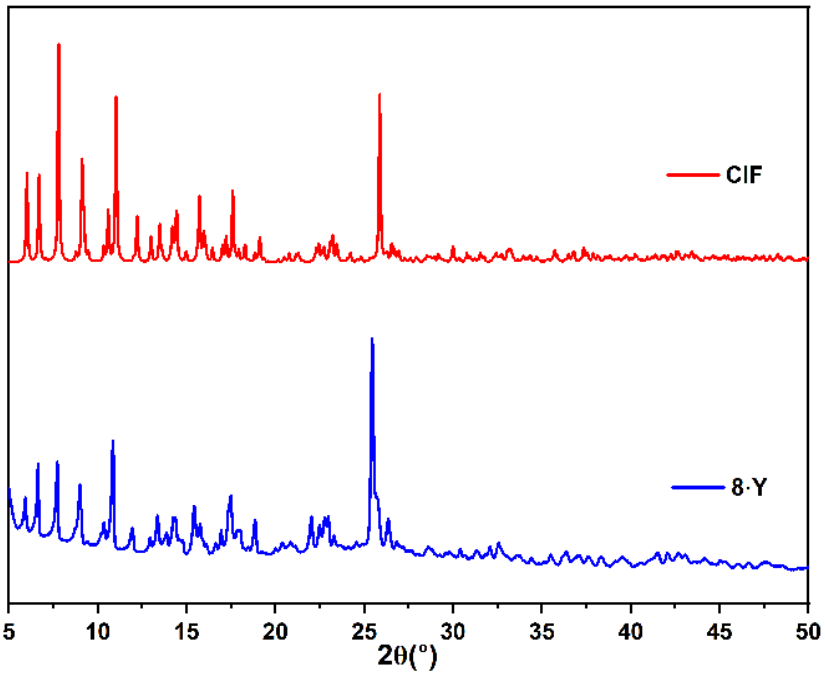

Fig. S36. The powder X-ray diffractograms of the *as-synthesized* solid sample (*solid blue line*) and the simulated pattern of the single-crystal X-ray molecular structure (*solid red line*) of the CO_3^{2-}-bridged dinuclear complex **8·Y**.

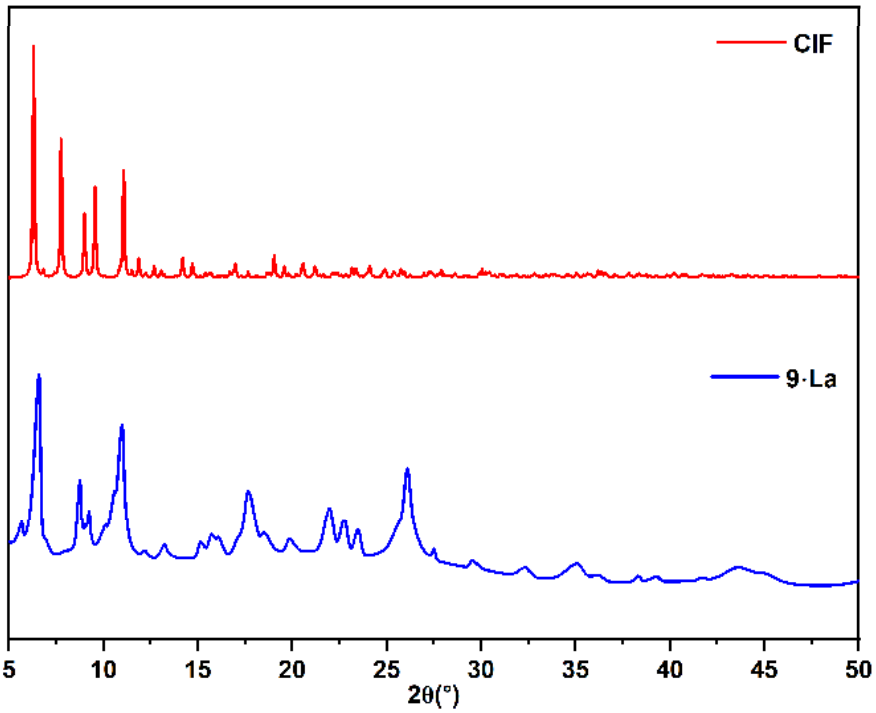

Fig. S37. The powder X-ray diffractograms of the *as-synthesized* solid sample (*solid blue line*) and the simulated pattern of the single-crystal X-ray molecular structure (*solid red line*) of the coordination polymer **9·La**.

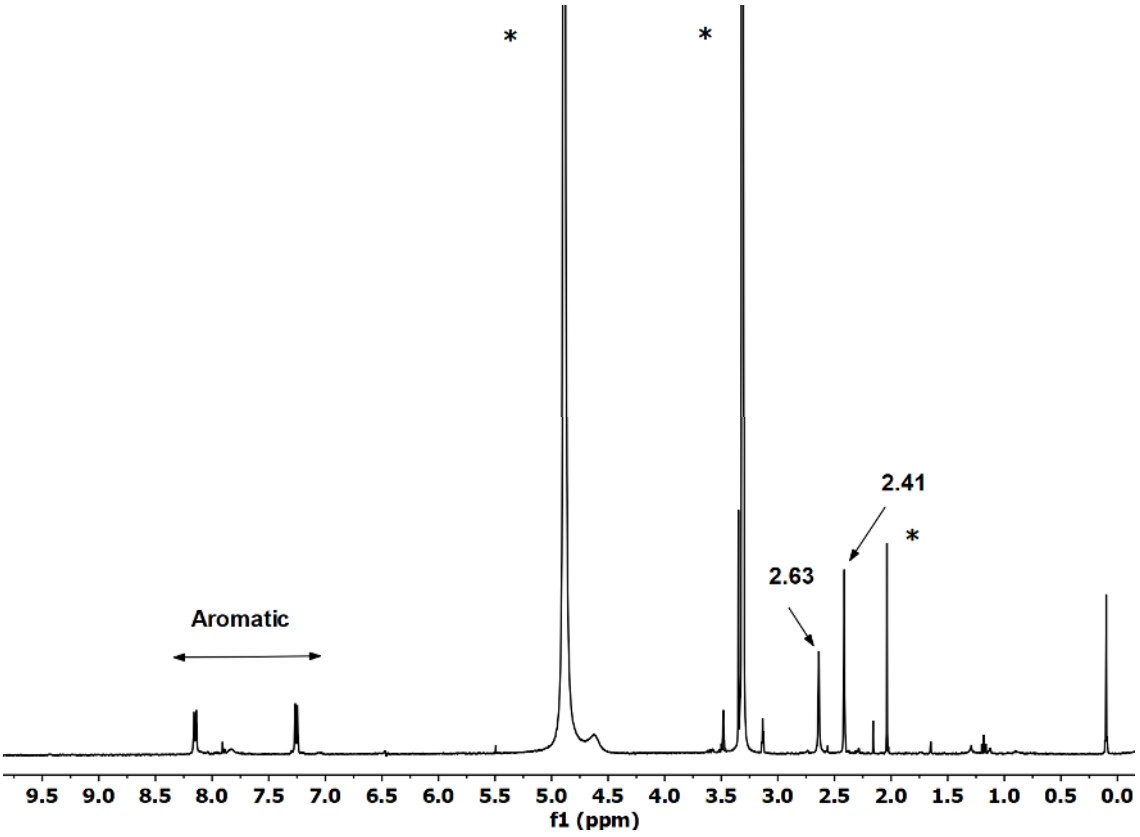

Fig. S38. The room temperature solution ^{1}H NMR spectrum recorded on the CD_3OD solution of the isolated single crystals of **8·Y**. The signals corresponding to the residual solvent / grease are indicated by asterisks. The characteristic signals corresponding to the CH_3 moieties of the imine functionality ($\delta_{CH_3}(imine)$, 2.63 ppm) and the toluene substituent ($\delta_{CH_3}(toluene)$, 2.41 ppm) of the ligand in **8·Y** are labelled with their chemical shift values.

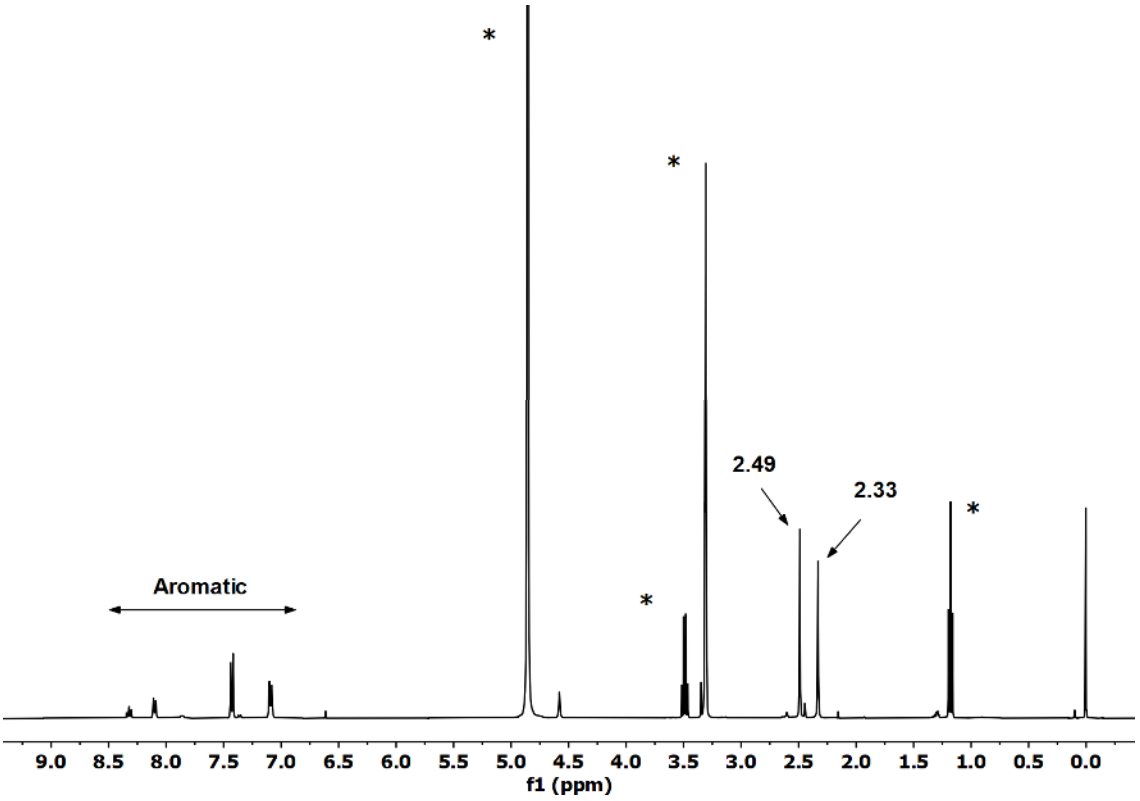

Fig. S39. The room temperature solution ^{1}H NMR spectrum recorded on the CD_3OD solution of the isolated single crystals of **9·La**. The signals corresponding to the residual solvent / grease are indicated by asterisks. The characteristic signals corresponding to the CH_3 moieties of the imine functionality ($\delta_{CH_3}(imine)$, 2.49 ppm) and the toluene substituent ($\delta_{CH_3}(toluene)$, 2.33 ppm) of the ligand in **9·La** are labelled with their chemical shift values.

Table S5: Selected crystallographic data and refinement parameters for **2·La, 8·Y and 9·La.**

	2·La	**8·Y**	**9·La**
Formula*	$C_{149}H_{134}N_{30}O_{15}Cl_{33}La_3$	$C_{54}H_{58}N_{10}O_{10}Y_2$	$C_{55}H_{67}N_{10}O_9La$
Mr (g mol^{-1})*	4171.43	1184.92	1151.09
crystal system	Orthorhombic	Triclinic	Monoclinic
space group	$P2_12_12_1$	P-1	$P2_1/c$
T (K)	100	100	100
a (Å)	14.5261(5)	13.2210(4)	12.9794(6)
b (Å)	22.8182(7)	13.3592(5)	23.8544(12)
c (Å)	52.0855(13)	15.4651(5)	17.3563(8)
α (°)	90	84.6720(10)	90
β (°)	90	71.9359(10)	94.125(2)
γ (°)	90	81.4930(10)	90
V (Å^3)	17262.2(9)	2565.05(15)	5359.9(4)
Z	4	2	4
$\rho_{calcd.}$ (g cm^{-3})	1.605	1.534	1.426
μ (mm^{-1})	1.308	2.322	0.863
collected reflns	311333	101933	75745
unique reflns	42887	11767	10984
No. of parameters	2116	751	601
Reflns for Refinement	311333	101933	75745
R (I > 3σ(I))[a]	0.0387	0.0292	0.0467
wR (I > 3σ(I))[b]	0.0952	0.0715	0.1258
GOF on *F*	1.035	1.023	1.050

[a] $R = \Sigma||F_o| - |F_c||/\Sigma|F_o|$, [b] $wR = [\Sigma(w(F_o^2 - F_c^2)^2)/\Sigma([w(F_o^2)^2]^{1/2}$ where $w = 1/(\sigma^2(F_o^2) + (aP)^2 + bP)$ with $P = (2F_c^2 + \max(F_o^2,0))/3$.

* Including squeezed out solvents

Table S6. Selected bond lengths (Å) and bond angles (°) of the complexes **2·La, 8·Y and 9·La.**

Complex **2·La**

La2 O7 2.666(4)	La2 O5 2.478(3)	La2 O6 2.481(4)	La2 O8 2.497(3)
La2 N19 2.760(4)	La2 N18 2.838(4)	La2 N17 2.705(4)	La2 N14 2.670(4)
La2 N12 2.703(4)	La2 N13 2.783(4)	La3 O10 2.478(4)	La3 O11 2.490(4)
La3 O9 2.483(4)	La3 O12 2.618(4)	La3 N29 2.797(4)	La3 N28 2.824(4)
La3 N27 2.686(4)	La3 N23 2.774(4)	La3 N24 2.694(5)	La3 N22 2.702(4)
La1 O3 2.494(4)	La1 O4 2.503(4)	La1 O1 2.448(4)	La1 O2 2.605(4)
La1 N9 2.783(4)	La1 N2 2.699(4)	La1 N10 2.730(4)	La1 N4 2.761(4)
La1 N3 2.819(4)	La1 N8 2.682(4)		

C102 N25 N24	109.5(4)	C109 N21 N22	108.2(4)	C132 N30 N29	114.4(4)
C125 N26 N27	110.9(4)	C63 N11 N12	108.8(4)	C56 N15 N14	109.8(4)
C86 N16 N17	110.9(4)	C79 N20 N19	115.6(4)	C10 N5 N4	114.6(4)
C17 N1 N2	109.6(4)	C40 N7 N8	109.2(4)	C33 N6 N10	108.3(4)
O10 La3 N24	59.01(12)	N24 La3 N23	58.96(13)	N22 La3 N23	58.14(13)

O9 La3 N22	58.94(12)	O12 La3 N29	56.36(12)	N29 La3 N28	56.41(12)
N27 La3 N28	58.60(12)	O11 La3 N27	60.15(12)	O5 La2 N12	58.65(12)
N12 La2 N13	58.15(12)	N14 La2 N13	58.40(13)	O6 La2 N14	59.48(13)
O8 La2 N17	59.61(12)	N17 La2 N18	57.74(12)	N19 La2 N18	56.06(13)
O7 La2 N19	56.97(12)	O4 La1 N10	57.60(13)	N10 La1 N9	57.76(13)
N8 La1 N9	58.81(13)	O3 La1 N8	59.65(12)	O1 La1 N2	59.80(13)
N2 La1 N3	58.16(13)	N4 La1 N3	56.57(13)	O2 La1 N4	57.02(12)

Complex **8·Y**

Y2 O7	2.2612(13)	Y2 O6	2.3638(13)	Y2 O5	2.3328(13)	Y2 O4	2.3345(13)
Y2 O10	2.3743(14)	Y2 N9	2.4571(16)	Y2 N8	2.4993(16)	Y2 N7	2.4586(16)
Y1 O1	2.3103(13)	Y1 O3	2.2747(13)	Y1 O2	2.2713(13)	Y1 O8	2.4101(14)
Y1 O9	2.3663(14)	Y1 N3	2.4822(16)	Y1 N2	2.4481(16)	Y1 N4	2.4458(16)
O2 C10	1.288(2)	N10 N9	1.383(2)	N1 N2	1.390(2)	N1 C18	1.317(3)
N7 N6	1.386(2)	N5 N4	1.384(2)	N5 C10	1.322(2)	N6 C44	1.326(2)
N10 C36	1.323(3)						

O1 Y1 N2	64.87(5)	N2 Y1 N3	64.16(5)	N4 Y1 N3	64.22(5)
O2 Y1 N4	65.02(5)	C18 N1 N2	109.70(15)	C10 N5 N4	109.21(15)
O7 Y2 N9	65.56(5)	N9 Y2 N8	63.75(5)	N7 Y2 N8	63.60(5)
O6 Y2 N7	64.59(5)	C36 N10 N9	109.31(15)	C44 N6 N7	110.50(15)

Complex **9·La**

La1 O1	2.521(3)	La1 O2	2.520(3)	La1 N4	2.706(3)	La1 O4	2.553(3)
La1 O3	2.475(3)	La1 N8	2.723(3)	La1 N3	2.732(3)	La1 N9	2.643(3)
La1 N7	2.643(3)	La1 N2	2.653(3)	O1 C18	1.274(5)	O2 C10	1.255(4)
N4 N5	1.388(4)	O4 C35	1.261(5)	O3 C43	1.271(5)	N5 C10	1.346(5)
N10 N9	1.385(5)	N10 C35	1.344(5)	N7 N6	1.404(5)	N6 C43	1.326(6)
N1 C18	1.327(6)	N2 N1	1.390(5)				

O4 La1 N9	59.22(10)	N9 La1 N8	59.12(10)	N7 La1 N8	59.84(11)
O3 La1 N7	59.63(11)	C35 N10 N9	112.2(3)	C43 N6 N7	108.5(3)
O2 La1 N4	58.62(9)	N4 La1 N3	58.69(10)	N2 La1 N3	59.79(10)
O1 La1 N2	59.51(10)	C10 N5 N4	111.6(3)	C18 N1 N2	109.9(3)

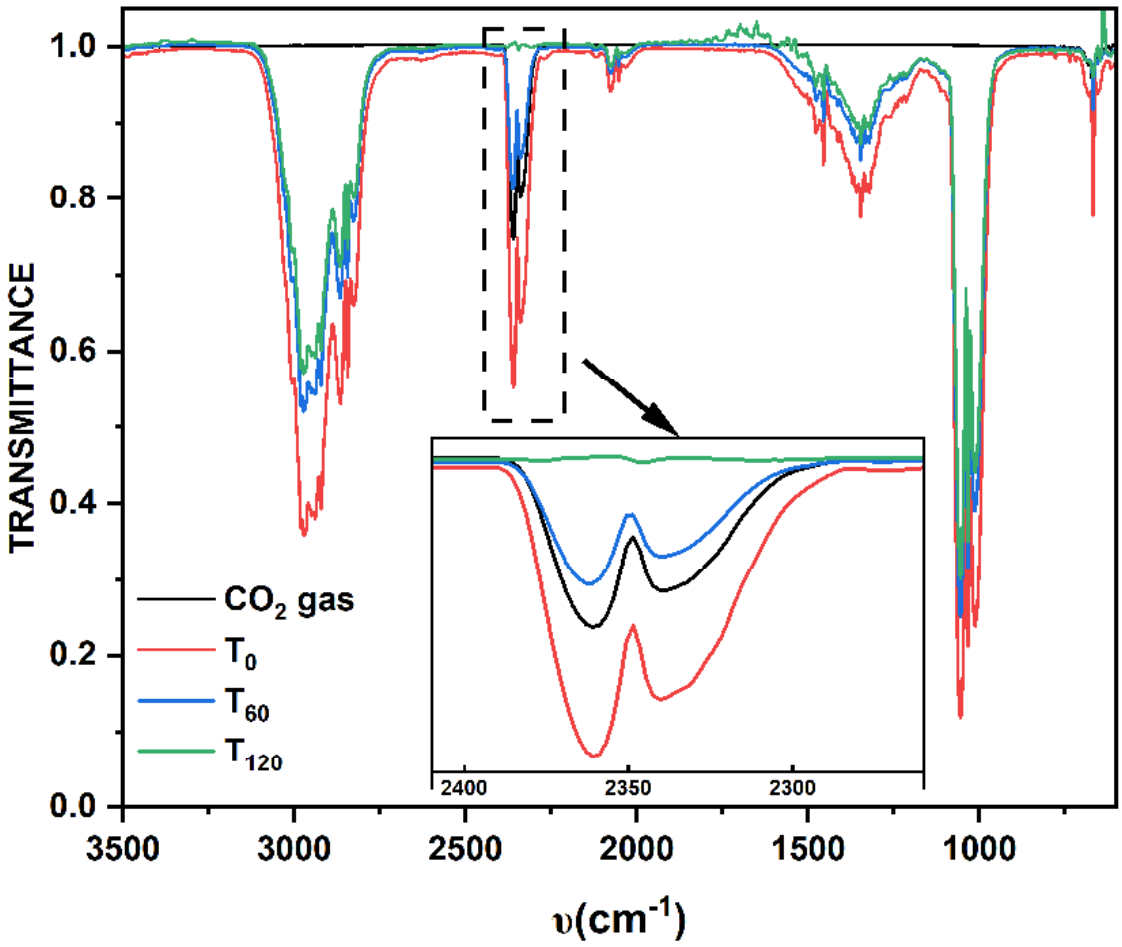

Fig. S40. The time-dependent gas-phase FT-IR spectra recorded on the head-space of the closed reaction container where the sample of **4·Y** was being treated with CO_2 gas in MeOH solvent medium in anhydrous condition under Ar atmosphere (see the experimental section for details). The gas-phase FT-IR spectra were recorded on the head-space of the reaction mixture in the beginning (T_0, *red solid line*), after 60 minutes (T_{60}, *blue solid line*) and after 120 minutes (T_{120}, *green solid line*) during the course of the reaction, and the spectra were compared with the reference gas-phase FT-IR spectra of CO_2 gas (*black solid line*). All the spectra were recorded at room temperature under Ar atmosphere. *Inset* shows the *zoomed-in* region of the spectra from 2260 to 2410 cm^{-1} where the characteristic stretching frequencies are prominent for CO_2 gas. The gradual decrement of the intensity of the characteristic peaks and finally the absence of the characteristic peaks for the CO_2 gas implied consumption of the employed CO_2 gas during the course of the reaction.

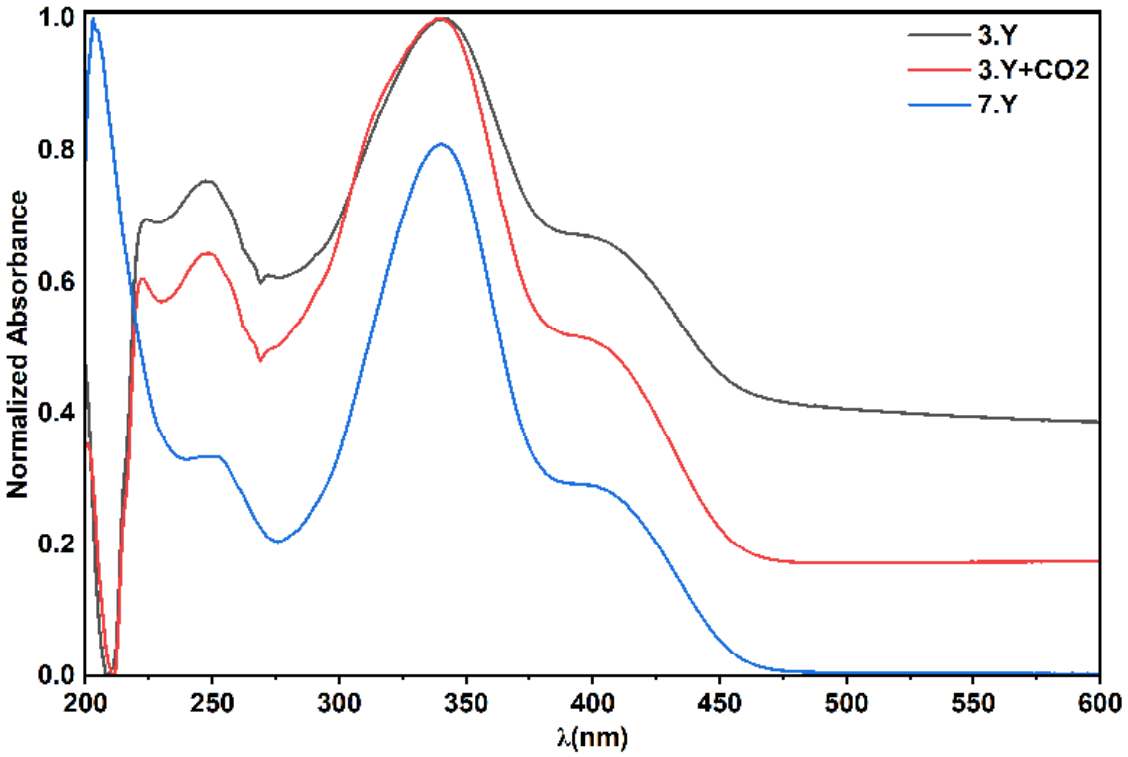

Fig. S41. The normalized comparative UV-Vis absorption spectra: ***black solid line*** – the UV-vis spectra recorded on the methanolic solutions of the isolated polycrystalline sample of **3·Y** at room temperature; ***red solid line*** – the UV-vis spectra recorded on the reaction mixture which was obtained upon treatment of **3·Y** with CO_2 gas in commercially available MeOH under Ar atmosphere at room temperature; and ***blue solid line*** – the UV-vis spectra recorded on the methanolic solutions of the isolated polycrystalline sample of **7·Y** at room temperature.

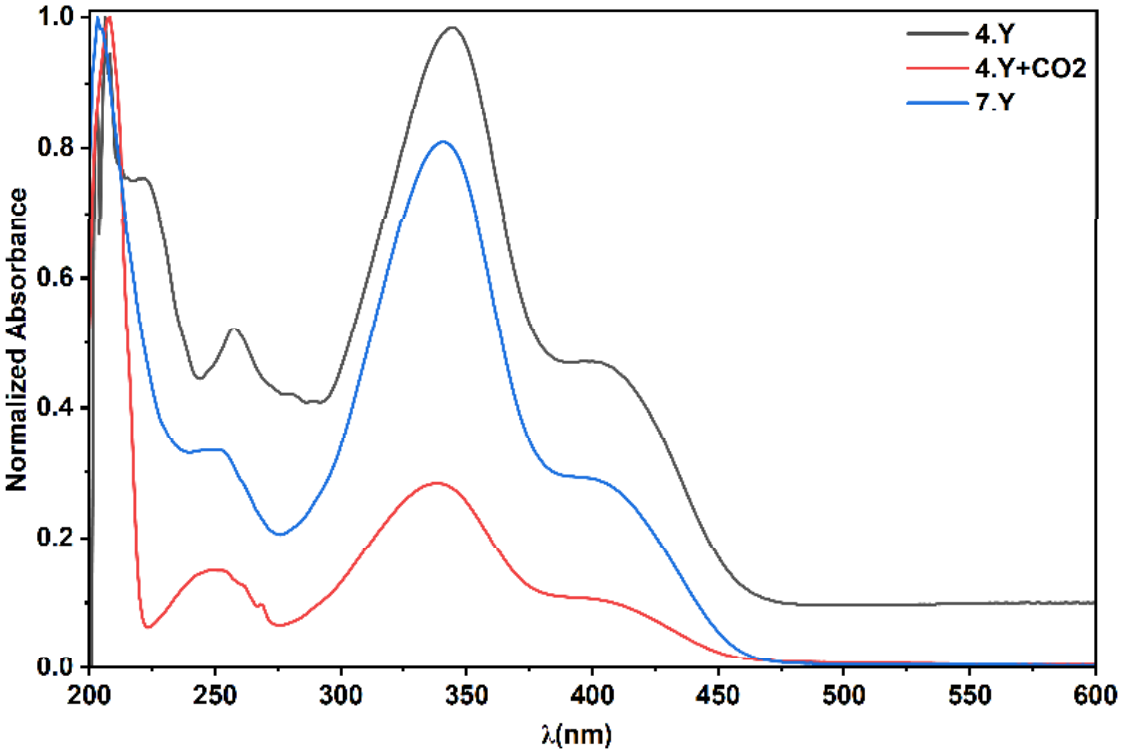

Fig. S42. The normalized comparative UV-Vis absorption spectra: ***black solid line*** – the UV-vis spectra recorded on the methanolic solutions of the isolated polycrystalline sample of **4·Y** at room temperature; ***red solid line*** – the UV-vis spectra recorded on the reaction mixture which was obtained upon treatment of **4·Y** with CO_2 gas in MeOH in anhydrous conditions under Ar atmosphere at room temperature; and ***blue solid line*** – the UV-vis spectra recorded on the methanolic solutions of the isolated polycrystalline sample of **7·Y** at room temperature.

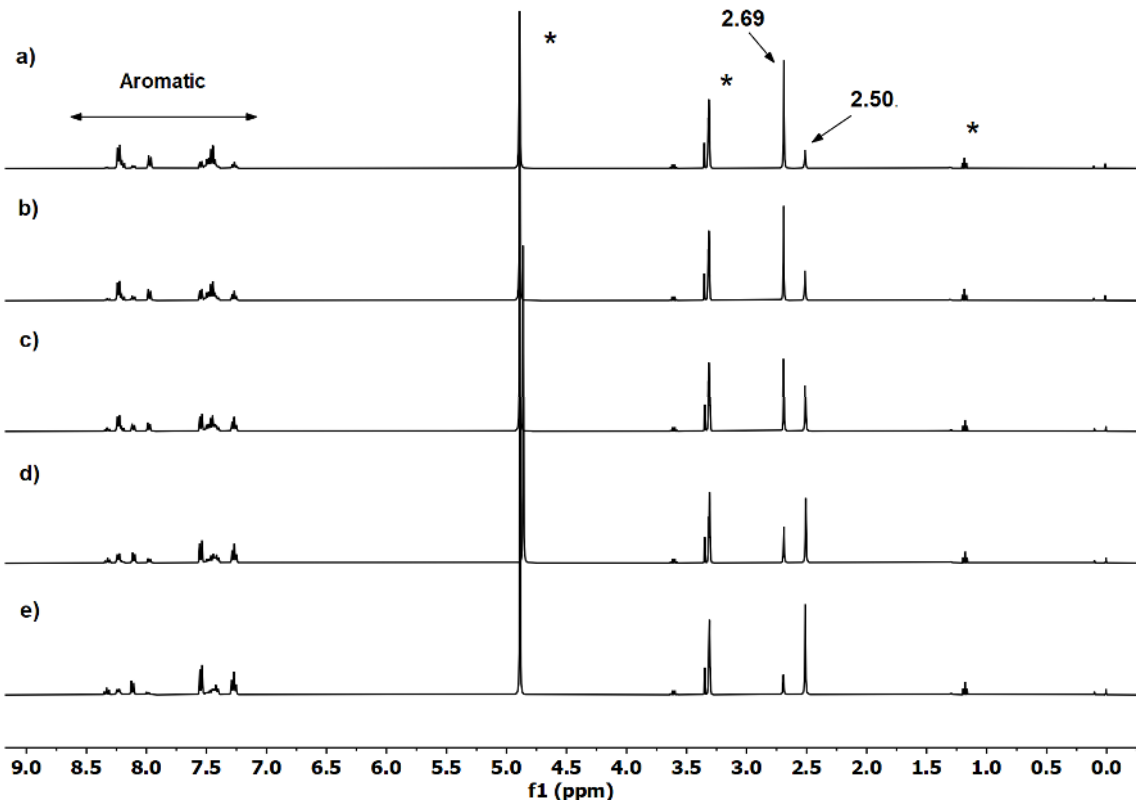

Fig. S43. The time-dependent solution ^{1}H NMR spectra recorded on the reaction mixture upon treatment of **4·La** with CO_2 gas in CD_3OD in anhydrous condition under Ar atmosphere at room temperature. The ^{1}H NMR spectra were recorded after the time periods of 30 minute (*a*), after 2 hours (*b*), after 4 hours (c), after 8 hours (d) and after 24 hours (*e*) during the progress of the reaction**.** The signals corresponding to the residual solvent / grease are indicated by asterisks. The characteristic signals corresponding to the CH_3 moieties of the imine functionality of the ligand ($\delta_{CH_3}(imine, \text{ppm})$) in the products of the reaction are labelled with their chemical shift values. The initial appearance of the signal at $\delta_{CH_3}(imine, \text{ppm})$ = 2.69 corresponds to the tetramethoxymethane-bridged ($C(OMe)_4$-bridged) dinuclear complex **10·La**. The signal at $\delta_{CH_3}(imine, \text{ppm})$ = 2.50 corresponds to the mononuclear decacoordinate neutral complex **2·La**. Slight up-filed shift of the $\delta_{CH_3}(imine, \text{ppm})$ signal towards 2.69 ppm correspond to the formation of CO_3^{2-}-bridged dinuclear complex **7·La**. The gradual decrement of the signal near $\delta_{CH_3}(imine, \text{ppm})$ = 2.69-2.68 and the concomitant enhancement of the signal at $\delta_{CH_3}(imine, \text{ppm})$ = 2.50 implied eventual conversion of **7·La** and **10·La** into **2·La** during the course of the reaction.

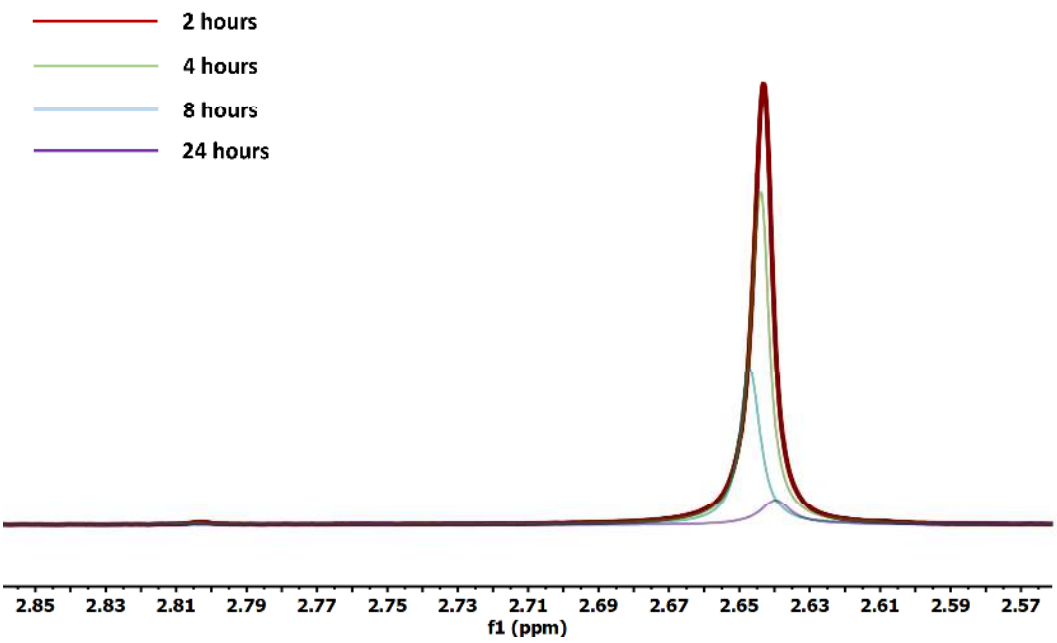

Fig. S44. The time-dependent solution ^{1}H NMR spectra recorded on the reaction mixture upon treatment of **4·Y** with CO_2 gas in CD_3OD in anhydrous condition under Ar atmosphere at room temperature. Only the *zoomed-in* segments around the characteristic $\delta_{CH_3}(imine$, ppm) signals of the ^{1}H NMR spectra are displayed for clarity. The ^{1}H NMR spectra were recorded after the time periods of 2 hours (*red solid line*), 4 hours (*green solid line*), 8 hours (*cyan solid line*) and 24 hours (*purple solid line*) during the progress of the reaction**.** The appearance of the signal peak at $\delta_{CH_3}(imine) = 2.65$ ppm in the initial stages corresponds to the tetramethoxymethane-bridged ($C(OMe)_4$-bridged) dinuclear complex **10·Y**. Slight up-field shift of the $\delta_{CH_3}(imine)$ signal towards 2.64 ppm in the later stage of the reaction corresponds to the formation of CO_3^{2-}-bridged dinuclear complex **7·Y**. The gradual decrement of the signal near $\delta_{CH_3}(imine$, ppm) = 2.65-2.64 was caused due to the crystallization of **7·Y** out of the reaction mixture.

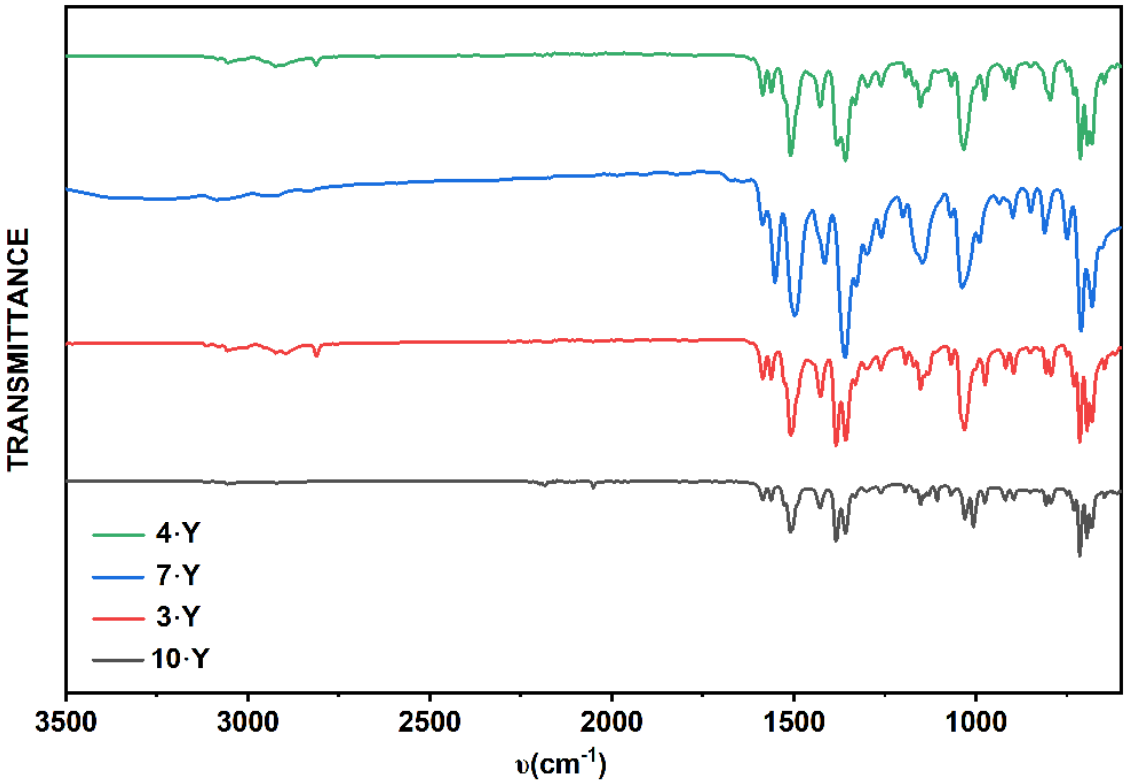

Fig. S45. Comparative FT-IR spectra: ***solid black line*** – the FT-IR spectrum recorded on the solid sample which was obtained upon drying the reaction mixture immediately after the disappearance of the suspended solid particles of the coordination polymer **4·Y** during its treatment with CO_2 gas in MeOH in anhydrous condition under Ar atmosphere at room temperature; ***solid green line*** – the FT-IR spectrum recorded on the freshly synthesized solid sample of the coordination polymer **4·Y**; ***solid red line*** – the FT-IR spectrum recorded on the freshly synthesized solid sample of the coordination polymer **3·Y**; and ***solid blue line*** – the FT-IR spectrum recorded on the isolated polycrystalline solid sample of the CO_3^{2-}-bridged dinuclear complex **7·Y**. All the spectral studies were carried out under Ar atmosphere at room temperature.

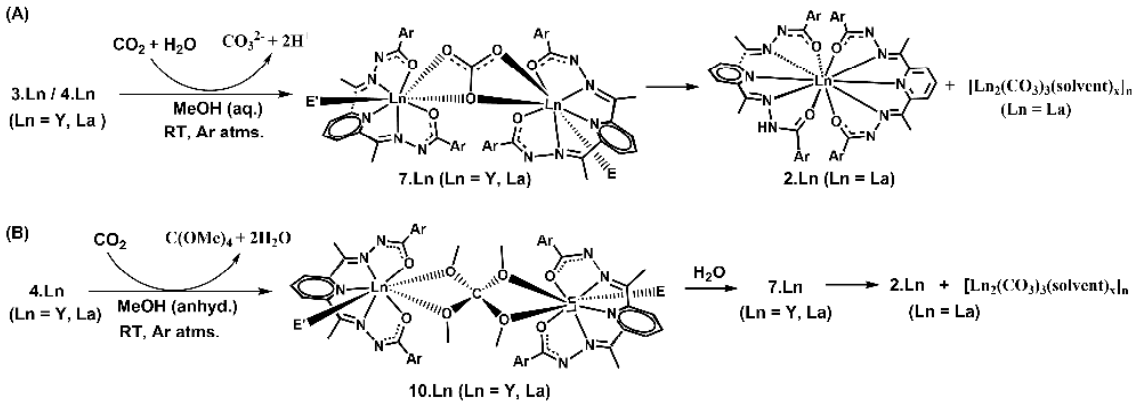

Scheme S5: Schematic representation for the reaction of **(A) 3·Ln** with CO_2 in aq. MeOH that leads to the formation of the CO_3^{2-}-bridged dinuclear complexes **7·Ln** and the decacoordinate mononuclear complexes **2·Ln**; **(B) 4·Ln** with CO_2 in MeOH in anhydrous conditions that leads to the formation of the $C(OMe)_4$-bridged dinuclear complexes **10·Ln**, the CO_3^{2-}-bridged dinuclear complexes **7·Ln** and the decacoordinate mononuclear complexes **2·Ln**; where E = E′= MeOH for **10a·Ln**; E= MeOH and E′= MeO^- for **10b·Ln**; E= E′= MeO^- for **10c·Ln** and E= E′= MeOH for **7·Ln**.

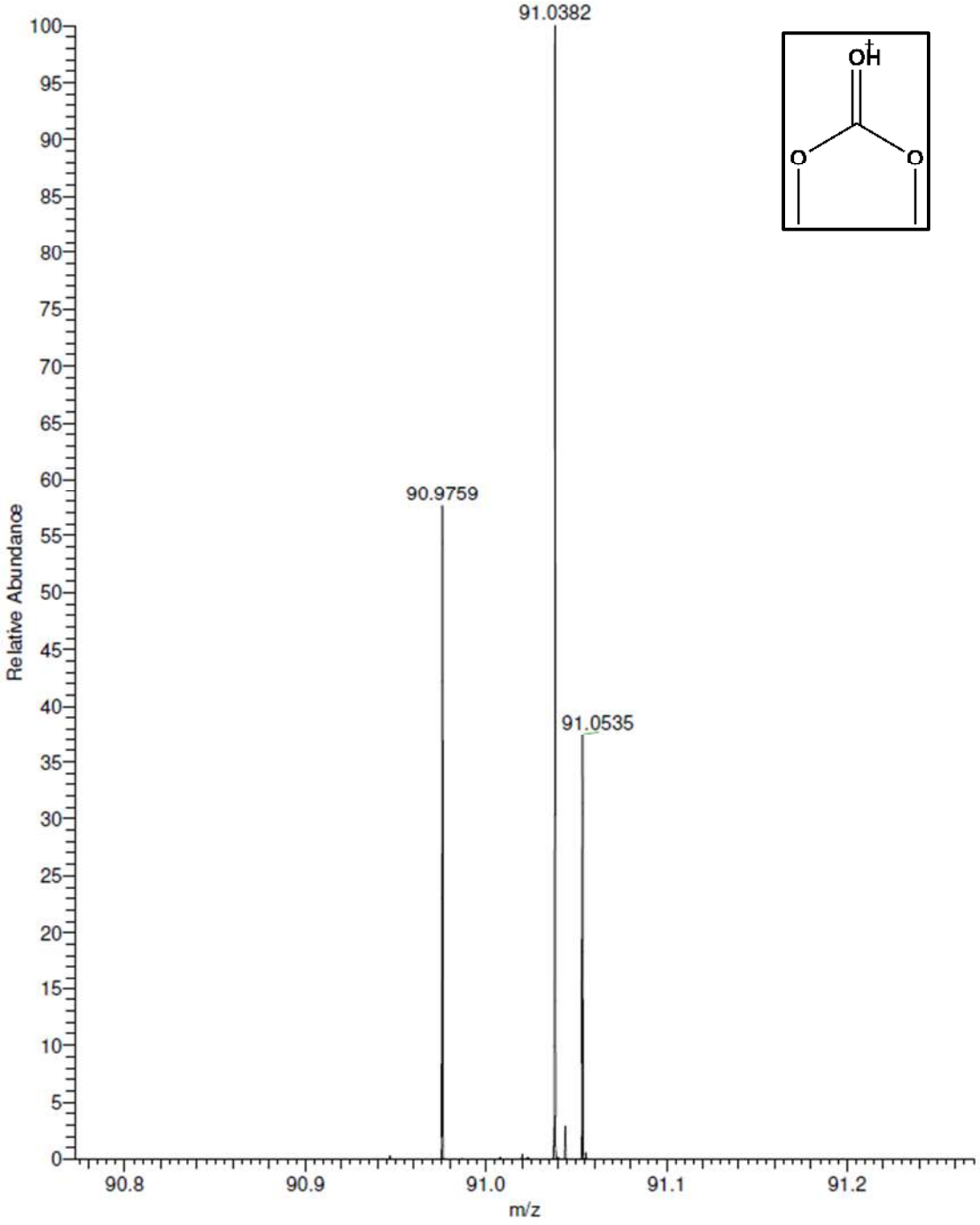

Fig. S46. The excerpt of high-resolution electron-spray ionization mass spectrogram (HR-ESI-MS) recorded on the reaction mixture during the course of the reaction of **4·La** with CO_2 gas in methanol in anhydrous conditions under Ar atmosphere at room temperature. The m/z value of 91.0382 correspond to the protonated form of dimethoxycarbonate.

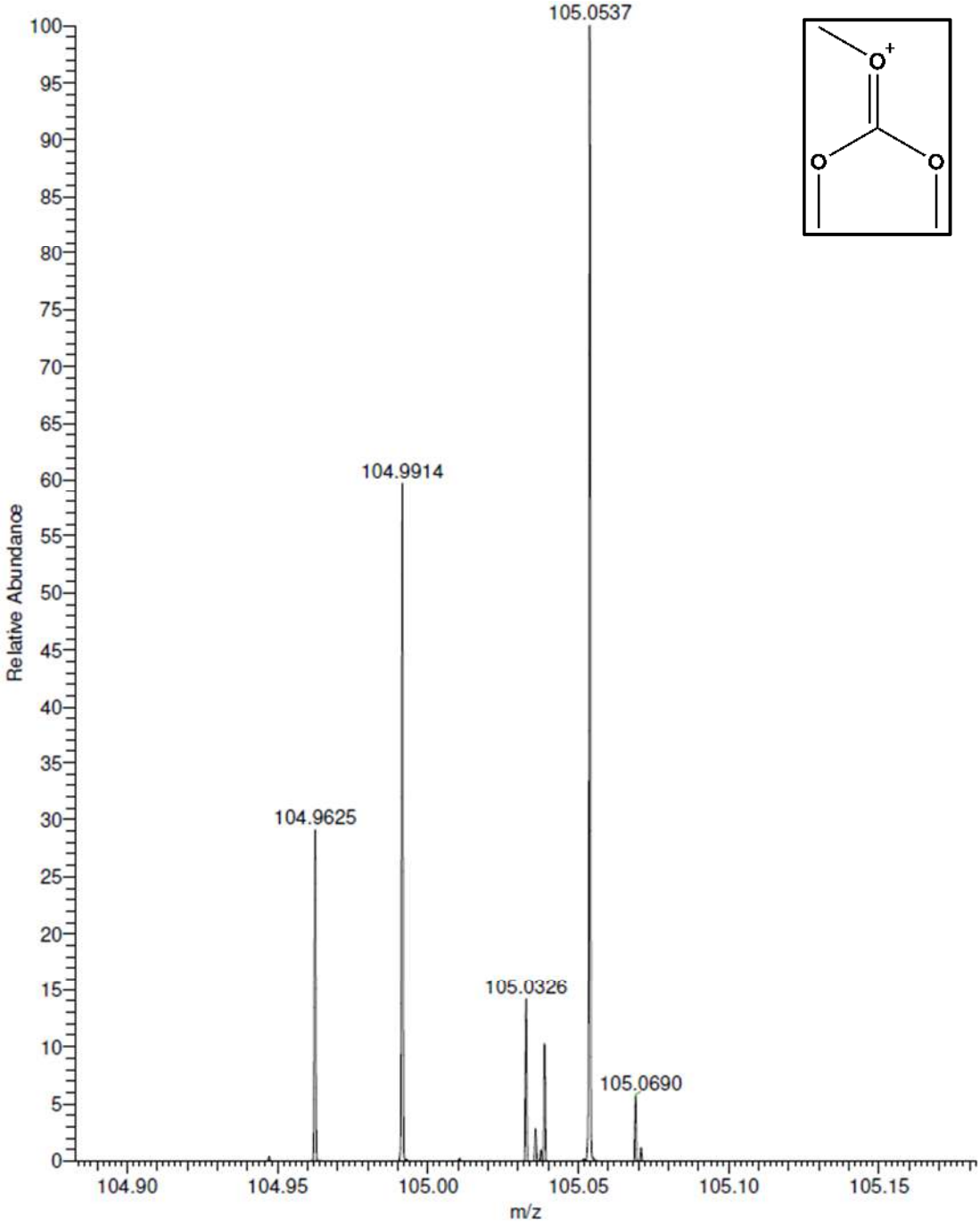

Fig. S47. The excerpt of high-resolution electron-spray ionization mass spectrogram (HR-ESI-MS) recorded on the reaction mixture during the course of the reaction of **4·La** with CO_2 gas in methanol in anhydrous conditions under Ar atmosphere at room temperature. The m/z value of 105.0537 correspond to the trimethoxycarbonium ion.

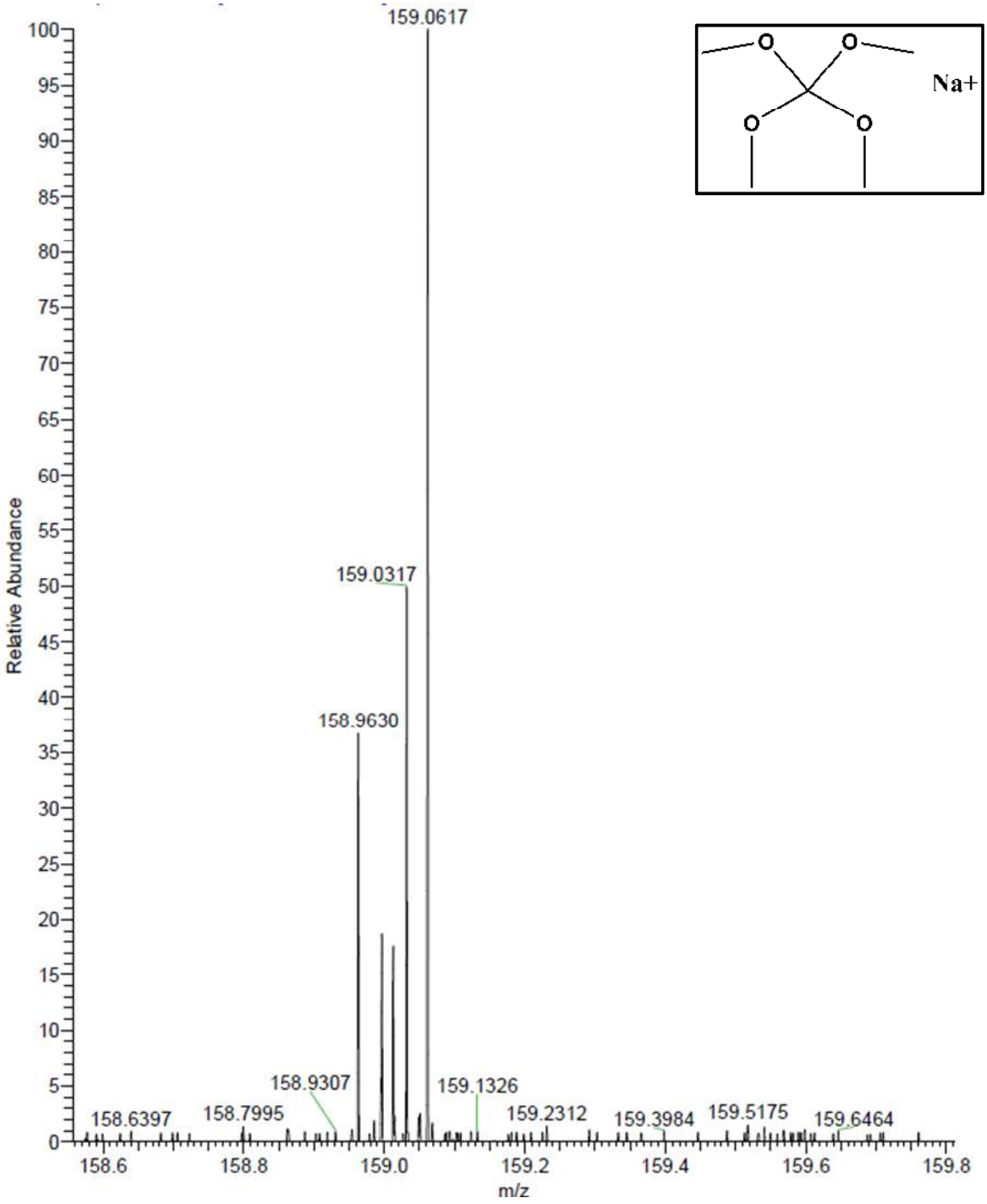

Fig. S48. The excerpt of high-resolution electron-spray ionization mass spectrogram (HR-ESI-MS) recorded on the reaction mixture during the course of the reaction of **4·La** with CO_2 gas in methanol in anhydrous conditions under Ar atmosphere at room temperature. The m/z value of 159.0617 sodiated form of tetramethoxymethane.

Table S7: Selected crystallographic data and refinement parameters for **10b·Y.**

	10b·Y
Formula*	$C_{55}H_{57}F_3N_{10}O_{13}SY_2$
Mr (g mol^{-1})*	1371.03
crystal system	Monoclinic
space group	C_2/c
T (K)	150
a (Å)	18.5467(8)
b (Å)	18.1073(7)
c (Å)	19.4790(7)
α (°)	90
β (°)	113.2300(10)
γ (°)	90
V (Å^3)	6011.3(4)
Z	4
$\rho_{calcd.}$ (g cm^{-3})	1.515
μ (mm^{-1})	2.039
collected reflns	79096
unique reflns	7604
No. of parameters	431
Reflns for Refinement	79096
R (I > 3σ(I))[a]	0.0492
wR (I > 3σ(I))[b]	0.1449
GOF on *F*	1.063

[a] $R = \Sigma||F_o| - |F_c||/\Sigma|F_o|$, [b] $wR = [\Sigma(w(F_o^2 - F_c^2)^2)/\Sigma([w(F_o^2)^2]^{1/2}$ where $w = 1/(\sigma^2(F_o^2) + (aP)^2 + bP)$ with $P = (2F_c^2 + \max(F_o^2,0))/3$.

*Including the squeezed out solvents.

Table S8. Selected bond lengths (Å) and bond angles (°) of the complex **10b·Y.**

Y1	O2	2.299(2)	N5	C10	1.326(4)	Y1	O3	2.351(2)	Y1	O1	2.254(2)
Y1	O4[1]	2.385(2)	Y1	O5	2.356(2)	Y1	N4	2.429(3)	Y1	N2	2.446(3)
Y1	N3	2.458(3)	Y1	C24	3.0456(4)	O2	C10	1.282(4)	O1	C17	1.288(4)
N1	N2	1.390(4)	N1	C17	1.319(4)	N4	N5	1.396(4)			

[1] 1-X,+Y,1/2-Z

O1	Y1	N2	65.28(9)	N4	Y1	N3	64.53(9)	N2	Y1	N3	64.65(9)
C17	N1	N2	109.5(3)	C10	N5	N4	108.8(3)	O2	Y1	N4	65.31(8)
C24	O3	Y1	103.76(12)								

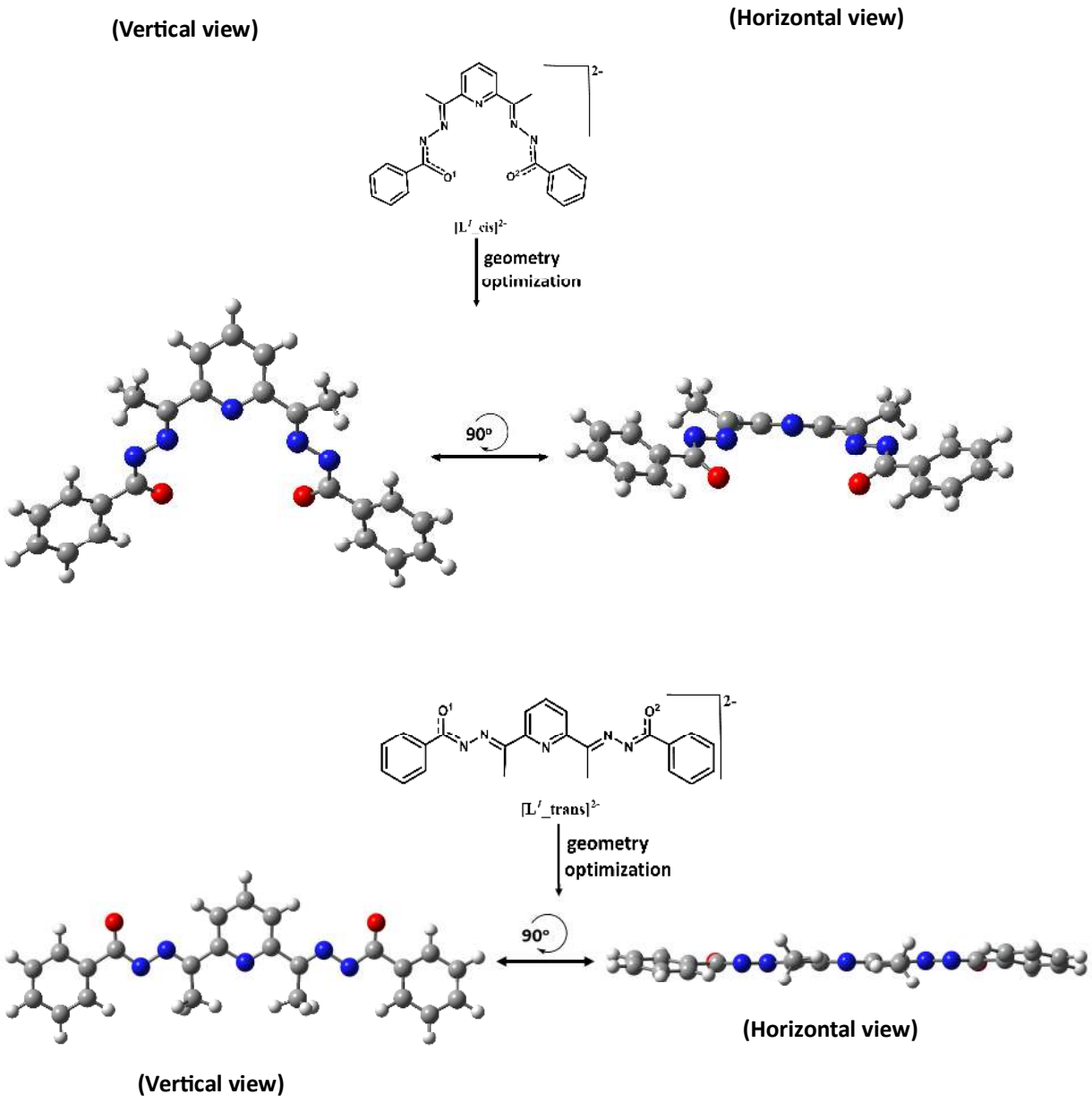

Fig. S49. The conventional *ChemDraw* structures as used for the initial guess for the energy optimization and the *ball-and-stick* model for the energy optimized geometries of the doubly deprotonated form of the ligand, $[\mathbf{L}^{I}]^{2-}$, in the gas phase under self-consistent MeOH for the cis form **(***top***)** and the trans form (*bottom*). The vertical views are those where the lines of eye-sight are perpendicular to the plane of pyridyl moiety of the structures, while the horizontal views are those where the lines of eye-sight are parallel to the plane of pyridyl moiety of the structures. Colour codes: red, O; blue, N; grey, C; light grey, H.

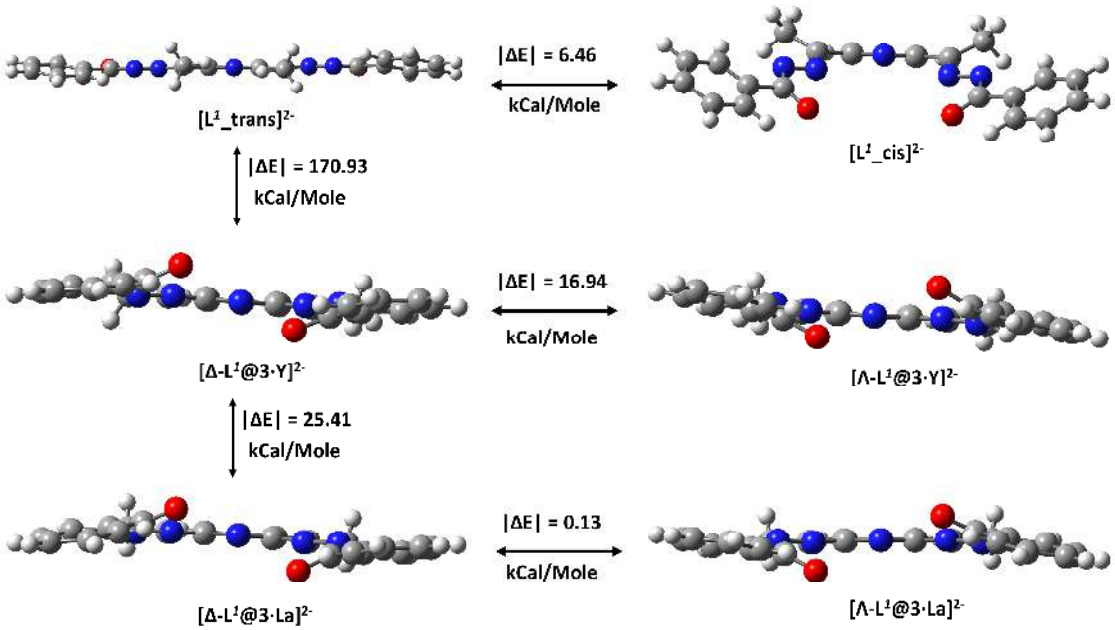

Fig. S50. Comparative horizontal views of the *ball-and-stick models* of the doubly deprotonated form of the ligand: [$\mathbf{L}^{\boldsymbol{1}}$**_trans**]$^{2-}$ - the energy optimized geometry of the trans isomer of [$\mathbf{L}^{\boldsymbol{1}}$]$^{2-}$; [$\mathbf{L}^{\boldsymbol{1}}$**_cis**]$^{2-}$ - the energy optimized geometry of the cis isomer of [$\mathbf{L}^{\boldsymbol{1}}$]$^{2-}$; [Δ-$\mathbf{L}^{\boldsymbol{1}}$**@3·Y**]$^{2-}$ - the conformation of [$\mathbf{L}^{\boldsymbol{1}}$]$^{2-}$ in the solid-state single-crystal X-ray molecular structure of the Δ-isomer of **3·Y**; [Δ-$\mathbf{L}^{\boldsymbol{1}}$**@3·La**]$^{2-}$ - the conformation of [$\mathbf{L}^{\boldsymbol{1}}$]$^{2-}$ in the solid-state single-crystal X-ray molecular structure of the Δ-isomer of **3·La**; [Λ-$\mathbf{L}^{\boldsymbol{1}}$**@3·Y**]$^{2-}$ - the conformation of [$\mathbf{L}^{\boldsymbol{1}}$]$^{2-}$ in the solid-state single-crystal X-ray molecular structure of the Λ-isomer of **3·Y**; and [Λ-$\mathbf{L}^{\boldsymbol{1}}$**@3·La**]$^{2-}$ - the conformation of [$\mathbf{L}^{\boldsymbol{1}}$]$^{2-}$ in the solid-state single-crystal X-ray molecular structure of the Λ-isomer of **3·La**. The value on a double-headed arrow corresponds to the energy difference between the two conformations of [$\mathbf{L}^{\boldsymbol{1}}$]$^{2-}$ on the both sides of the arrow. The relative energies of these conformations of [$\mathbf{L}^{\boldsymbol{1}}$]$^{2-}$ are portrayed on Fig.S63 below. Colour codes: red, O; blue, N; grey, C; light grey, H.

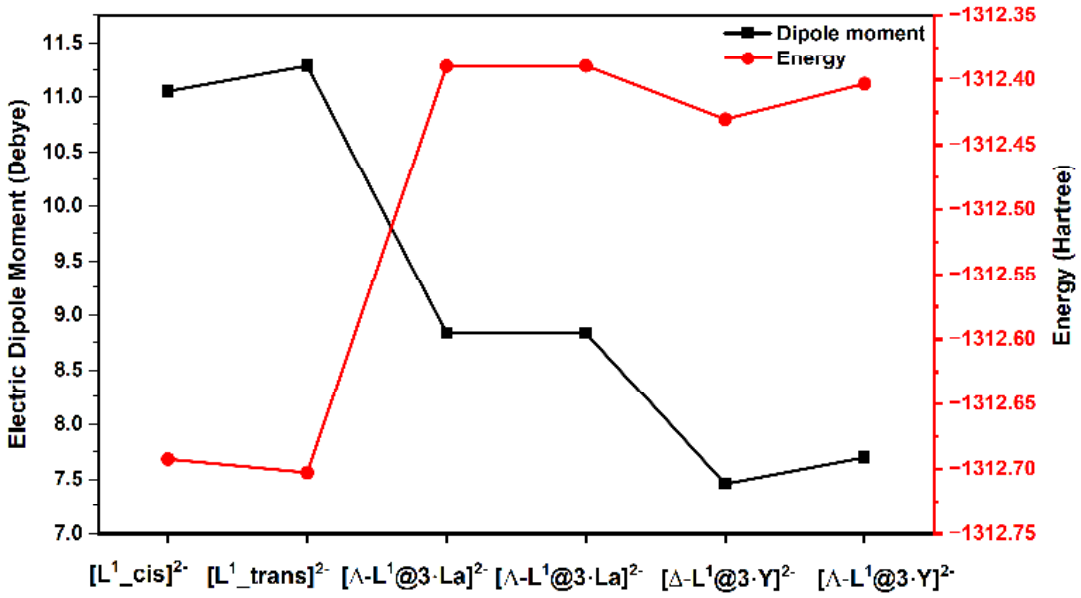

Fig. S51. The computed energies (in Hartree, red solid circles) and the computed electronic dipole moments (in Debye, black solid squares) at the level of the Density Functional Theory (DFT) for the doubly deprotonated forms of the ligand, $[\mathbf{L}^{I}]^{2-}$, at its energy optimized geometries (cis and trans) and at its different conformations in the solid state single-crystal X-ray molecular structures of the coordination polymers **3·Ln** (Ln = Y and La) as mentioned in the abscissa labels. See the experimental section for the computational details. While the energies correspond to the total electronic energies of $[\mathbf{L}^{I}]^{2-}$ at its optimized geometries and its different conformations in the solid-state molecular structures of the coordination polymers, the electronic dipole moments stand for the degrees of distortion of $[\mathbf{L}^{I}]^{2-}$ at its optimized geometries and its different conformations in the solid-state molecular structures of the coordination polymers.

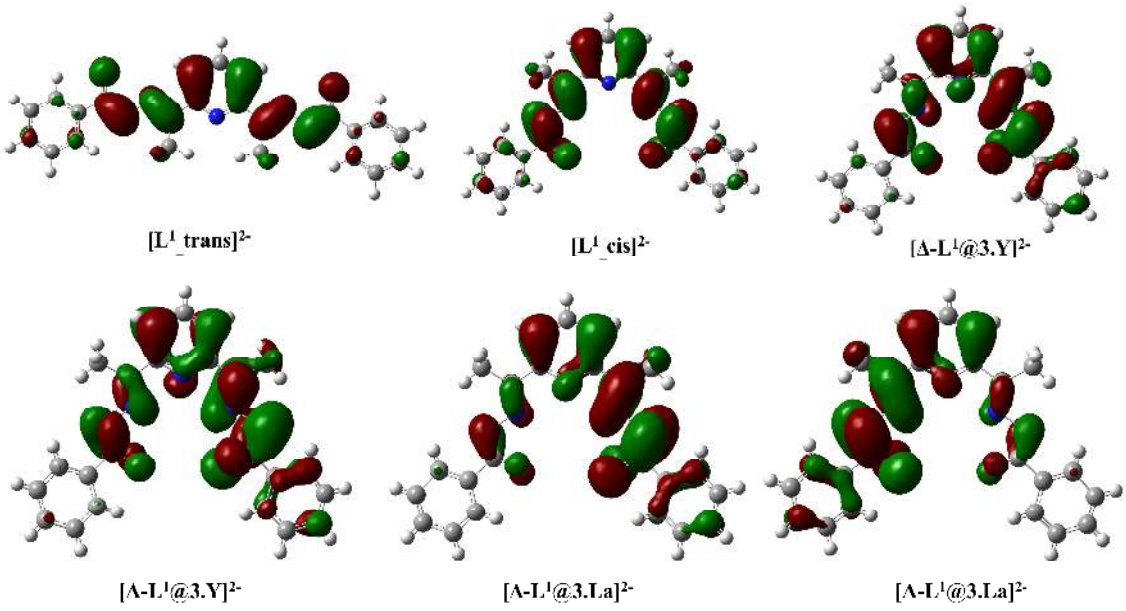

Fig. S52. The comparative horizontal views of the *ball-and-stick models* of the doubly deprotonated form of the ligand, $[\mathbf{L}^{\mathit{I}}]^{2-}$, along with the isosurfaces (isovalue = 0.02; the green and brown coloured surfaces representing the mutually opposite phases of the corresponding wave function) corresponding to the Highest Occupied Molecular Orbital (HOMO) for: $[\mathbf{L}^{\mathit{I}}\mathbf{\_trans}]^{2-}$ - the energy optimized geometry of the trans isomer of $[\mathbf{L}^{\mathit{I}}]^{2-}$; $[\mathbf{L}^{\mathit{I}}\mathbf{\_cis}]^{2-}$ - the energy optimized geometry of the cis isomer of $[\mathbf{L}^{\mathit{I}}]^{2-}$; $[\Delta\text{-}\mathbf{L}^{\mathit{I}}\mathbf{@3\cdot Y}]^{2-}$ - the conformation of $[\mathbf{L}^{\mathit{I}}]^{2-}$ in the solid-state single-crystal X-ray molecular structure of the Δ-isomer of **3·Y**; $[\Delta\text{-}\mathbf{L}^{\mathit{I}}\mathbf{@3\cdot La}]^{2-}$ - the conformation of $[\mathbf{L}^{\mathit{I}}]^{2-}$ in the solid-state single-crystal X-ray molecular structure of the Δ-isomer of **3·La**; $[\Lambda\text{-}\mathbf{L}^{\mathit{I}}\mathbf{@3\cdot Y}]^{2-}$ - the conformation of $[\mathbf{L}^{\mathit{I}}]^{2-}$ in the solid-state single-crystal X-ray molecular structure of the Λ-isomer of **3·Y**; and $[\Lambda\text{-}\mathbf{L}^{\mathit{I}}\mathbf{@3\cdot La}]^{2-}$ - the conformation of $[\mathbf{L}^{\mathit{I}}]^{2-}$ in the solid-state single-crystal X-ray molecular structure of the Λ-isomer of **3·La**. The relative energies of these HOMOs are portrayed on Fig.S65.

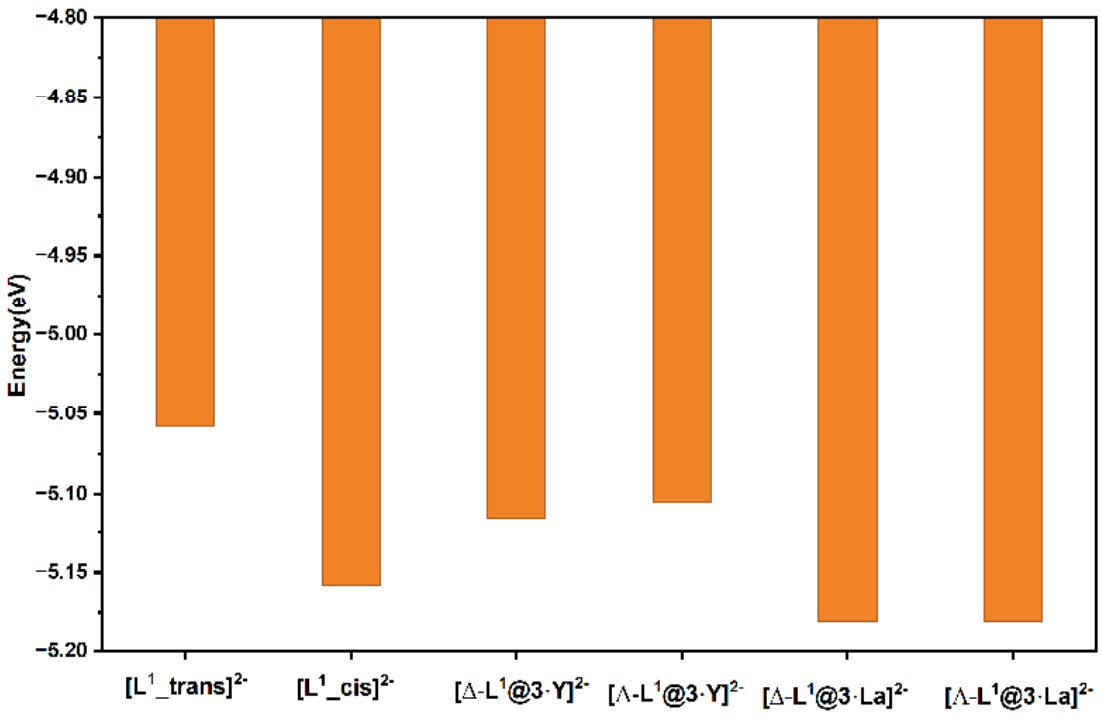

Fig. S53. The computed energies (in eV, orange solid bars) at the level of the Density Functional Theory (DFT) for the doubly deprotonated forms of the ligand, $[\mathbf{L}^{1}]^{2-}$, at its energy optimized geometries (cis and trans) and at its different conformations in the solid state single-crystal X-ray molecular structures of the coordination polymers **3·Ln** (Ln = Y and La) as mentioned in the abscissa labels.

Table S9: The relative atomic coordinates corresponding to the energy optimized geometries

$[L^1\_cis]^{2-}$

N	-0.000003	2.291038	0.137293
O	2.657012	-1.620387	-0.873519
N	3.632567	0.278298	0.088115
N	2.442100	0.931870	-0.112749
C	4.893330	-1.756517	-0.051994
C	6.009186	-1.165072	0.561238
C	1.162565	2.938673	-0.057889
C	3.607000	-1.000599	-0.312432
C	2.436775	2.197037	0.160147
C	1.198503	4.284006	-0.461457
H	2.142836	4.787709	-0.623334
C	4.981485	-3.102983	-0.432414
C	6.145200	-3.837960	-0.208625
H	6.190947	-4.879094	-0.510986
C	7.172921	-1.897495	0.784898
H	8.024482	-1.421535	1.260248
C	7.246973	-3.238099	0.400702
H	8.153682	-3.807773	0.575279
C	3.648283	2.952147	0.651978
H	3.387349	3.942118	1.026114
H	4.129736	2.391851	1.456978
H	4.397449	3.068571	-0.139905
C	-0.000001	4.953207	-0.673978
H	0.000001	5.986050	-1.005721
O	-2.656977	-1.620430	-0.873427
N	-3.632562	0.278287	0.088113
N	-2.442095	0.931860	-0.112753
C	-4.893321	-1.756530	-0.051966
C	-6.009203	-1.165056	0.561191
C	-1.162570	2.938670	-0.057903
C	-3.606975	-1.000628	-0.312373
C	-2.436782	2.197031	0.160120
C	-1.198506	4.284003	-0.461476
H	-2.142838	4.787702	-0.623370
C	-4.981464	-3.103011	-0.432338
C	-6.145192	-3.837974	-0.208572
H	-6.190929	-4.879120	-0.510894
C	-7.172951	-1.897466	0.784826
H	-8.024532	-1.421483	1.260118

C	-7.246991	-3.238085	0.400681
H	-8.153709	-3.807749	0.575239
C	-3.648302	2.952138	0.651927
H	-3.387384	3.942121	1.026041
H	-4.129750	2.391854	1.456940
H	-4.397466	3.068531	-0.139961
H	4.128151	-3.572756	-0.906215
H	-4.128111	-3.572805	-0.906082
H	5.957990	-0.126882	0.861647
H	-5.958016	-0.126855	0.861562

$[L^1\_trans]^{2-}$

N	-0.000002	0.073545	0.000059
O	5.872718	1.885282	-0.074127
N	4.684708	-0.132240	0.004264
N	3.532949	0.607033	0.005425
C	7.080075	-0.172748	0.011596
C	7.109635	-1.546708	0.298468
C	1.167073	0.745016	-0.024747
C	5.793853	0.622613	-0.018251
C	2.420787	-0.058001	-0.047936
C	1.201093	2.149434	-0.026796
H	2.150393	2.665942	-0.049114
C	8.294486	0.478498	-0.246912
C	9.501277	-0.219665	-0.227439
H	10.429065	0.302868	-0.436337
C	8.315346	-2.244138	0.325463
H	8.317759	-3.304774	0.554756
C	9.517239	-1.584310	0.060337
H	10.455475	-2.128728	0.079224
C	2.352628	-1.559888	-0.125672
H	1.324919	-1.901439	-0.223360
H	2.936970	-1.925317	-0.975530
H	2.789790	-2.011954	0.771308
C	0.000003	2.846086	0.000031
H	0.000006	3.931304	0.000025
O	5.872726	1.885286	0.074021
N	-4.684708	-0.132240	-0.004098
N	-3.532952	0.607037	-0.005305
C	-7.080074	-0.172753	-0.011638
C	-7.109599	-1.546735	-0.298415

C	-1.167075	0.745021	0.024845
C	-5.793856	0.622610	0.018314
C	-2.420790	-0.057993	0.048086
C	-1.201089	2.149439	0.026873
H	-2.150387	2.665951	0.049193
C	-8.294519	0.478512	0.246666
C	-9.501308	-0.219652	0.227092
H	-10.429121	0.302896	0.435834
C	-8.315307	-2.244166	-0.325511
H	-8.317691	-3.304819	-0.554727
C	-9.517234	-1.584318	-0.060586
H	-10.455467	-2.128738	-0.079551
C	-2.352632	-1.559876	0.125887
H	-1.324922	-1.901425	0.223578
H	-2.789805	-2.011983	-0.771067
H	-2.936963	-1.925266	0.975769
H	-6.180848	-2.063308	-0.502727
H	6.180909	-2.063266	0.502937
H	8.288463	1.538927	-0.468387
H	-8.288523	1.538957	0.468063

$[\Delta\text{-}L^1\ @3{\cdot}Y]^{2-}$

O	-1.960430	-1.188383	0.949959
N	2.178444	1.163773	-0.022526
N	0.005990	2.559961	-0.017805
O	1.926099	-1.239987	-0.917548
N	-2.195680	1.154027	-0.003737
N	-3.330815	0.376004	-0.098865
N	3.316221	0.337126	0.076771
C	-1.168217	3.230123	0.024547
C	2.392342	2.405594	-0.036380
C	-3.701317	3.097574	-0.032610
C	1.157381	3.242008	0.015084
C	-3.079303	-0.847353	0.373743
C	3.073954	-0.884198	-0.367267
C	-3.740990	-3.220737	0.123199
H	-2.831072	-3.473708	0.231593
C	3.723945	-3.213018	-0.040831
H	2.808877	-3.457248	-0.095298
C	4.108029	-1.875531	-0.159764
C	-4.112889	-1.853338	0.194852

C	-2.382005	2.434202	-0.001359
C	1.220977	4.624113	0.028031
H	2.050262	5.084446	0.032977
C	-5.462647	-1.527714	-0.022210
H	-5.733624	-0.617864	-0.004716
C	-1.137454	4.639796	0.032915
H	-1.963831	5.110958	0.038062
C	-4.696950	-4.180602	-0.100968
H	-4.441392	-5.094253	-0.152366
C	6.046030	-3.838023	0.275008
H	6.711713	-4.496201	0.440160
C	4.716793	-4.195034	0.158506
H	4.468997	-5.110483	0.214769
C	5.429190	-1.503783	-0.059313
H	5.684269	-0.590107	-0.126130
C	3.750624	3.065921	-0.009673
H	3.983964	3.294221	0.913672
H	3.726321	3.882856	-0.551992
H	4.419228	2.451091	-0.375101
C	-6.413249	-2.535300	-0.266703
H	-7.319917	-2.305991	-0.439299
C	6.396033	-2.505837	0.144983
H	7.312908	-2.261961	0.194659
C	-0.034069	5.327945	0.032834
H	-0.054099	6.276827	0.036087
C	-6.024575	-3.830291	-0.253432
H	-6.677181	-4.514258	-0.351915
H	-3.566870	4.159094	-0.032666
H	-4.226982	2.804589	-0.917333
H	-4.265841	2.809603	0.829530

[Λ-L^{1} @3·Y]$^{2-}$

O	1.961111	-1.187712	0.949881
N	-2.178354	1.163408	-0.022510
N	-0.006243	2.560136	-0.017906
O	-1.925420	-1.240296	-0.917414
N	2.195776	1.154749	-0.003835
N	3.331100	0.377008	-0.098860
N	-3.315917	0.336479	0.076598
C	1.167793	3.230590	0.024537
C	-2.392561	2.405176	-0.036372

C	3.700925	3.098670	-0.032627
H	4.378187	2.467372	-0.351950
H	3.664779	3.871714	-0.634826
H	3.936350	3.401018	0.870318
C	-1.157799	3.241897	0.014882
C	3.079898	-0.846409	0.373658
C	-3.073361	-0.884788	-0.367132
C	3.742169	-3.219630	0.123230
H	2.832319	-3.472827	0.231529
C	-3.722768	-3.213767	-0.040776
H	-2.807635	-3.457770	-0.095344
C	-4.107180	-1.876376	-0.159818
C	4.113733	-1.852138	0.194772
C	2.381779	2.434970	-0.001366
C	-1.221748	4.623986	0.028018
H	-2.051142	5.084113	0.032863
C	5.463404	-1.526180	-0.022198
H	5.734156	-0.616263	-0.004711
C	1.136680	4.640256	0.032894
H	1.962935	5.111623	0.038134
C	4.698371	-4.179259	-0.101032
H	4.443035	-5.092974	-0.152323
C	-6.044692	-3.839347	0.274975
H	-6.710215	-4.497689	0.440234
C	-4.715367	-4.196029	0.158471
H	-4.467348	-5.111415	0.214840
C	-5.428443	-1.504956	-0.059165
H	-5.683744	-0.591344	-0.126089
C	-3.751007	3.065165	-0.009667
H	-3.984397	3.293414	0.913578
H	-3.726914	3.882102	-0.551891
H	-4.419455	2.450167	-0.375187
C	6.414256	-2.533532	-0.266686
H	7.320862	-2.303999	-0.439186
C	-6.395032	-2.507249	0.145041
H	-7.311967	-2.263600	0.194718
C	0.033128	5.328130	0.032712
H	0.052918	6.277017	0.036057
C	6.025909	-3.828619	-0.253503
H	6.678685	-4.512425	-0.351983

[Δ-L^1 @3·La]$^{2-}$

O	2.159109	-1.312173	-0.900025
O	-2.130566	-1.327851	0.958408
N	-2.269914	1.107794	0.077487
N	2.254327	1.110878	-0.003024
N	3.449352	0.350855	0.074959
N	-3.468387	0.324592	0.006730
N	-0.018462	2.492192	0.036702
C	2.391599	2.405592	-0.026203
C	3.213137	-0.884120	-0.341551
C	-2.424697	2.369211	0.018366
C	-3.231276	-0.888234	0.410260
C	1.162710	3.167436	-0.015646
C	4.346168	-1.847604	-0.129168
C	3.701748	3.103391	-0.040397
H	3.840609	3.552574	0.819928
H	3.709898	3.767852	-0.760498
H	4.417855	2.451686	-0.187959
C	-1.177870	3.179354	0.000186
C	-4.333167	-1.843607	0.201972
C	-4.003985	-3.231150	0.127610
H	-3.116267	-3.527327	0.292762
C	4.014245	-3.233711	-0.098681
H	3.130068	-3.544403	-0.242880
C	5.051717	-4.085051	0.151544
H	4.859407	-5.011626	0.252884
C	-3.765459	3.106911	0.027861
H	-4.493940	2.461595	-0.094548
H	-3.783571	3.760671	-0.701920
H	-3.878820	3.568465	0.883996
C	5.654930	-1.435466	-0.051764
H	5.887809	-0.522460	-0.172839
C	6.640622	-2.399063	0.210652
H	7.539648	-2.130841	0.353265
C	1.230918	4.586079	-0.034818
H	2.054538	5.056317	-0.034698
C	6.315902	-3.689268	0.261553
H	7.000795	-4.338404	0.377610
C	-5.622709	-1.428814	0.012914
H	-5.865214	-0.512108	0.091653
C	-1.190187	4.543415	-0.012237

H	-2.018597	5.007114	0.007742
C	-4.990894	-4.123528	-0.188051
H	-4.772017	-5.039650	-0.305590
C	-0.019224	5.248058	-0.052663
H	-0.046165	6.197091	-0.094291
C	-6.315678	-3.703242	-0.339284
H	-6.999775	-4.350765	-0.461458
C	-6.617443	-2.456126	-0.313668
H	-7.509667	-2.192554	-0.512929

[Λ-L^{1} @3·Y]$^{2-}$

O	-2.159046	-1.312174	-0.900046
O	2.130551	-1.327931	0.958383
N	2.269924	1.107857	0.077566
N	-2.254395	1.110895	-0.003041
N	-3.449283	0.350856	0.074943
N	3.468315	0.324591	0.006806
N	0.018479	2.492261	0.036687
C	-2.391602	2.405530	-0.026215
C	-3.213072	-0.884118	-0.341570
C	2.424774	2.369193	0.018350
C	3.231201	-0.888237	0.410233
C	-1.162632	3.167430	-0.015657
C	-4.346187	-1.847659	-0.129089
C	-3.701750	3.103333	-0.040406
H	-3.840528	3.552575	0.819921
H	-3.709899	3.767797	-0.760406
H	-4.417778	2.451691	-0.187969
C	1.177809	3.179360	0.000171
C	4.333149	-1.843693	0.201943
C	4.003961	-3.231234	0.127678
H	3.116244	-3.527408	0.292730
C	-4.014248	-3.233627	-0.098706
H	-3.130153	-3.544382	-0.242908
C	-5.051803	-4.085025	0.151517
H	-4.859416	-5.011541	0.252855
C	3.765477	3.106968	0.027844
H	4.493957	2.461650	-0.094568
H	3.783590	3.760730	-0.701835
H	3.878821	3.568379	0.883981
C	-5.654867	-1.435457	-0.051782
H	-5.887823	-0.522510	-0.172855

C	-6.640622	-2.398972	0.210632
H	-7.539586	-2.130826	0.353247
C	-1.230974	4.586093	-0.034827
H	-2.054534	5.056254	-0.034604
C	-6.315928	-3.689317	0.261629
H	-7.000881	-4.338372	0.377584
C	5.622771	-1.428843	0.012985
H	5.865279	-0.512138	0.091727
C	1.190210	4.543480	-0.012248
H	2.018601	5.007037	0.007832
C	4.990868	-4.123615	-0.188086
H	4.771988	-5.039736	-0.305627
C	0.019250	5.248128	-0.052671
H	0.046114	6.197101	-0.094297
C	6.315673	-3.703193	-0.339320
H	6.999688	-4.350779	-0.461497
C	6.617443	-2.456079	-0.313702
H	7.509587	-2.192569	-0.512964

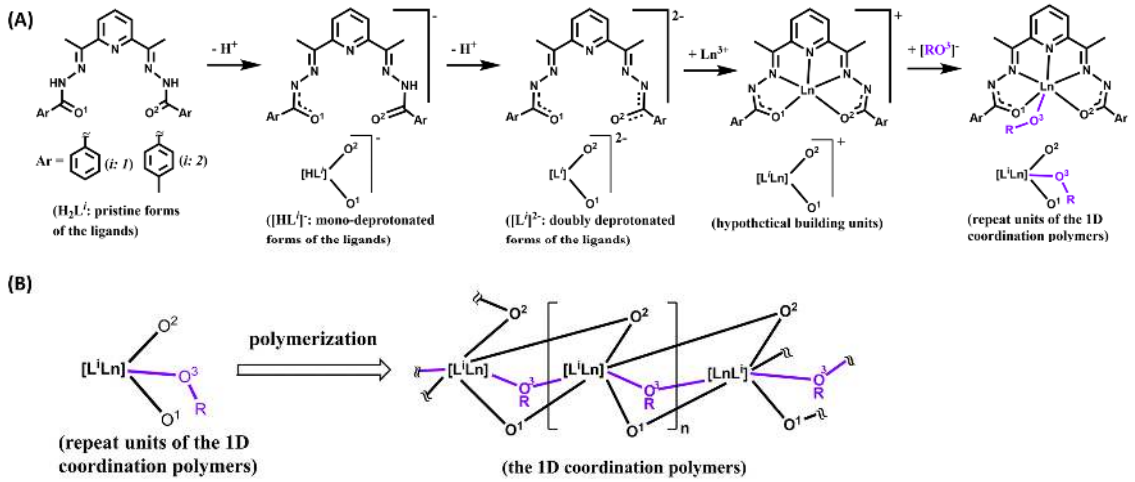

Scheme S6. (***A***) – The schematic representation for the *step-by-step* formation of the singly deprotonated form ($[\mathbf{HL}^{i}]^{-}$), doubly deprotonated form ($[\mathbf{L}^{i}]^{2-}$) of the generalized pentadentate chelating ligands form their pristine forms (**H_2L**), the hypothetical Ln(III)-based mono-cationic pentagonal planar building blocks ($[\mathbf{(L}^{i}\mathbf{)Ln}]^{+}$), and the neutral building blocks ($[\mathbf{(L}^{i}\mathbf{)Ln(OR)}]$) that are formed upon coordination of the anionic ancillary ligands $[\mathbf{RO}]^{-}$ with the cationic pentagonal building blocks $[\mathbf{(L}^{i}\mathbf{)Ln}]^{+}$ to result in the repeat units for the 1D coordination polymers. The diagrams below each of the conventional *ChemDraw* structures are the simplified *ChemDraw* representations for the corresponding chemical composites. The colour codes are the eye-guides to distinguish the segments from the ancillary ligands (*purple in colour*) from the segments from the basis building blocks (*grey in colour*) in a chemical composite or in a molecular structure. The O atomic centres of the pentadentate chelating ligands are labelled as O1 and O2, while the O atomic centres of the ancillary ligands are labelled as O3 in a chemical composite or in a molecular structure for convenient mechanistic understanding. (***B***) – the hypothetical schematic representation for the formation of the 1D coordination polymers $[\mathbf{(L}^{i}\mathbf{)Ln(OR)}]_n$ from the neutral building blocks $[\mathbf{(L}^{i}\mathbf{)Ln(OR)}]$. The 1D coordination polymers, $[\mathbf{(L}^{i}\mathbf{)Ln(OR)}]_n$, and the neutral building blocks, $[\mathbf{(L}^{i}\mathbf{)Ln(OR)}]$, are depicted with the simplified *ChemDraw* representations.

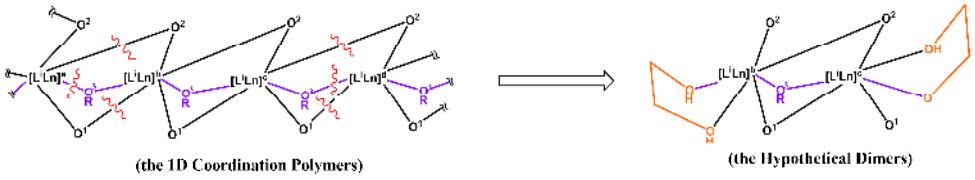

(C)

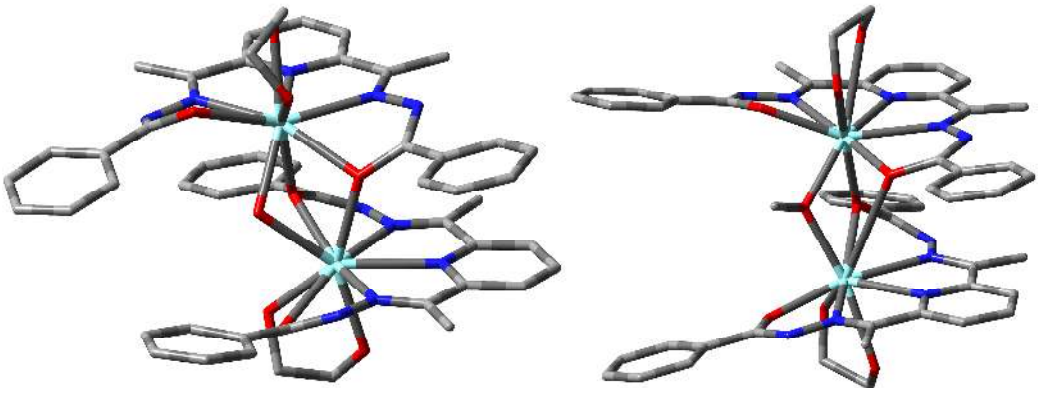

Scheme S7. (***A***) – The simplified *ChemDraw* representations for the 1D coordination polymers, $[(\mathbf{L}^{i})\mathbf{Ln(OR)}]_n$. The colour codes are the eye-guides to distinguish the segments from the ancillary ligands (*purple in colour*) from the segments from the basis building blocks (*grey in colour*). The O atomic centres of the pentadentate chelating ligands are labelled as O1 and O2, while the O atomic centres of the ancillary ligands are labelled as O3 in a chemical composite or in a molecular structure for convenient mechanistic understanding. The curly red solid lines stand for the cleavage of the chemical bonds to generate the hypothetical dinuclear segments of the coordination polymers. (***B***) – the simplified *ChemDraw* representations for the hypothetical dinuclear model complexes that could mimic the chemical reactivity of the coordination polymers. The segments in black and purple colours were kept as such in the molecular structure of the coordination polymers. The segments in orange colour were amended to obtain the chemically realistic and computationally economic models. The labels *a-d* on the pentagonal building blocks, $[(\mathbf{L}^{i})\mathbf{Ln}]$, in the simplified *ChemDraw* representations are the eye-guides to distinguish different Ln centres in the dinuclear model complexes or in the coordination polymers. (***C***)-(***D***) – the *capped-sticks* models of the molecular structures of the hypothetical dinuclear model complexes $[(\mathbf{L}^{1})\mathbf{Y(OH)(OCH_2CH_2OH)(HOCH_2CH_2OH)}]$ (***C***) and $[(\mathbf{L}^{1})\mathbf{Y(OMe)(OCH_2CH_2OH)(HOCH_2CH_2OH)}]$ (***D***) which represent the mimicking model chemical composites of the coordination polymers **3**·**Y** and **4**·**Y**, respectively. The H atoms are omitted in the figures for clarity. The geometries of these dinuclear model complexes were used as the initial *input* geometries for the computational analyses at the level DFT (see the experimental computational section for details). Colour codes: cyan, Y; red, O; blue, N; grey, C.

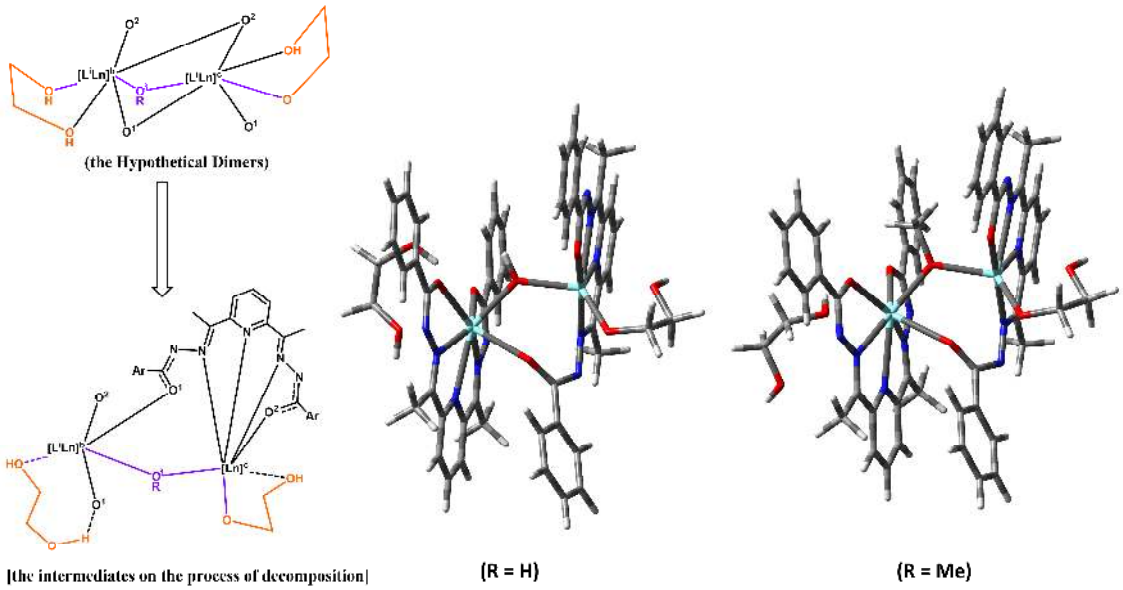

Scheme S8. (***A***) – The simplified *ChemDraw* representations for the hypothetical dinuclear model complexes that could mimic the chemical reactivity of the coordination polymers. The segments in black and purple colours were kept as such in the molecular structure of the coordination polymers. The segments in orange colour were amended to obtain the chemically realistic and computationally economic models. The labels *b-c* on the pentagonal building blocks, [**(L^i)Ln**], in the simplified *ChemDraw* representations are the eye-guides to distinguish different Ln centres in the dinuclear model complexes or in the coordination polymers. These dinuclear model complexes were used as the initial *input* chemical composites for the computational analyses at the level DFT. (***B***) – the *ChemDraw* representations for the intermediates at the break-down divergence during the energy optimization of the hypothetical dinuclear model complexes. The labels and the colour codes remain the same as above. (***C***)-(***D***) – the *capped-sticks* models of the intermediates at the break-down divergence during the energy optimization of the hypothetical dinuclear model complexes **[(L^1)Y(OH)(OCH$_2$CH$_2$OH)(HOCH$_2$CH$_2$OH)]** (***C***) and **[(L^1)Y(OMe)(OCH$_2$CH$_2$OH)(HOCH$_2$CH$_2$OH)]** (***D***). Colour codes: cyan, Y; red, O; blue, N; grey, C; light grey, H.

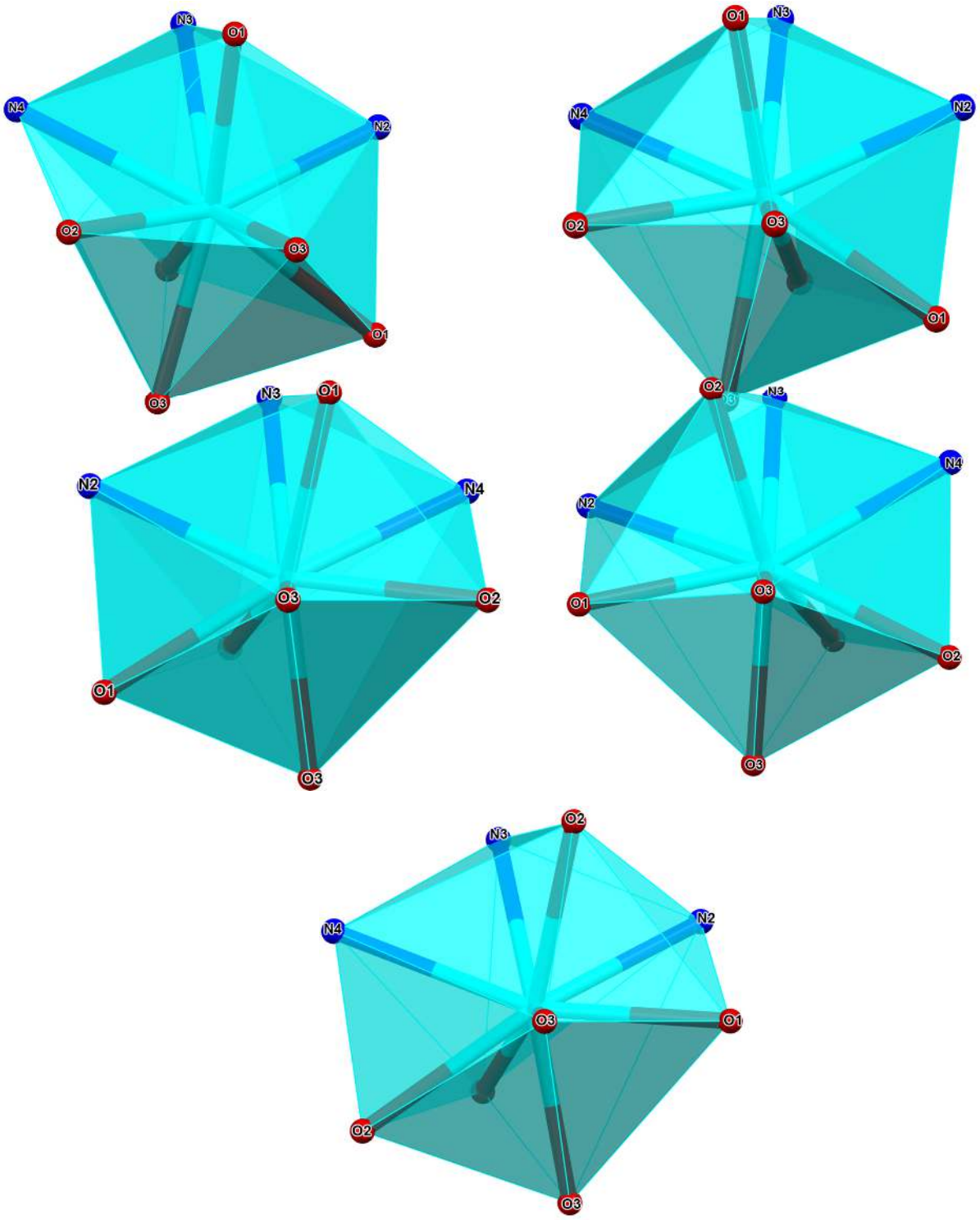

Fig. S54. The coordination polyhedra around the Ln centre of the coordination polymers **3·La** (*top left*), **3·Y** (*top right*), **4·La** (*middle left*), **5·La** (*middle right*) and **6·La** (*bottom*). The labels of the coordinating atoms are as per the atomic labels in the crystallographic Tables of the corresponding complexes.

Table S10. The outputs from the *Continuous Shape Measures* (CShM's) analyses employing the SHAPE program based on the Pinsky-Avnir algorithm for the calculation of continuous shape measures for the **3·La-6·La and 3·Y** nona-coordinated fragments around the Ln centers in the complexes with highlighted closest geometry (minimal distortion paths values) for each metal center.

Complex **3·La**

Metal Centre Polyhedron*	**La1**
EP-9	28.732
OPY-9	23.650
HBPY-9	17.411
JTC-9	15.435
JCCU-9	5.806
CCU-9	4.500
JCSAPR-9	5.436
CSAPR-9	4.714
JTCTPR-9	4.422
TCTPR-9	4.706
JTDIC-9	11.966
HH-9	6.007
MFF-9	**4.173**

Complex **4·La**

Metal Centre Polyhedron*	**La1**
EP-9	28.665
OPY-9	23.487
HBPY-9	17.607
JTC-9	15.642
JCCU-9	6.057
CCU-9	4.637
JCSAPR-9	5.649
CSAPR-9	4.841
JTCTPR-9	4.554
TCTPR-9	4.830
JTDIC-9	12.226
HH-9	6.172
MFF-9	**4.231**

Complex **5·La**

Metal Centre Polyhedron*	**La1**
EP-9	29.173
OPY-9	23.491
HBPY-9	17.144
JTC-9	15.261
JCCU-9	5.879
CCU-9	4.495
JCSAPR-9	5.406
CSAPR-9	4.611
JTCTPR-9	4.509
TCTPR-9	4.584
JTDIC-9	11.507
HH-9	5.531
MFF-9	**3.938**

Complex **6·La**

Metal Centre Polyhedron*	**La1**
EP-9	28.675
OPY-9	23.111
HBPY-9	17.641
JTC-9	15.393
JCCU-9	6.105
CCU-9	4.681
JCSAPR-9	5.600
CSAPR-9	4.784
JTCTPR-9	4.551
TCTPR-9	4.776
JTDIC-9	12.033
HH-9	6.142
MFF-9	**4.147**

Complex **3·Y**

Metal Centre Polyhedron*	**La1**
EP-9	29.894
OPY-9	24.226
HBPY-9	16.910
JTC-9	16.018
JCCU-9	5.719
CCU-9	4.433
JCSAPR-9	5.002
CSAPR-9	4.200
JTCTPR-9	4.086

TCTPR-9	4.050
JTDIC-9	12.301
HH-9	5.954
MFF-9	**3.841**

* EP-9: Enneagon (D9h); OPY-9: Octagonal pyramid(C8v); HBPY-9: Heptagonal bipyramid(D7h); JTC-9: Johnson triangular cupola J3(C3v); JCCU-9: Capped cube J8(C4v); CCU-9: Spherical-relaxed capped cube (C4v); JCSAPR-9: Capped square antiprism J10(C4v); CSAPR-9: Spherical capped square antiprism(C4v); JTCTPR-9: Tricapped trigonal prism J51(D3h); TCTPR-9: Spherical tricapped trigonal prism (D3h); JTDIC-9: Tridiminished icosahedron J63(C3v); HH-9: Hula-hoop (C2v); MFF-9: Muffin(Cs)

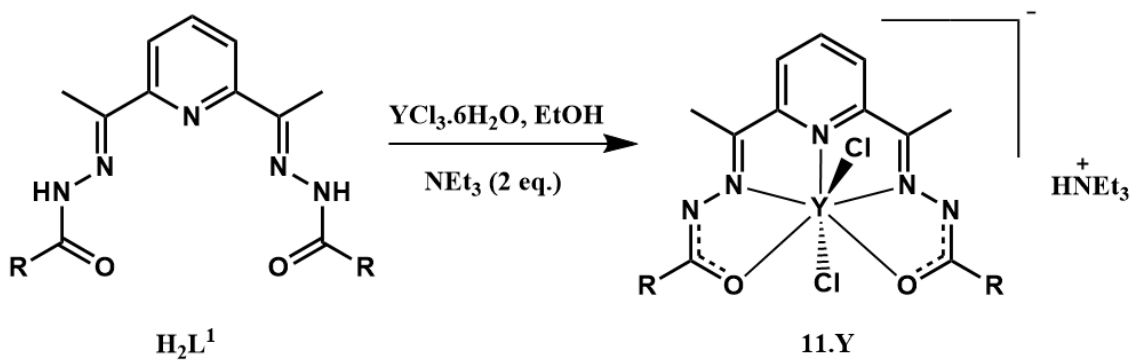

Scheme S9: Schematic representation for the synthesis of the heptacoordinate mononuclear complex **11·Y**.

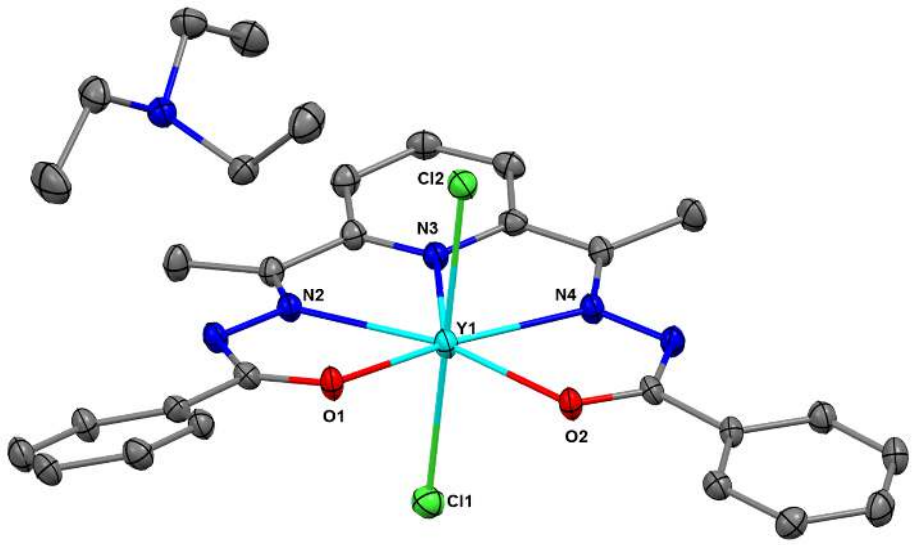

Fig. S55. ORTEP representations with 40% ellipsoid probability for the solid-state single crystal X-ray molecular structure of **11·Y**. The H atoms and the co-crystallized solvent molecules are omitted for clarity. Color codes: cyan, Y; green, Cl; red, O; blue, N; and grey, C.

Table S11. Selected crystallographic data and refinement parameters for the complex **11·Y.**

	11·Y
Formula	$C_{31}H_{41}Cl_2N_6O_3Y_2$
Mr (g mol^{-1})	705.51
crystal system	Triclinic
space group	P-1
T (K)	150
a (Å)	8.5659(5)
b (Å)	11.7521(7)
c (Å)	16.3880(10)
α (°)	92.739(2)
β (°)	93.857(2)
γ (°)	96.821(2)
V (Å^3)	1631.76(17)
Z	2
$\rho_{calcd.}$ (g cm^{-3})	1.436
μ (mm^{-1})	1.992
collected reflns	62136
unique reflns	6692
No. of parameters	395
Reflns for Refinement	62136
R (I > 3σ(I))[a]	0.0380
wR (I > 3σ(I))[b]	0.1095
GOF on *F*	1.023

[a] $R = \Sigma||F_o| - |F_c||/\Sigma|F_o|$, [b] $wR = [\Sigma(w(F_o^2 - F_c^2)^2)/\Sigma([w(F_o^2)^2]^{1/2}$ where $w = 1/(\sigma^2(F_o^2) + (aP)^2 + bP)$ with $P = (2F_c^2 + \max(F_o^2,0))/3$.

Table S12. Selected bond lengths (Å) and bond angles (°) of the complex **11·Y.**

Y1 Cl2	2.6243(8)	Y1 Cl1	2.6210(8)	Y1 O2	2.2700(19)	Y1 O1	2.2787(18)
Y1 N4	2.435(2)	Y1 N2	2.451(2)	Y1 N3	2.453(2)	O2 C10	1.287(3)
O1 C17	1.274(3)						

O1 Y1 N2	65.09(7)	N2 Y1 N3	64.51(7)	N4 Y1 N3	64.45(7)
O2 Y1 N4	65.56(7)	Cl1 Y1 Cl2	178.78(3)	C17 N1 N2	109.4(2)
C10 N5 N4	109.2(2)				

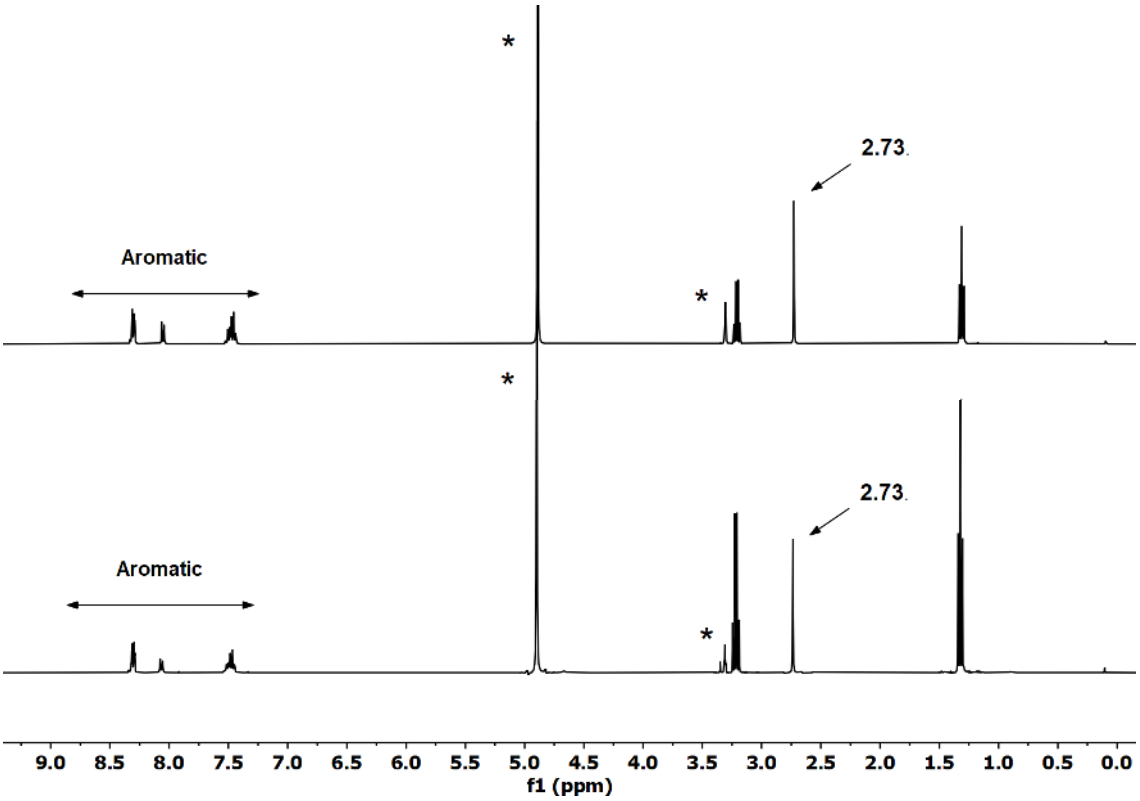

Fig. S56. The comparative room temperature solution ^{1}H NMR spectra of: ***Top*** – the ^{1}H NMR spectrum recorded on the CD_3OD solution of the isolated polycrystalline sample of **11·Y**; ***Bottom*** – the ^{1}H NMR spectrum recorded on the reaction mixture which was obtained upon treatment of the isolated polycrystalline sample of **11·Y** with CO_2 gas in CD_3OD medium after stirring at room temperature for 6h under Ar atmosphere. The solvent peaks / grease are indicated by asterisks. The characteristic signals corresponding to the CH_3 moieties of the imine functionality of the ligand ($\delta_{CH_3}(imine$, ppm)) in **11·Y** are labelled with the chemical shift values. No visible change in the spectral patterns implied the inertness of **11·Y** towards CO_2 gas in CD_3OD at room temperature.

Mechanistic Proposition: For simplicity, the building-blocks and the CPs are abbreviated to the generic structures as shown in Scheme S7 (see ESI). Segments with four consecutive Ln centers of the CPs were considered for easy understanding of the mechanistic aspects. A conventional portrayal for the rational flow of electrons during the course of the reactions is provided step-wise in ESI (Schemes S11-S17). As discussed earlier, **11·Y** exhibited inertness towards CO_2 despite it having relatively lower coordinate Ln center and more accessibility for CO_2 towards the Ln center in contrast to the CPs. One could presume that the close proximity of the Lewis acidic (Ln(III)) and basic (μ_2-OH/OMe) centers in the CPs plays a pivotal role in this regard. Obviously, the oxygen atoms (O^3) of the bridging ancillary ligands (μ_2-OH/OMe) are the most electron-rich centers, while the Ln centers being the most electron deficient centers in the CPs (Scheme S11). Thus, one of the oxygen atoms of a CO_2 molecule could approach the Ln center in one of the building blocks of any two consecutive Ln centers of the CPs – ca. either $[L^iLn]^a$ or $[L^iLn]^b$ of the first two consecutive Ln centers as depicted in Scheme S11. At the same time, O^3 approaches the carbon center of the CO_2 molecule - leading to a transition state (***TS1*** or ***TS1′***), which could eventually transform into several intermediates, such as ***I1*** - ***I4*** (or, ***I1′*** - ***I4′***; Scheme S11). Notably, it's obvious that the transformation of ***TS1*** (or ***TS1′***) into ***I1*** (or ***I1′***) requires significant mechanical movements of the backbone of the CPs (Scheme S11). Consequently, one could anticipate high resistivity of the CPs towards CO_2 in their solid-state matrix or in their crystal-packing. It is indeed evidenced from the experimental observation of indefinite stability of the CPs in their solid-states even in the presence of CO_2 under solvent-free conditions. However, after insertion of a CO_2 molecule between two adjacent Ln centers of a polymeric molecule (***I4*** or ***I4′***; Scheme S11), the further processing is dependent on the nature of the ancillary bridging ligands (μ_2-OH/OMe in CPs herein). In the cases of **3·Ln** or **5·Ln**, the inserted CO_2 is converted into nothing but a bicarbonate moiety (HCO_3^- ; Scheme S12). The coordinated HCO_3^- is prone to release the proton (H^+) to assume carbonate moiety (CO_3^{2-}) in order for more uniform electron density distribution. Worth to mention that though ***I4*** and ***I4′*** are stereochemically different from each other by their formation, they could scramble to each other through the mechanism as depicted in Scheme S13. However, at this juncture, the reaction could proceed via two obvious pathways: (i) the released H^+ being attracted by the adjacent μ_2-OH group to form the intermediate ***I5*** (or ***I5′;*** Scheme S12); and (ii) the released H^+ being attracted by the adjacent amide N center of the doubly deprotonated form ($[\mathbf{L}^i]^{2-}$) of the pentadentate chelating ligand in the CPs to form the intermediate ***I25*** (Scheme S16). Both of the pathways rupture the backbone of the CPs. However, the former pathway eventually leads to the formation of the CO_3^{2-}-bridged dinuclear chemical species as the end-products, while the latter pathway eventually renders the formation of decacoordinate mononuclear complexes and solvated lanthanide carbonates. Worth mentioning that the latter pathway is sterically demanding at the Ln centers. Moreover, it associates with the hopping of $[\mathbf{HL}^i]^-$ from one Ln center to other Ln center (ca. from $[Ln]^b$ to $[Ln]^c$; Scheme S16). Hence, the latter pathway is expected to be facilitated for the CPs having relatively larger Ln ions and weaker coordination bond enthalpy. The ionic size is considerably larger for La(III) than Y(III). Moreover, as revealed by the computation analyses, $[\mathbf{L}^I]^{2-}$ renders significantly more stable CPs with Y(III) compared to La(III). It could be ascribed to why the treatment of CO_2 with the Y-based CPs (**3·Y** or **5·Y**) resulted in CO_3^{2-}-bridged dinuclear complexes, while the treatment of CO_2 with the La-based CPs (**3·La** or **5·La**) resulted in the decacoordinate mononuclear complexes and lanthanide carbonates in addition to the CO_3^{2-}bridged dinuclear complexes. Notably, Ln(III) and CO_3^{2-} result in layered structures with significantly high heat of formation . Thus, it could facilitate further reaction of the CO_3^{2-}-bridged dinuclear complexes with CO_2 to result in lanthanide carbonates and decacoordinate mononuclear complexes as depicted in Scheme S17. It is worth reiterating the experimental observations that the *in-situ* formed La-based CO_3^{2-}-bridged dinuclear complexes were found to decompose spontaneously into the decacoordinate mononuclear complexes and solvated carbonates. On the other hand, the Y-based CO_3^{2-}-bridged dinuclear complexes were found to be stable indefinitely. It could be attributed to the differences in the ionic sizes of Ln(III) and the binding energy between the Ln(III) and the pentadentate chelating ligands.

In the cases of **4·Ln** or **6·Ln**, the bridging moiety between $[L^{i}Ln]^{a}$ and $[L^{i}Ln]^{b}$ in ***I4*** (or ***I4'***) is methoxycarbonate ($MeOCO_2^-$). The C center in the bridging $[MeOCO_2]$ moiety is still significantly electrophilic in nature. If the reaction is carried out in MeOH solvent medium, the $[MeOCO_2]$ moiety could react with MeOH molecules eventually leading to the formation of tetramethoxymethane ($C(OMe)_4$) via the cascade method as illustrated in Scheme S14 (see ESI). Notably, H_2O is substantially stronger nucleophile than MeOH. As H_2O is a byproduct of these reactions (Scheme 1), a competitive reaction of H_2O with the $[MeOCO_2]$ moiety is inevitable, which results in the CO_3^{2-}-based products as well. The C center in the $C(OMe)_4$ moiety is also considerably electrophilic in nature. Thus, the bridging $[C(OMe)_4]$ moiety could undergo substitution reactions with H_2O leading to CO_3^{2-}-based products as depicted in Scheme S15 (see ESI). Obviously, Ln dependent trends of the reactivity of the CPs **4·Ln** or **6·Ln** towards CO_2, and the formation of decacoordinate mononuclear complexes alongside lanthanide carbonates remain the same as described before for the CPs **3·Ln** or **5·Ln**.

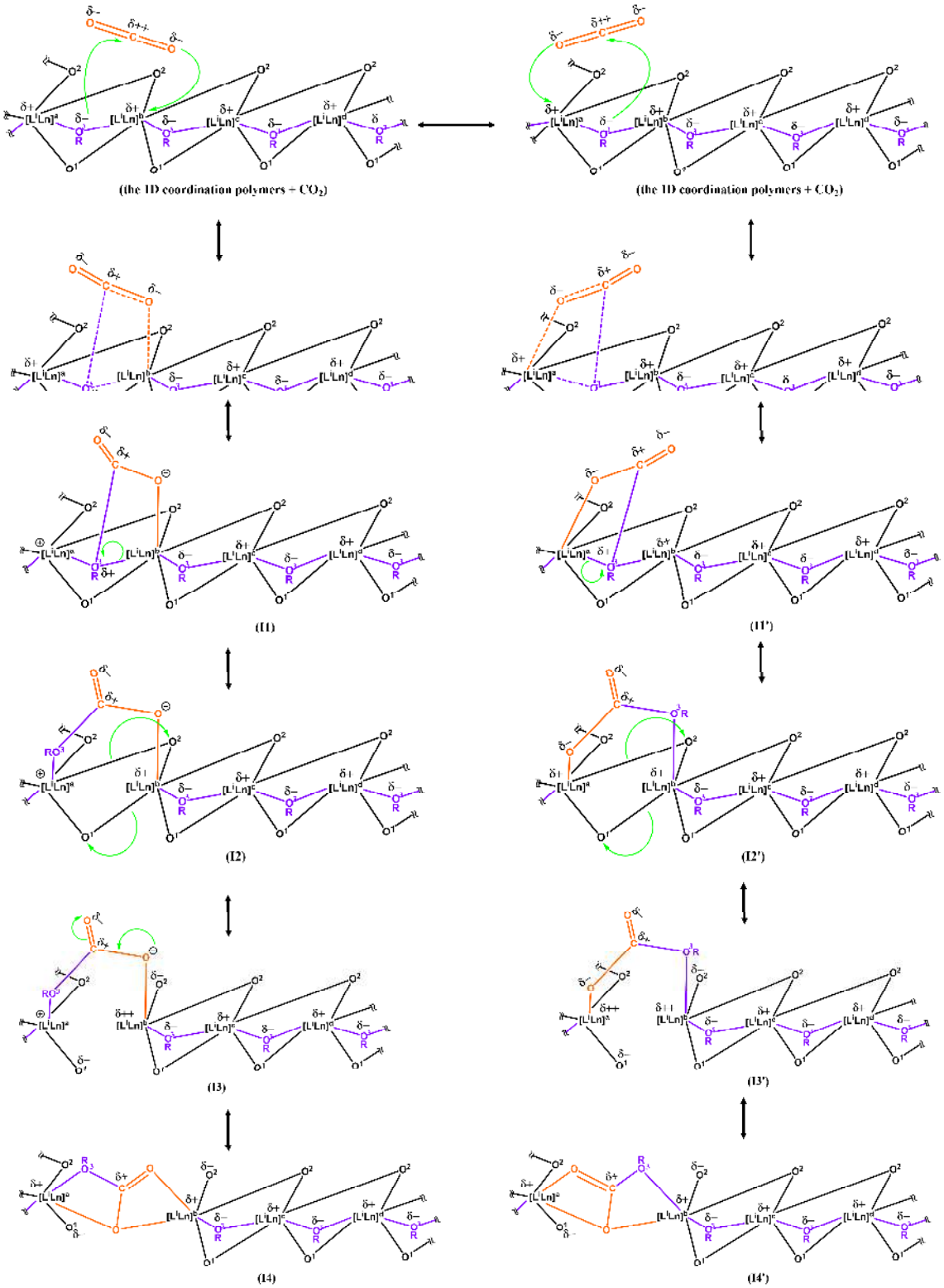

Scheme S10. The most probable reaction mechanism for the activation of CO_2 by the coordination polymers and insertion of alkoxycarbonate (when R = alkyl group) or bicarbonate (when R = H) between two adjacent Ln centres (ca. $[\mathbf{L}^{i}\mathbf{Ln}]^{a}$ and $[\mathbf{L}^{i}\mathbf{Ln}]^{b}$ here in) to form the intermediates ***I4*** (or ***I4'***) via the transition states ***TS1*** or (or ***TS1'***) and via the subsequent intermediates ***I1 – I3*** (or ***I1' – I3'***). The

coordination polymers and the intermediates are depicted in simplified *ChemDraw* representations where the segments in grey colour are from the basis building blocks, the segments in purple colour are from the ancillary bridging ligands and the segments in orange colour are from the CO_2 molecules. The O atomic centres of the pentadentate chelating ligands are labelled as O1 and O2, while the O atomic centres of the ancillary bridging ligands are labelled as O3. In view of the fundamental elementary properties, the O atoms are nucleophilic in nature, while the C centre is electrophilic in nature in a CO_2 molecule. On the other hand, the Ln(III) centre are the most electrophilic in nature, while the O atoms in the ancillary bridging ligands (O3) are the most nucleophilic in nature in the coordination polymers. Conventionally, the electrophilic centres are labelled with δ+, while the nucleophilic centres are labelled with δ-. Considering the overall electro-neutrality of the coordination polymers and CO_2, positive and negative charges are assigned to the appropriate centres accordingly (ca. δ++ for C and δ- for O in CO_2). The simplified *ChemDraw* structures where all the chemical bonds are presented as solid lines are either the pristine coordination polymers or the *intermediates* (*Is*) formed during the course of the reactions. On the other hand, the simplified *ChemDraw* structures where some of the chemical bonds are presented as dashed lines are the *transition states* (***TS****s*) formed during the course of the reactions. The chemical bonds which are presented as dashed lines in the ***TS***s stand for the state of the formation or cleavage of the chemical bonds. Conventionally, the directions indicated with the green solid curly arrows stand for the directions of the flows of the frontier electrons during the formation or cleavage of the chemical bonds. The double headed black solid arrows conventionally represent the bidirectionality of the reactions of interconversions without involving any mass change.

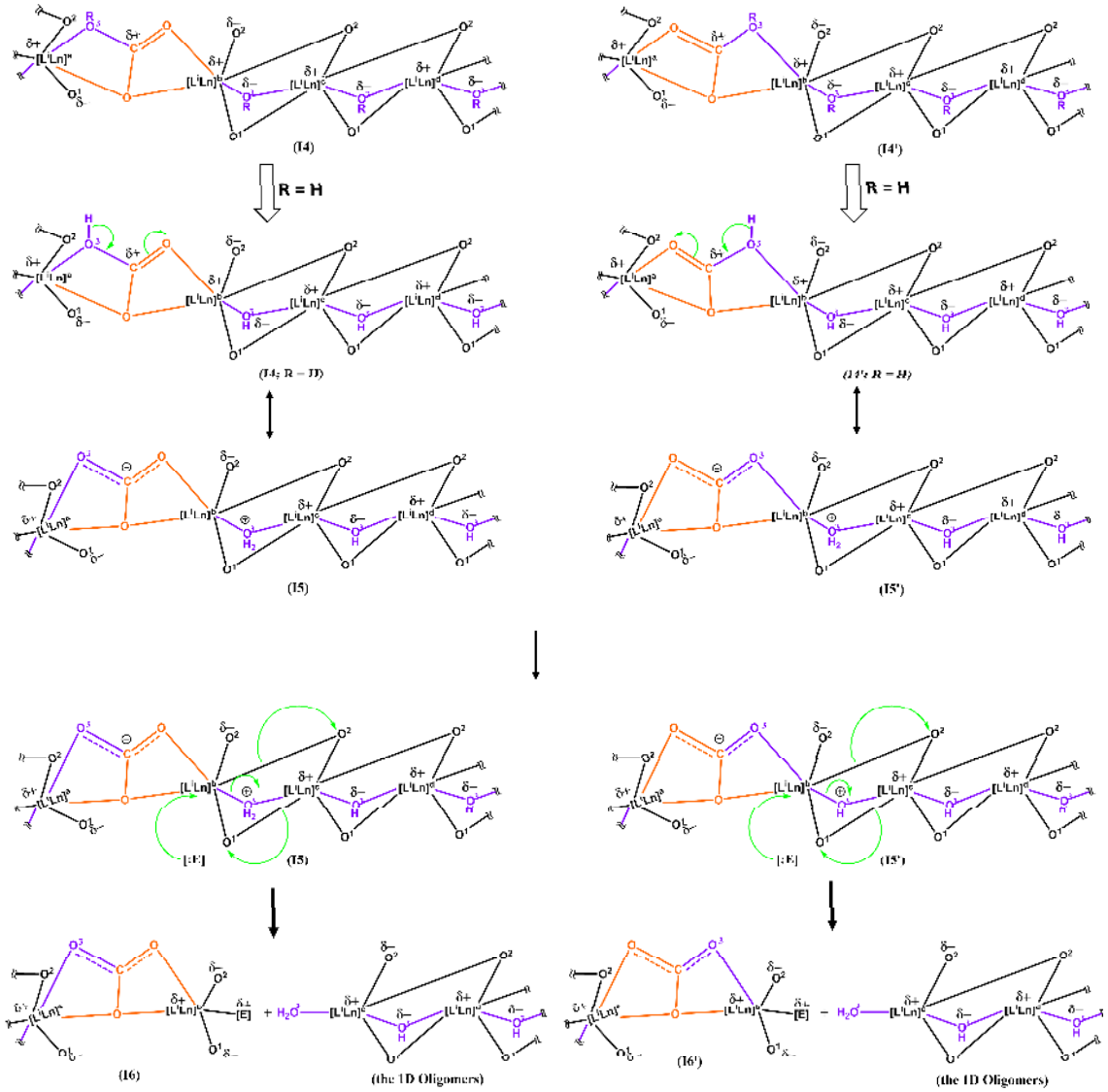

Scheme S11. The most probable reaction mechanism for the transformation of the bicarbonate-bridged (HCO_3^--bridged) intermediates (***I4*** or ***I4'*** where R = H) into the CO_3^{2-}-bridged intermediates (***I6*** or ***I6'***) and the 1D oligomers through the intermediates ***I5*** or ***I5'***. The 1D oligomers and the intermediates are depicted in simplified *ChemDraw* representations where the segments in grey colour are from the basis building blocks, the segments in purple colour are from the ancillary bridging ligands and the segments in orange colour are from the CO_2 molecules. The O atomic centres of the pentadentate chelating ligands are labelled as O1 and O2, while the O atomic centres of the ancillary bridging ligands are labelled as O3. In view of the fundamental elementary properties, the Ln(III) centre are the most electrophilic in nature, while the O atoms in the ancillary bridging ligands (O3) are the most nucleophilic in nature in the coordination polymers/oligomers. Conventionally, the electrophilic centres are labelled with δ+, while the nucleophilic centres are labelled with δ-. Considering the overall electro-neutrality, positive and negative charges are assigned to the appropriate centres accordingly. The chemical bonds which are presented as the dashed lines in the intermediates (***I***s) stand for the conventional conjugation of π-electron(s) in the segment(s) of the chemical composites/structures. Conventionally, the directions indicated with the green solid curly arrows stand for the directions of the flows of the frontier electrons during the formation or cleavage of the chemical bonds. The double headed black solid arrows

conventionally represent the bidirectionality of the reactions of interconversions without involving any mass change. The single headed black solid arrows conventionally represent the irreversible reactions moving only towards the directions of the arrows.

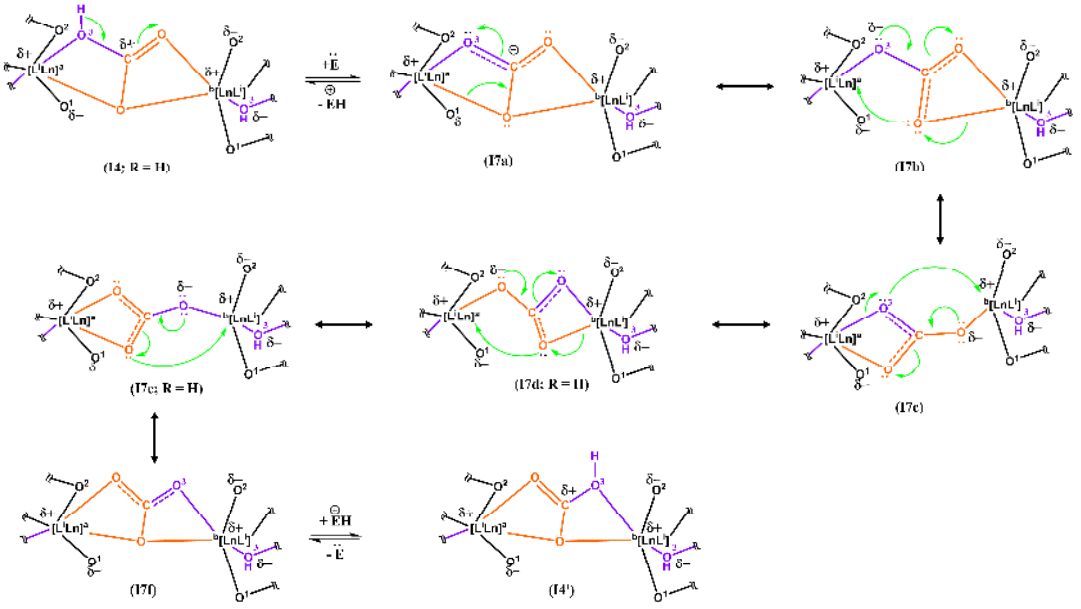

Scheme S12. The schematic presentation for the interconversion between the HCO_3^--bridged intermediates ***I4*** and ***I4'*** (where R = H) upon scrambling the positions of the O atoms of the bicarbonate (HCO_3^-) moieties. It implies that the final outcomes are expected to be the same irrespective to the formation of any one or both of the initial intermediates ***I4*** and ***I4'***. In the simplified *ChemDraw* representations, the segments in grey colour are from the basis building blocks, the segments in purple colour are from the ancillary bridging ligands and the segments in orange colour are from the CO_2 molecules. The O atomic centres of the pentadentate chelating ligands are labelled as O1 and O2, while the O atomic centres of the ancillary bridging ligands are labelled as O3. In view of the fundamental elementary properties, the Ln(III) centre are the most electrophilic in nature, while the O atoms in the ancillary bridging ligands (O3) are the most nucleophilic in nature in the coordination polymers/oligomers. Conventionally, the electrophilic centres are labelled with δ+, while the nucleophilic centres are labelled with δ-. Considering the overall electro-neutrality, positive and negative charges are assigned to the appropriate centres accordingly. The chemical bonds which are presented as the dashed lines in the intermediates (***I***s) stand for the conventional conjugation of π-electron(s) in the segment(s) of the chemical composites/structures. Conventionally, the directions indicated with the green solid curly arrows stand for the directions of the flows of the frontier electrons during the formation or cleavage of the chemical bonds. The double headed black solid arrows conventionally represent the bidirectionality of the reactions of interconversions without involving any mass change. The double half-headed black solid arrows conventionally represent the reactions steps which are kinetically in equilibrium.

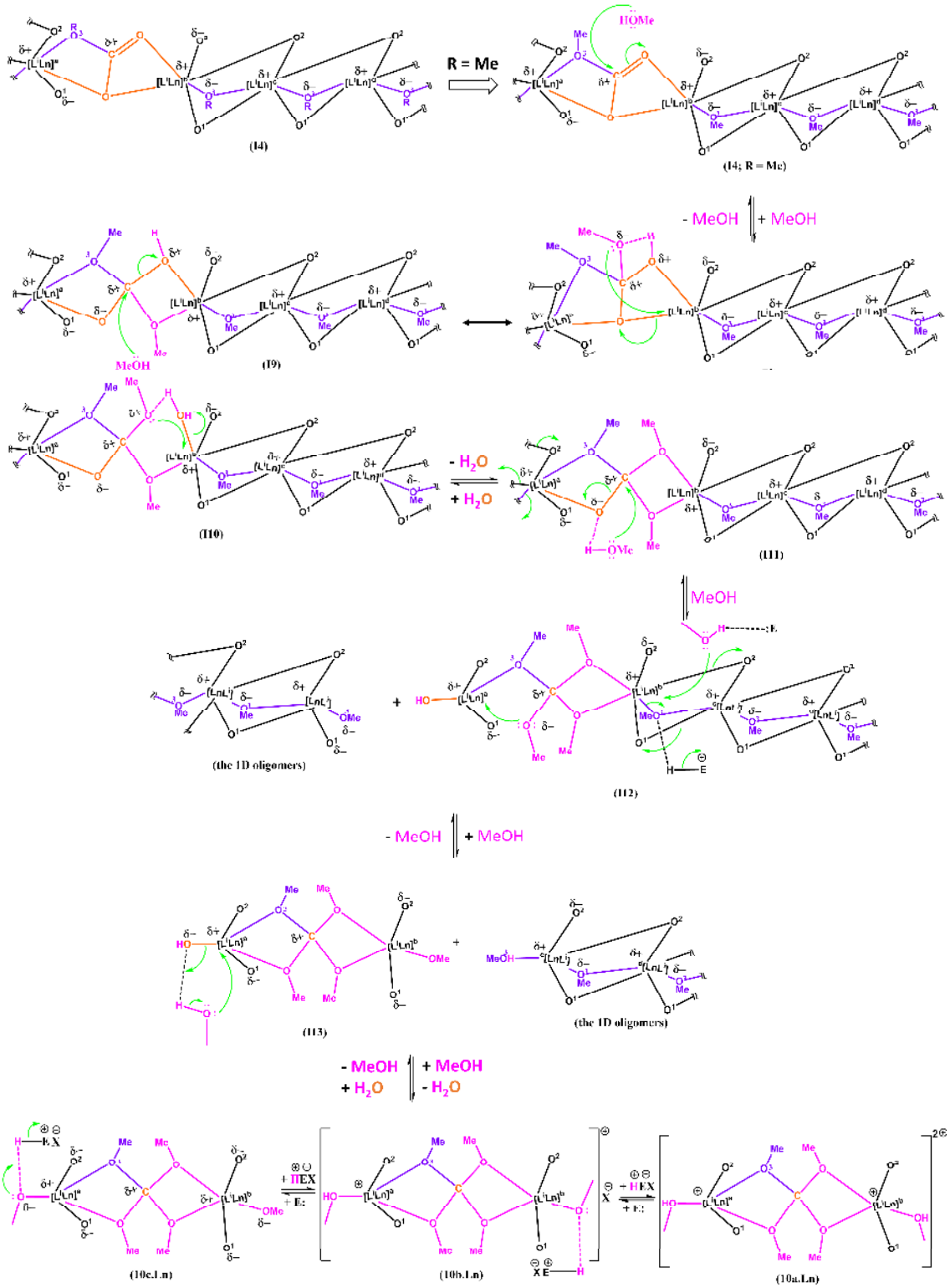

Scheme S13. The most probable reaction mechanism for the transformation of the methoxycarbonate-bridged ($MeOCO_2^-$-bridged) intermediates (***I4*** or ***I4'*** where R = Me) into the tetramethoxymethane-bridged ($C(OMe)_4$-bridged) products **10·Ln** (**10a·Ln**, **10b·Ln** and **10c·Ln**) and the 1D oligomers via the intermediates ***I8*** or ***I13***. The 1D oligomers, the intermediates ***I4***, ***I8-I13***, and the products **10·Ln** (**10a·Ln**, **10b·Ln** and **10c·Ln**) are depicted in simplified *ChemDraw* representations where the

segments in grey colour are from the basis building blocks, the segments in purple colour are from the ancillary bridging ligands, the segments in orange colour are from the CO_2 molecules and the segments in pink colour are MeOH solvent molecules. The O atomic centres of the pentadentate chelating ligands are labelled as O1 and O2, while the O atomic centres of the ancillary bridging ligands are labelled as O3. In view of the fundamental elementary properties, the Ln(III) centre are the most electrophilic in nature, while the O atoms in the ancillary bridging ligands (O3) are the most nucleophilic in nature in the coordination polymers/oligomers. Conventionally, the electrophilic centres are labelled with δ+, while the nucleophilic centres are labelled with δ-. Considering the overall electro-neutrality, positive and negative charges are assigned to the appropriate centres accordingly. The chemical bonds which are presented as the dotted lines herein stand for the H-bonding interactions. Conventionally, the directions indicated with the green solid curly arrows stand for the directions of the flows of the frontier electrons during the formation or cleavage of the chemical bonds. The double headed black solid arrows conventionally represent the bidirectionality of the reactions of interconversions without involving any mass change. The double half-headed black solid arrows conventionally represent the reactions steps which are kinetically in equilibrium.

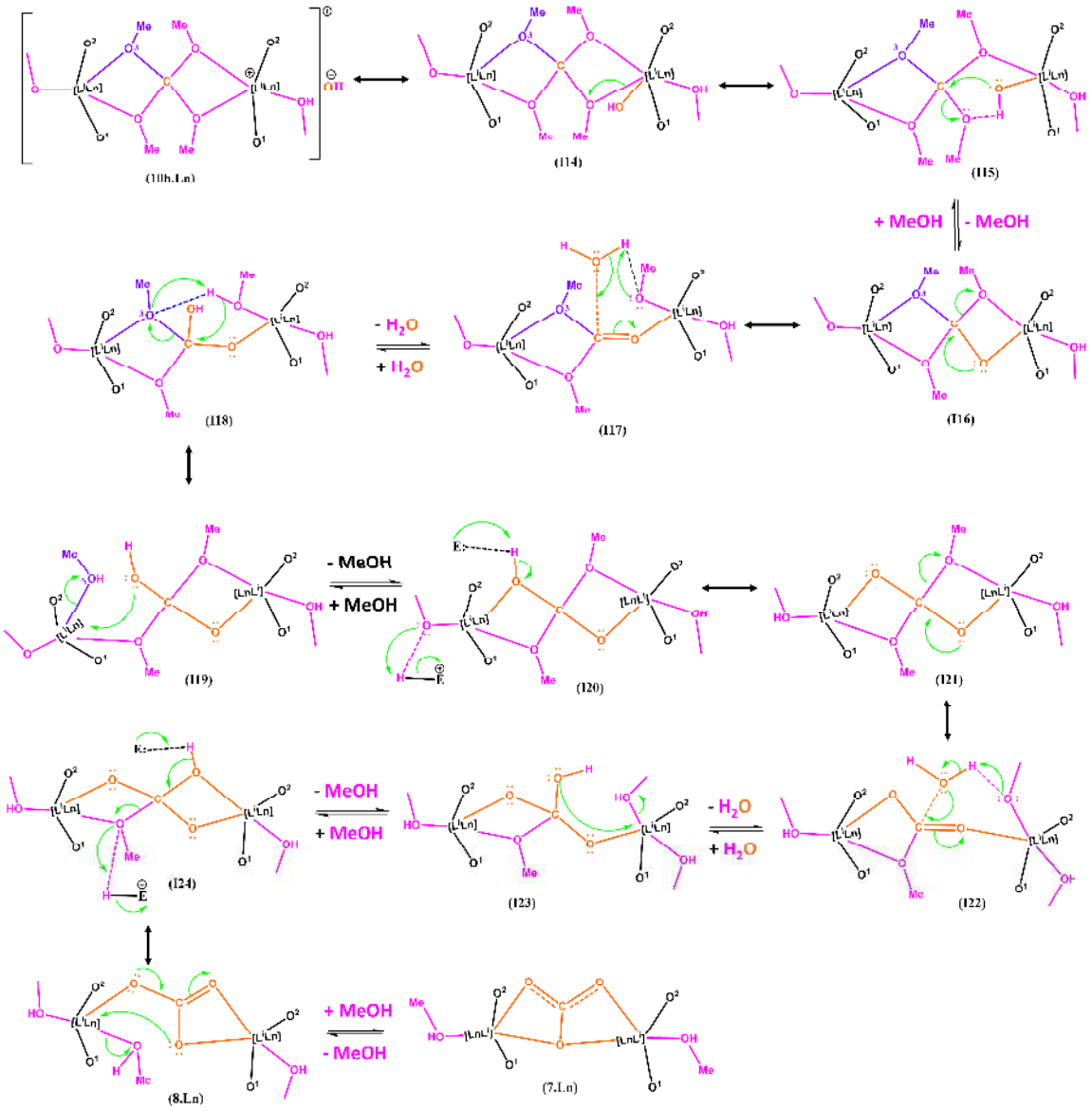

Scheme S14. The most probable reaction mechanism for the reactions of the *in-situ* formed tetramethoxymethane-bridged ($C(OMe)_4$-bridged) products **10a·Ln** with the *in-situ* generated water to result in the CO_3^{2-}-bridged products **7·Ln** and **8·Ln** via the intermediates ***I14*** or ***I22***. The intermediates ***I4***, ***I8-I13***, and the products **7·Ln**, **8·Ln** and **10a·Ln** are depicted in simplified *ChemDraw* representations where the segments in grey colour are from the basis building blocks, the segments in purple colour are from the ancillary bridging ligands, the segments in orange colour are from the CO_2 molecules and the segments in pink colour are MeOH solvent molecules. The O atomic centres of the pentadentate chelating ligands are labelled as O1 and O2, while the O atomic centres of the ancillary bridging ligands are labelled as O3. In view of the fundamental elementary properties, the Ln(III) centre are the most electrophilic in nature, while the O atoms in the ancillary bridging ligands (O3) are the most nucleophilic in nature in the coordination polymers/oligomers. Conventionally, the electrophilic centres are labelled with δ+, while the nucleophilic centres are labelled with δ-. Considering the overall electro-neutrality, positive and negative charges are assigned to the appropriate centres accordingly. The chemical bonds which are presented as the dashed lines in the structures stand for the conventional

conjugation of π-electron(s) in the segment(s) of the chemical composites/structures. The chemical bonds which are presented as the dotted herein stand for the H-bonding interactions. Conventionally, the directions indicated with the green solid curly arrows stand for the directions of the flows of the frontier electrons during the formation or cleavage of the chemical bonds. The double headed black solid arrows conventionally represent the bidirectionality of the reactions of interconversions without involving any mass change. The double half-headed black solid arrows conventionally represent the reactions steps which are kinetically in equilibrium.

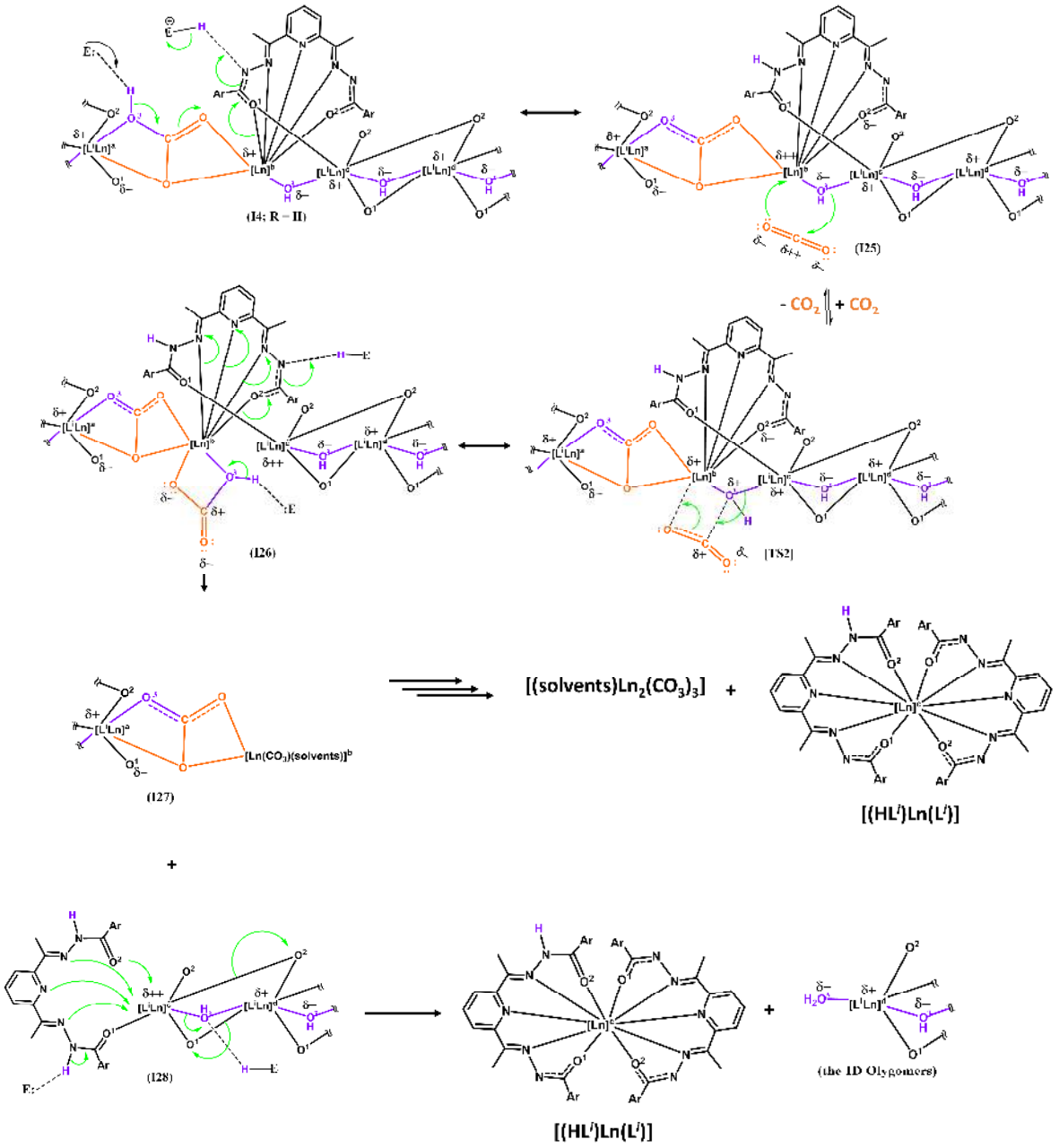

Scheme S15. The most probable mechanism for the further reactions of the *in-situ* formed HCO_3^--bridged intermediates ***I4*** (or ***I4'***) with CO_2 to result in eventually the decacoordinate mononuclear neutral complexes ([**(HL^i)Ln(L^i)**]) and the solvated lanthanide carbonate salts (**[(solvents)Ln$_2$(CO$_3$)$_3$]**). The intermediates ***I25-I28,*** the transition states ***TS2*** and the 1D oligomers are depicted in simplified *ChemDraw* representations where the segments in grey colour are from the basis building blocks, the segments in purple colour are from the ancillary bridging ligands, the segments in orange colour are from the CO_2 molecules and the segments in pink colour are MeOH solvent molecules. The O atomic centres of the pentadentate chelating ligands are labelled as O1 and O2, while the O atomic centres of the ancillary bridging ligands are labelled as O3. In view of the fundamental elementary properties, the Ln(III) centre are the most electrophilic in nature, while the O atoms in the ancillary bridging ligands (O3) are the most nucleophilic in nature in the coordination polymers/oligomers. Conventionally, the

electrophilic centres are labelled with δ+, while the nucleophilic centres are labelled with δ-. Considering the overall electro-neutrality, positive and negative charges are assigned to the appropriate centres accordingly. The chemical bonds which are presented as the dashed lines in the structures stand for the conventional conjugation of π-electron(s) in the segment(s) of the chemical composites/structures. The chemical bonds which are presented as the dotted herein stand for the H-bonding interactions. Conventionally, the directions indicated with the green solid curly arrows stand for the directions of the flows of the frontier electrons during the formation or cleavage of the chemical bonds. The double headed black solid arrows conventionally represent the bidirectionality of the reactions of interconversions without involving any mass change. The single headed black solid arrows conventionally represent the irreversible reactions moving only towards the directions of the arrows. The single headed multiple (triple herein) black solid arrows conventionally represent the multistep obvious reactions to result in the final products.

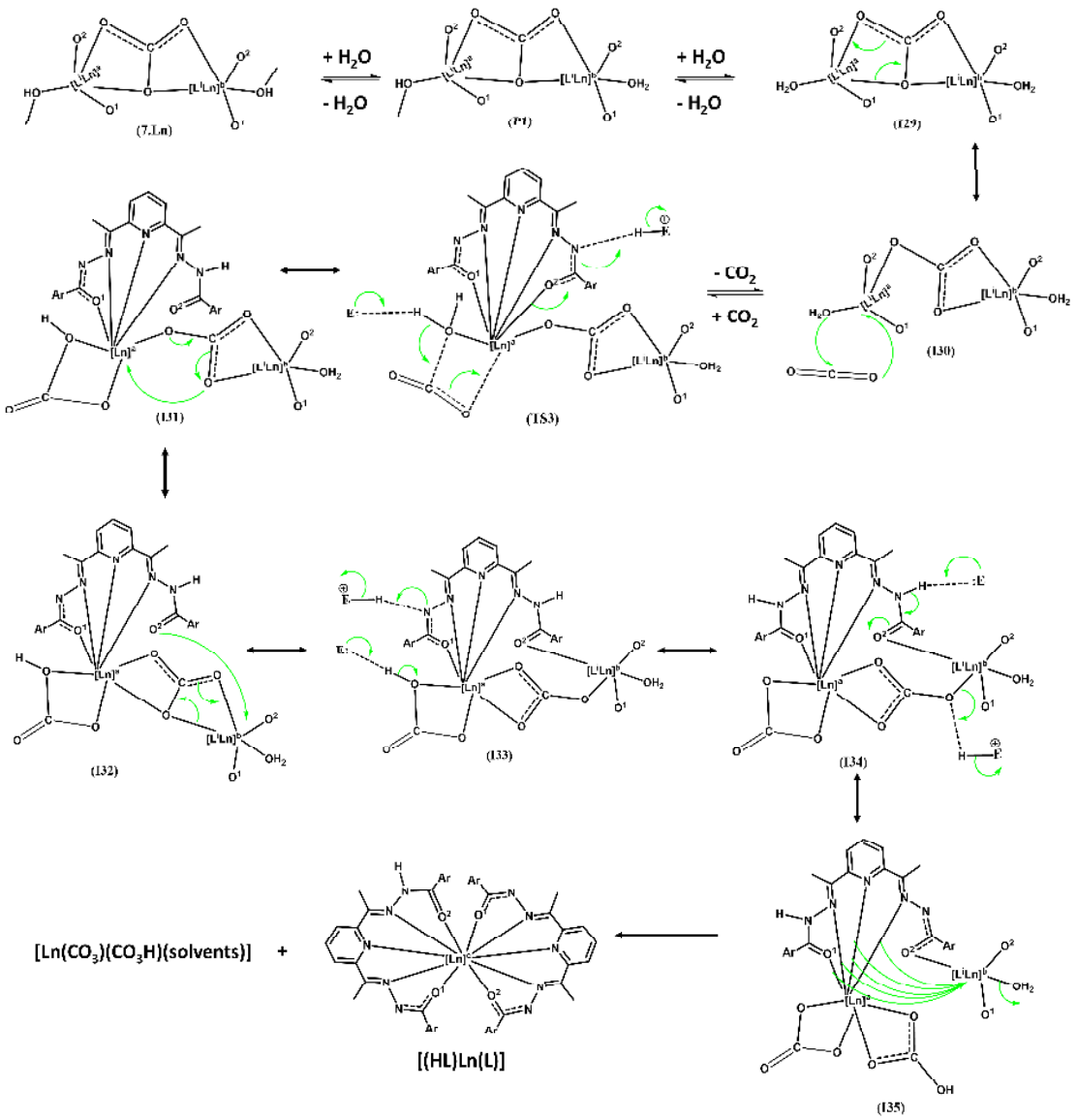

Scheme S16. The most probable mechanism for the further reactions of the *in-situ* formed CO_3^{2-}-bridged products **7·Ln** with CO_2 in the presence of water to result in eventually the decacoordinate mononuclear neutral complexes ([**(HL^i)Ln(L^i)**]) and the solvated lanthanide carbonate salts (**[(solvents)Ln$_2$(CO$_3$)$_3$]**). The precursors, **7·Ln**, the intermediates ***I29-I35*** and the products ***P1*** are depicted in simplified *ChemDraw* representations where the segments in grey colour are from the basis building blocks, the segments in purple colour are from the ancillary bridging ligands, the segments in orange colour are from the CO_2 molecules and the segments in pink colour are MeOH solvent molecules. The O atomic centres of the pentadentate chelating ligands are labelled as O1 and O2, while the O atomic centres of the ancillary bridging ligands are labelled as O3. In view of the fundamental elementary properties, the Ln(III) centre are the most electrophilic in nature, while the O atoms in the ancillary bridging ligands (O3) are the most nucleophilic in nature in the coordination polymers/oligomers. Conventionally, the electrophilic centres are labelled with δ+, while the nucleophilic centres are labelled with δ-. Considering the overall electro-neutrality, positive and

negative charges are assigned to the appropriate centres accordingly. The chemical bonds which are presented as the dashed lines in the structures stand for the conventional conjugation of π-electron(s) in the segment(s) of the chemical composites/structures. The chemical bonds which are presented as the dotted herein stand for the H-bonding interactions. Conventionally, the directions indicated with the green solid curly arrows stand for the directions of the flows of the frontier electrons during the formation or cleavage of the chemical bonds. The double headed black solid arrows conventionally represent the bidirectionality of the reactions of interconversions without involving any mass change. The single headed black solid arrows conventionally represent the irreversible reactions moving only towards the directions of the arrows. The double half-headed black solid arrows conventionally represent the reactions steps which are kinetically in equilibrium.

Video S1. Reaction of the CPs **3·Y** and **3·La** with CO_2 in degassed methanol

Schlenk tube A:1.4 mg of **3·Y** (0.0024 mmol) was taken in 1 ml of degassed methanol and after stirring for 5 minutes, CO_2 gas was purged.

Schlenk tube B:1.53 mg of **3·La** (0.0028 mmol) was taken in 1 ml of degassed methanol and after stirring for 5 minutes, CO_2 gas was purged.

Video S2. Comparative reactivity of the *in-situ* formed CP **3·Y** and *as-synthesized* solid samples of the CPs **3·Y** in degassed methanol on treatment with CO_2 gas

Schlenk tube A:13.2 mg of $Y(OTf)_3.6H_2O$ (0.0205 mmol), 8.2 mg of $\mathbf{H_2L^1}$ (0.0205 mmol) was taken in 2 ml of degassed methanol. Into this solution 17μL of NEt_3 (0.123 mmol) was added and after stirring for 15 minutes, CO_2 gas was purged.

Schlenk tube B:5.0 mg of **3·Y** (0.00831 mmol) was taken in 2 ml of degassed methanol and after stirring for 15 minutes, CO_2 gas was purged**.**

Video S3. Comparative video illustrating the change in reactivity of CP **3·Y** with varying base equivalents and water content in degassed methanol.

Schlenk tube A: 1.1 mg of **3·Y** (0.0018 mmol) was taken in 2 ml of degassed methanol into which 0.5 equivalence of NEt_3((100 times diluted in MeOH; 15 μL, 0.0011 mmol) was added and after stirring for 15 minutes, CO_2 gas was purged.

Schlenk tube B: 1.1 mg of **3·Y** (0.0018 mmol) was taken in 2 ml of degassed methanol into which 1 equivalence of NEt_3(100 times diluted in MeOH; 30 μL, 0.0022 mmol) was added and after stirring for 15 minutes, CO_2 gas was purged.

Schlenk tube C: 1.1 mg of **3·Y** (0.0018 mmol) was taken in 2 ml of degassed aq. methanol (5% water, v/v) and after stirring for 15 minutes, CO_2 gas was purged.

Schlenk tube D: 1.1 mg of **3·Y** (0.0018 mmol) was taken in 2 ml of degassed aq. methanol (10% water, v/v) and after stirring for 15 minutes, CO_2 gas was purged.

Video S4. Comparative video illustrating the reaction rate of *in-situ* generated CP **3·Y** with CO_2 under closed and continuous purging conditions in degassed methanol.

Schlenk tube A: 11.5 mg of $Y(OTf)_3.6H_2O$ (0.0177 mmol), 7.1 mg of $\mathbf{H_2L^1}$ (0.0177 mmol) was taken in 1.5 ml of degassed methanol. Into this solution 14.8µL of NEt_3 (0.1062 mmol) was added and after stirring for 15 minutes, CO_2 gas was purged with a bleed needle.

Schlenk tube B: 11.5 mg of $Y(OTf)_3.6H_2O$ (0.0177 mmol), 7.1 mg of $\mathbf{H_2L^1}$ (0.0177 mmol) was taken in 1.5 ml of degassed methanol. Into this solution 14.8µL of NEt_3 (0.1062 mmol) was added and after stirring for 15 minutes, CO_2 gas was purged without a bleed needle.

References:

1. C. Lorenzini, C. Pelizzi, G. Pelizzi and G. Predieri, *J. Chem. Soc.,* Dalton Trans., 1983, 721.
2. A. F. Santos, I. P. Ferreira, C. B. Pinheiro, J. A. Takahashi, L. R. Teixeira and H. Beraldo, *Polyhedron*, 2017, **138**, 270.
3. International Tables for Crystallography. DOI: 10.1107/97809553602060000001.
4. M. J. Frisch, G. W. Trucks, H. B. Schlegel, G. E. Scuseria, M. A. Robb, J. R. Cheeseman, G. Scalmani, V. Barone, B. Mennucci, G. A. Petersson, H. Nakatsuji, M. Caricato, X. Li, H. P. Hratchian, A. F. Izmaylov, J. Bloino, G. Zheng, J. L. Sonnenberg, M. Hada, M. Ehara, K. Toyota, R. Fukuda, J. Hasegawa, M. Ishida, T. Nakajima, Y. Honda, O. Kitao, H. Nakai, T.Vreven, J. A. Montgomery Jr., J. E. Peralta, F. Ogliaro, M. Bearpark, J.J. Heyd, E.Brothers, K. N. Kudin, V. N. Staroverov, R. Kobayashi, J. Normand, K. Raghavachari, A. B. Rendell, J. C. Burant, S. S. Iyengar, J.Tomasi, M. Cossi, N. Rega, M. J. Millam, M. Klene, J. E. Knox, J. B.Cross, V. Bakken, C. Adamo, J. Jaramillo, R. Gomperts, R. E. Stratmann,O. Yazyev, A. J. Austin, R. Cammi, C. Pomelli, J. W. Ochterski, R. L.Martin, K. Morokuma, V. G. Zakrzewski, G. A. Voth, P. Salvador, J. J.Dannenberg, S. Dapprich, A. D. Daniels, O. Farkas, J. B. Foresman, J.V. Ortiz, J. Cioslowski, D. J. Fox, *Gaussian 09*; Gaussian, Inc.,Wallingford CT (2009).
5. A. D. J. Becke, *J. Chem. Phys.,* 1993*,* **98**, 5648.
6. T. H. J. Dunning, P. J. Hay, *Modern Theoretical Chemistry*, Schaefer, H.F., III, Ed.; Plenum: New York, **Vol. *3*** (1976).
7. P. J. Hay and R. J. Wadt, *Chem. Phys. Chem.*, 1985, **82**, 299.
8. V. Singh, V. Urunikulavan and A. K. Bar, *Dalton Trans.*, 2025, **54**, 4566.

==========*****==========